INFORMATION TO USERS

This manuscript has been reproduced from the microfilm master. UMI films the text directly from the original or copy submitted. Thus, some thesis and dissertation copies are in typewriter face, while others may be from any type of computer printer.

The quality of this reproduction is dependent upon the quality of the copy submitted. Broken or indistinct print, colored or poor quality illustrations and photographs, print bleedthrough, substandard margins, and improper alignment can adversely affect reproduction.

In the unlikely event that the author did not send UMI a complete manuscript and there are missing pages, these will be noted. Also, if unauthorized copyright material had to be removed, a note will indicate the deletion.

Oversize materials (e.g., maps, drawings, charts) are reproduced by sectioning the original, beginning at the upper left-hand corner and continuing from left to right in equal sections with small overlaps.

Photographs included in the original manuscript have been reproduced xerographically in this copy. Higher quality 6" x 9" black and white photographic prints are available for any photographs or illustrations appearing in this copy for an additional charge. Contact UMI directly to order.

Bell & Howell Information and Learning
300 North Zeeb Road, Ann Arbor, MI 48106-1346 USA

UMI®
800-521-0600

Preparation of Magnetic Carriers Through Functionalization of Nanosized Maghemite Particles

by

Stéphanie Gélinas

A thesis submitted to the Faculty of Graduate Studies and Research of McGill University in partial fulfillment of the requirements for the degree of Doctor of Philosophy.

Department of Mining and Metallurgical Engineering

McGill University, Montreal

February, 1999

To Jörg, and my family

for their insights, support and patience since the beginning.

Abstract

A novel method for preparing magnetic carriers, the functionalization of magnetic particles by molecular self-assembly, is described. Oriented and stable monolayers of a dibenzoic acid diamide bolaamphiphile were prepared on the surface of nanosized maghemite (γ-Fe_2O_3) particles. The nature of the monolayer was characterized by X-ray photoelectron spectroscopy (XPS), while the structure and stability were characterized by diffuse reflectance infrared Fourier transform spectroscopy (DRIFTS). The results show that the bolaamphiphile anchors on the surface through chemical bonding between one of the carboxylic head groups and the iron of the maghemite, leaving a pendant carboxylic moiety reactive. A density of the self-assembled films on γ-Fe_2O_3 was assessed from potentiometric titration studies of the coated particles in dimethylformamide (DMF). Modification of the carboxy-terminated carriers through a reaction with the ligand diethylenetriamine (DETA), using a typical carbodiimide, enabled the preparation of highly selective magnetic carriers. Potentiometric titration of the reacted carriers indicates a 50% yield of DETA-reacted surfaces. An application of the prepared magnetic carriers in the recovery of metals, such as Cu^{2+} ions from dilute streams, is demonstrated. The efficiency of carriers in the chelation of copper ions was assessed by complexometric titration. Imaging of the prepared magnetic carriers, using an advanced Pt/C replica technique of transmission electron microscopy (TEM), is presented.

Résumé

Une nouvelle méthode de préparation de transporteurs magnétiques, par la modification de la fonctionnalité de particules magnétiques par auto-assemblage, est décrite. Des monocouches orientées et stables d'un bolaamphiphile dibenzoïque acide diamide ont été préparées à la surface de particules nanométriques de maghémite (γ-Fe_2O_3). La nature de la monocouche a été caractérisée par spectroscopie photo-électrique à rayons-X (XPS), alors que la structure et la stabilité ont été caractérisées par spectroscopie infrarouge à transformée de Fourier par réflection diffuse (DRIFTS). Les résultats démontrent que le bolaamphiphile s'ancre à la surface par liaison chimique entre un des groupes carboxyliques terminaux et le fer de la maghémite, laissant une entité carboxylique pendante et réactive. La densité des films auto-assemblés sur la maghémite a été déterminée par des études de titration potentiométrique des particles couvertes dans le solvant diméthylformamide (DMF). La modification des transporteurs aux terminaisons carboxyl par réaction avec le ligand diéthylènetriamine (DETA), en utilisant un carbodiimide typique, permet la préparation de transporteurs magnétiques hautement sélectifs. La titration potentiométrique des transporteurs réactifs indique un rendement de surfaces réactives au DETA de 50%. L'utilisation des transporteurs magnétiques ainsi préparés, dans la récupération de métaux, plus spécifiquement d'ions Cu^{2+} provenant d'effluents dilués, est démontrée. L'efficacité des transporteurs dans la chélation d'ions de cuivre a été déterminée par titration complexométrique. L'imagerie des transporteurs magnétiques ainsi préparés, par l'utilisation d'une technique avancée de replica de Pt/C par microscopie à transmission électronique (TEM), est présentée.

Foreword

This thesis was prepared in accordance with article B2 of the Guidelines Concerning Thesis Preparation of McGill University. This article reads as follows:

> "Candidates have the option of including, as part of the thesis, the text of a paper(s) submitted or to be submitted for publication, or the clearly-duplicated text of a published paper(s). These texts must be bound as an integral part of the thesis.
> -If this option is chosen, connecting texts that provide logical bridges between the papers are mandatory. The thesis must be written in such a way that it is more than a mere collection of manuscripts; in other words, results of a series of papers must be integrated.
> -The thesis must still conform to all other requirements of the "Guidelines for Thesis Preparation". The thesis must include: a Table of Contents, an abstract in English and French, an introduction which clearly states the rationale and objectives of the study, a comprehensive review of the literature, a final conclusion and summary and a thorough bibliography or reference list.
> -Additional material must be provided where appropriate (e.g. in appendices) and in sufficient detail to allow a clear and precise judgment to be made of the importance and originality of the research reported in the thesis.
> -In the case of manuscripts co-authored by the candidate and others, the candidate is required to make an explicit statement in the thesis as to who contributed to such work and to what extent. Supervisors must attest to the accuracy of such statements at the doctoral oral defense. Since the task of the examiners is made more difficult in these cases, it is in the candidate's interest to make perfectly clear the responsibilities of all the authors of the co-authored papers."

This thesis consists of seven chapters. Chapter 1 presents a general introduction to magnetic carriers, their associated technology and role in wastewater treatment. Chapter 2 contains a summary of the preparation and characterization techniques of magnetic carriers. Chapters 3, 4, 5 and 6 present the main results of the research and are written in publication format. Chapter 7 includes general conclusions and contributions to original knowledge.

The following are manuscripts written by the author and were used in preparation of this thesis. Manuscripts 1, 2 comprise Chapters 3, 4 respectively. Manuscript 3 and 4 make up Chapter 5, while manuscript 5, comprises Chapter 6. The manuscripts are to be submitted as indicated.

1. Stéphanie A. Gélinas, James A. Finch, Zhenghe Xu, and Peter Böhme, "Characterization of rigid and stable monolayers of a dibenzoic acid diamide bolaamphiphile on nanosized maghemite particles" to be submitted for publication in *Langmuir*.

2. Stéphanie A. Gélinas, James A. Finch and Andrew J. Vreugdenhil, "Determination of monolayer density by potentiometric titration", to be submitted for publication in *The Journal of Physical Chemistry*.

3. Stéphanie A. Gélinas, James A. Finch and Andrew J. Vreugdenhil, "Coupling of diethylenetriamine to carboxyl-terminated magnetic particles", to be submitted for publication in the *Journal of the American Chemical Society*.

4. Stéphanie A. Gélinas, Hojatollah Vali and James A. Finch, "TEM imaging of DETA-terminated magnetic carriers", to be submitted for publication in the *Journal of Materials Science*.

5. Stéphanie A. Gélinas, James A. Finch and Andrew J. Vreugdenhil, "Complexation of copper ions by DETA-terminated magnetic carriers", to be submitted for publication in the *International Journal of Mineral Processing*.

All of the manuscripts presented above are co-authored by Dr. James Finch in his capacity as research supervisor. Manuscript 3 includes Dr. Zhenghe Xu (Department of Chemical and Materials Engineering, University of Alberta) and Dr. Peter Böhme (formerly of the Department of Chemical Engineering at the Rensselaer Polytechnic Institute, NY) as co-authors, recognizing their contribution as initiators of the research into the preparation of magnetic carriers by self-assembly onto maghemite (Dr. Xu), using a novel diacid diamide

bolaamphiphile (original synthesis by Dr. Böhme). Dr. Andrew Vreugdenhil (formerly of the Department of Mining and Metallurgy, McGill University) is included as a co-author on manuscripts 2,3, and 5 in recognition of his contributions to the characterization by spectroscopy techniques (DRIFTS, XPS) and to the general chemistry aspects of the analysis of the carriers. Finally, Chapter 4 includes Dr. Hojatollah Vali (Department of Earth and Planetary Science, McGill University) as co-author, recognizing is contribution into the characterization of carriers by transmission electron microscopy (TEM). Beyond the contributions of the co-authors mentioned here, all of the work presented in this dissertation was performed by the author.

Acknowledgments

For their contributions to this research I wish to thank the following people:

Dr. Jim Finch, for the guidance provided throughout this work.

Dr. Andrew Vreugdenhil for his friendship, support and countless helpful and refreshing research ideas.

Colleagues from the chemistry research group, past and present, including:

Dr. Ram Rao, Ferehsteh, Caroline, Volkan, David, Qingxia, Joachim, Fu, Tony, Mitra and Jolanda.

And to my friends and colleagues from the column flotation group, Colin and Gunther, for all the wonderful ultimate outdoor experiences, giving me the energy and motivation to complete this work.

Table of Contents

Abstract i
Résumé ii
Foreword iii
Acknowledgments vi
List of Abbreviations xi
List of Figures xii
List of Tables xv

Chapter 1: General Introduction 1

Thesis Outline 5

Chapter 2: Background 8
2.1 Review of Magnetic Carriers 8
2.1.1 Introduction 9
2.1.2 Bare Magnetite 9
2.1.3 Polymer Assisted Magnetite 9
2.1.4 Polymer Adsorption and Polymerization 10
2.1.5 Silanation on Metal Oxides and Silica Coated Metal Oxides 11
2.1.6 Magnetic Carriers Derived from Drug Carriers 11
2.2 Characterization Techniques 13
2.2.1 Introduction 14
2.2.2 Infrared Spectroscopy 14
2.2.2.1 DRIFTS 17
2.2.3 XPS 21
2.2.4 Potentiometry 26
2.2.5 TEM 29

Chapter 3: Characterization of Rigid and Stable Monolayers of a Dibenzoic Acid Diamide Bolaamphiphile on Nanosized Maghemite Particles 34

3.1 Introduction 36

3.2 Experimental 37

3.2.1 Materials 37

3.2.2 Synthesis 38

3.2.3 Monolayer Preparation 38

3.2.4 Stability Experiment 38

3.2.5 Infrared Measurement 39

3.2.6 XPS 39

3.2.7 TEM 40

3.3 Results and Discussion 40

3.3.1 Maghemite Particles 40

3.3.2 Molecular Self-Assembled Monolayers 44

3.4 Conclusions 56

Chapter 4: Determination of Monolayer Density by Potentiometric Titration 59

4.1 Introduction 61

4.2 Experimental 63

4.2.1 Materials 63

4.2.2 Synthesis 64

4.2.3 Monolayer Preparation 64

4.2.4 Titration Apparatus 64

4.2.5 Titration Procedure 64

4.2.6 Infrared Measurement 65

4.3 Results and Discussion 66

4.3.1 DBSC-10 Titration 66

4.3.2 Titration of DBSC-10 Coated Particles 68
4.4 Conclusions 74

Chapter 5: DETA Modification 76
5.1 Coupling of Diethylenetriamine to Carboxyl-Terminated Magnetic Particles 76
5.1.1 Introduction 78
5.1.2 Experimental 79
5.1.2.1 Materials 79
5.1.2.2 Preparation of Stock Solutions 79
5.1.2.3 Coupling of DETA Procedure 79
5.1.2.4 Titration Apparatus 80
5.1.2.5 Titration Procedure 81
5.1.2.6 Infrared Measurement 81
5.1.2.7 XPS 81
5.1.3 Results and Discussion 82
5.1.3.1 DRIFTS 82
5.1.3.2 XPS 86
5.1.3.3 Titration 90
5.1.4 Conclusions 95
5.2 TEM Imaging of DETA-Terminated Magnetic Carriers 98
5.2.1 Introduction 100
5.2.2 Experimental 101
5.2.2.1 Materials 101
5.2.2.2 TEM 101
5.2.3 Results and Discussion 102
5.2.4 Conclusions 109

Chapter 6: Complexation of Copper Ions by DETA-Terminated Magnetic Carriers 111

6.1 Introduction 113

6.2 Experimental 114

6.2.1 Materials 114

6.2.2 Titration Apparatus 114

6.2.3 Titration Procedure 115

6.2.4 Copper Calibration Curve 115

6.2.5 XPS 116

6.3 Results and Discussion 117

6.3.1 Complexometric Titration 117

6.3.2 XPS 121

6.4 Conclusions 124

Chapter 7: Summary 126

7.1 Conclusions 127

7.2 Contributions to Original Knowledge 129

List of Abbreviations

DETA	diethylenetriamine
DBSC-10	dibenzoic acid diamide bolaamphiphile
EDCI	dimethylaminopropyl ethylcarbodiimide hydrochloride
DMF	dimethylformamide
MCT	magnetic carrier technology
SAM	self-assembled monolayer
XPS	X-ray photoelectron spectroscopy
DRIFTS	diffuse reflectance infrared Fourier transform spectroscopy
TEM	transmission electron microscopy
AFM	atomic force microscopy
STEM	scanning transmission electron microscopy
MS	mass spectrometry
FT-IR	Fourier transform infrared

List of Figures

Figure 1-1: Magnetic Carrier Technology 4
Figure 2-2-1: Three types of reflections from a powdered surface 18
Figure 2-2-2: Optical diagram of a DRIFTS accessory 19
Figure 2-2-3: Schematic of a typical XPS spectrometer 22
Figure 2-2-4: Principles of XPS 23
Figure 2-2-5: Schematic ray path for a TEM equipped for additional x-ray and electron energy-loss spectroscopy 31
Figure 3-1: Maghemite sample by transmission electron microscopy (TEM) with nanodiffraction patterns in circled particle 41
Figure 3-2: DRIFTS spectra of not treated, washed and dried maghemite particles 42
Figure 3-3: DRIFTS spectra of (a) pure DBSC-10, and (b) monolayer, with the structure of DBSC-10 in (c) 44
Figure 3-4: DRIFTS spectra of (a) pure DBSC-10, (b) monolayer, and (c) bare maghemite 46
Figure 3-5: Coordination modes of the carboxylate ion 47
Figure 3-6: DRIFTS spectra of methylene associated peaks for (a) pure DBSC-10, and (b) monolayer 48
Figure 3-7: XPS spectra of narrow scans for the elements of interest on γ-Fe_2O_3 surfaces with (a) and without (b) self-assembled DBSC-10 51
Figure 3-8: Structure of DBSC-10 with labeled atoms 53
Figure 3-9: DRIFTS spectra of monolayer at (a) neutral pH and (b) pH 3, with acid related peaks presented in insert (c) 54
Figure 4-1: Schematic of a DBSC-10 monolayer onto a maghemite (γ-Fe_2O_3) particle 63
Figure 4-2: Titration curves from the neutralization of (a) 4.4 mg and (b) 8 mg of DBSC-10 67

Figure 4-3: Titration curves of 50 mg of (a) bare maghemite and (b) DBSC-10 coated particles 68
Figure 4-4: Titration of 50 mg of DBSC-10 coated particles by KOH 69
Figure 4-5: Titration of DBSC-10 coated particles (a) 25 mg, (b) 50 mg, (c) 75 mg, (d) 100 mg, and 75 mg of bare maghemite 70
Figure 4-6: Inflexion points of DBSC-10 coated particles (a) 25 mg, (b) 50 mg, (c) 75 mg, (d) 100 mg 71
Figure 4-7: DRIFTS of DBSC-10 coated particles (a) after and (b) before titration with KOH 73
Figure 5-1-1: DRIFTS spectra of the DBSC-10 monolayer before (a) and after (b) reaction with DETA 83
Figure 5-1-2: DRIFTS spectra of methylene associated peaks for the DBSC-10 monolayer before (a) and after (b) reaction with DETA 84
Figure 5-1-3: DRIFTS spectra of the DBSC-10 monolayer before (a) and after (b) reaction with DETA 85
Figure 5-1-4: XPS spectrum of narrow scans for the elements of interest on carboxy-terminated maghemite surfaces before (a) and after (b) reaction with DETA 87
Figure 5-1-5: Structures of DBSC-10 and DETA-reacted DBSC-10 with labeled atoms 88
Figure 5-1-6: Titration of DETA reacted particles (—) 25 mg, (—) 50 mg, and (···) 75 mg 91
Figure 5-1-7: Inflexion points of DETA reacted particles (—) 25 mg, (—) 50 mg, and (···) 75 mg 92
Figure 5-1-8: Acid-base properties of amino acids 93
Figure 5-2-1: TEM image of a bare maghemite sample 103
Figure 5-2-2: TEM image of a carboxy-functionalized maghemite sample 106
Figure 5-2-3: TEM image of DETA-modified maghemite, i.e. magnetic carriers 107

Figure 5-2-4: TEM images, at higher magnifications, of samples (a) bare, (b) carboxy-functionalized, and (c) DETA-modified maghemite, with special features (D) dodecahedron shape, (E) hexagonal perimeter, and (F) halo 108
Figure 6-1: Calibration curve of the copper selective electrode 116
Figure 6-2: Titration of magnetic carriers and 200 mg of bare maghemite particles 118
Figure 6-3: Titration of carboxy-terminated particles and 100 mg bare maghemite 120
Figure 6-4: XPS spectra of narrow scans for the elements of interest on magnetic carriers after (a) and before (b) copper loading 122
Figure 6-5: XPS spectrum of narrow scans for copper and nitrogen on magnetic carriers after (a) and before (b) copper loading 123

List of Tables

Table 3-1: Assignment of IR peaks obtained from DRIFTS spectra of the surfactant pure and self-assembled 49

Table 3-2: Binding energies (eV) of X-ray photoelectrons at band maxima 52

Table 3-3: Binding energies (eV) of X-ray photoelectrons and related area percentages 53

Table 4-1: Reproducibility of the volume difference between 25 mg increments of coated particles 72

Table 5-1-1: Assignment of IR peaks obtained from DRIFTS spectra of the DBSC-10 monolayer before and after reaction with DETA 86

Table 5-1-2: Binding energies (eV) of X-ray photoelectrons and related area percentages 88

Table 5-1-3: Inflexion points results of DETA-reacted particles 94

Table 5-1-4: Titration results of replicates 94

Table 5-1-5: Reproducibility of the titration results between 25 mg increments of DETA-reacted particles 94

Table 6-1: Reproducibility of the volume differences 118

Table 6-2: Binding energies (eV) of photoelectrons 123

Chapter 1

General Introduction

The recovery of base metals, such as zinc, copper or nickel, and toxic heavy metals, such as cadmium and selenium, from processing effluents, is receiving growing interest as part of developing wastewater management strategies. Such efforts are not only directed towards creating a less toxic residue for disposal, but also to preserving resources and providing some revenue to help offset the cost of treatment. The use of ion flotation, neutralization, and flocculation to recover metals from industrial effluents has been widely described.[1,2] A novel method, magnetic carrier technology (MCT), offers the possibility of replacing the traditional separation techniques by more rapid and practical means of separating particles from treated water and wastewater, especially those containing suspended solids.[3]

In magnetic carrier technology (Figure 1-1), magnetic carriers are first added to a heterogeneous suspension to capture the desired target, forming a magnetic carrier-target complex. The complex is then removed from the suspension by magnetic separation, producing a cleaned effluent. Subsequent regeneration of the magnetic carriers is carried out by stripping the target with an appropriate reagent. The target can vary in nature from metal ions in hydrometallurgy[4] to biological cells, bacteria, and viruses in biological and medical applications.[5,6]

For practical purposes, the magnetic carriers should be of small particle size to provide optimal reaction kinetics between the functional groups on the magnetic carriers and the targets. They should also be spherical in shape to eliminate nonspecific binding, and of uniform surface area to provide efficient use and optimal accessibility of the

functional groups on their surface. Finally, the magnetic carriers should be mechanically strong and resistant to solution leaching, which otherwise translates into back contamination of the product effluent by leached iron and even sometimes into toxic iron exposures of living targets.

To achieve these criteria in the production of magnetic carriers, the molecular self-assembly technique is proposed. This method employs amphiphilic molecules, exhibiting both hydrophilic and lipophilic solubility tendencies to form oriented monolayers on the surface of nano-sized magnetic particles. The molecular orientation is produced by a *spontaneous* chemical synthesis at the interface as the system approaches equilibrium.[7] Molecular self-assembly by bolaamphiphiles, which are molecules composed of a head group on each end of a hydrophobic skeleton is also possible.[8] Bolaamphiphiles offer the unique opportunity to bind the monolayers chemically to the maghemite surface via one head group and to modify the magnetic particle surface properties *ad lib* by chemical reactions with the other head group.

Once the extent to which magnetic particles can be coated with close-packed, defect-free monolayers with well-defined functionality is established, it is possible to modify the reactivity of a magnetic carrier in the desired way. In particular, ligands may bind to a magnetic carrier to form a ligand-terminated carrier. Since a ligand containing a donor group may combine with a metal ion to form a chelate, these carriers could potentially be applied to the selective recovery of metals in wastewater treatment.[9]

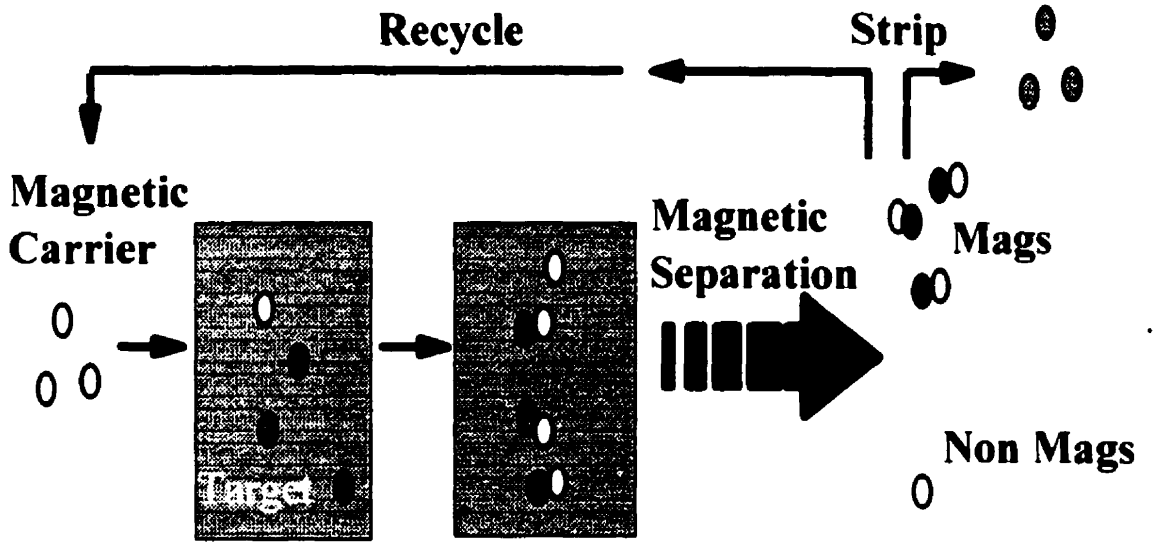

Figure 1-1: Magnetic Carrier Technology.

Thesis Outline

In this thesis, the step-by-step preparation and characterization of magnetic carriers, are presented. Application of these prepared magnetic carriers in metal ion recovery is also demonstrated. Section 1 of Chapter 2 summarizes the different preparation methods of magnetic carriers. The second section of Chapter 2 outlines the pertinent characterization techniques used in this research.

Chapter 3 discusses the preparation of a self-assembled monolayer of a dibenzoic acid diamide bolaamphiphile on nanosized maghemite particles. Characterization of the monolayer is performed by diffuse reflectance infrared Fourier transform spectroscopy (DRIFTS) and X-ray photoelectron spectroscopy (XPS). Chapter 4 presents a novel technique, potentiometric titration, used in the assessment of the DBSC-10 monolayer density.

The first section of Chapter 5 describes the preparation of a reactive DETA-modified monolayer, based on the reaction with a typical carbodiimide, of carboxylic and amine groups. Characterization is performed through the use of DRIFTS and XPS spectroscopy techniques, and potentiometric titration. Section 2 of Chapter 5 concentrates on the imaging of the prepared magnetic carriers, using an advanced Pt/C replica technique of transmission electron microscopy (TEM).

Chapter 6 demonstrates the application of the prepared magnetic carriers in the removal of Cu^{2+} ions from dilute effluents. A technique, complexometric titration, is introduced to assess the efficiency of recovery.

Chapter 7 contains final conclusions and the claims to original research of this thesis.

References

[1] Rao, S.R., Xu, Z., Finch, J.A., in "Waste Processing and Recycling in Mineral and Metallurgical Industries II", Rao, S.R., Amaratunga L.M., Boateng, D.A.A., Chalkley, M.E., eds, Proceedings of the International Symposium, 3-11, Canada (1992).

[2] Rousseau, R.W., "Handbook of Separation Process Technology", John Wiley & Sons, USA (1987).

[3] Bolto, B.A., Waste Management, **10**, 11-21 (1990).

[4] Dixon, D.R., Hawthorne, D.B., J. Appl. Chem. Biotechnol., **28**, 10-16 (1978).

[5] Ølsvik, O., Popovic, T., Skjerve, E., Cudjoe, K.S., Hornes, E., Ugelstad, J., Uhlen, M., Clinical Microbiology Reviews, 7 (1), 43-54 (1994).

[6] Ugelstad, J., Berge, A., Ellingsen, T., Aune, O., Kilaas, L., Nilsen, T.N., Schmid, R., Stenstad, P., Funderud, S., Kvalheim, G., Nustad, K., Lea, T., Vartdal, F., Danielsen, H., Makromol. Chem., Macromol. Symp. , **17**, 177-211 (1988).

[7] Ulman, A., "Ultrathin Organic Films", Academic Press, USA (1991).

[8] Böhme, P., Hicke H-G., Boettcher, C., Fuhrhop, J-H., J. Am. Chem. Soc., **117**, 5824-5828 (1995).

[9] Rao, S.R., Xu, Z., Finch, J.A., in "Waste Processing and Recycling in Mineral and Metallurgical Industries II", Rao, S.R., Amaratunga L.M., Richards,G.G., Kondos,P.D. eds, Proceedings of the International Symposium, 69-77, Canada (1995).

Chapter 2

Section 1:

Review of Magnetic Carriers

2.1.1 Introduction

Various magnetic carriers have been developed using iron oxide particles. The attachment of the targets to the magnetic carriers is through specific binding mechanisms, such as electrostatic adsorption or chemical affinity. This section introduces the general principles for the design of magnetic carriers, used in magnetic carrier technology applications from water treatment to drug delivery systems. Some limitations of these carriers are also discussed.

2.1.2 Bare Magnetite

The use of magnetite as magnetic carriers is reported by De Latour and Terashima *et al.*[1,2], who studied the precipitation of metal ions and their co-precipitates after addition of magnetite seed. Their work show that magnetic agglomerates can be formed by coagulating precipitates with magnetic seeds through adjustment of the chemistry.

2.1.3 Polymer Assisted Magnetite

Polymers used as adjuncts to magnetic iron oxide, employed as the primary coagulant, have been described.[3] Negatively surface charged contaminants heterocoagulate with positively charged iron oxides. Since a loaded oxide has a reduced positive charge, a cationic polyelectrolyte is added to scavenge the remaining impurities and attach them by bridging to the oxide.

2.1.4 Polymer Adsorption and Polymerization

Magnetic particles incorporating ferromagnetic particles within synthetic polymer beads may be prepared in three main forms.[4] The first contains magnetic materials such as maghemite or magnetite evenly distributed throughout a polymeric network. They are prepared by adding a magnetic filler with suitable dispersants to the conventional polymerisation process. The spherical particles are obtained by suspension polymerisation after bulk polymerisation. The second type is prepared by placing small particles of active polymer with the magnetic material inside an inert but permeable crosslinked polymer. Whisker type particles constitute a third type. They have a shell structure and are prepared by grafting active polymer chains onto a magnetic polymeric core that is formed by including magnetic particles within an inert polymer matrix.

Another type of microspheres consisting of magnetic particles within an organic polymer matrix have been described by Ugelstad *et al.*[5], who have prepared hydrophilic micrometer-sized particles consisting of polymer latex impregnated with approximately 20% w/w single domain maghemite. These composite particles were synthesised by the *in situ* oxidation of iron salts within the polymer latex and are commercially available as magnetic carriers.

More recently Senna and Lee[6] and Furusawa *at al.*[7], have prepared particles consisting of a micrometer-sized polystyrene latex core coated with a shell of ultrafine ($d<20$ nm) magnetic particles, while another study reports on the successful synthesis of colloidal dispersions of polypyrrole-magnetite silica nanocomposites by polymerizing pyrrole (C_4H_5N) in ultrafine silica-coated magnetite suspensions.[8]

In general, magnetic carriers prepared either by polymer adsorption or polymerization, have the disadvantage of offering less magnetism than other types of carriers, because of the lower percentage of iron oxide they contain.

2.1.5 Silanation on Metal Oxides and Silica Coated Metal Oxides

Another type of commercially available magnetic carrier originates from the work of Whitehead *et al.*[9] Their preparation is based on the formation of silane polymers by condensation of 3-aminopropyltrimethoxysilane on the surface of magnetite particles. The silane polymers associate with the metal oxide either by forming a covalent bond with surface hydroxy groups through dehydration, or by adsorption of silane polymers onto the metal oxides. The resulting magnetic particles can be further functionalized to amine or carboxylic acid terminated carriers. The same method has been applied to the silanation of maghemite particles by Liu *et al.*[10], who prepared a much more stable magnetic carrier by silane condensation on silica coated maghemite particles.

2.1.6 Magnetic Carriers Derived from Drug Carriers

Liposomes have been used as carriers to promote controlled release of drugs in the body. Liposomes consist of nearly spherical unilamellar or multilamellar lipid bilayers alternating with thin aqueous resevoirs.[11] A similar, but synthetic unilamellar magnetic liposome was engineered by Hwang *et al.*[12] on the surface of a magnetic particles by sequential layering of amphiphilic molecules. The inner layer amphiphile has a functional group with an affinity for the metal oxide surface, and the outer layer of amphiphile can be

built on top of the inner one through hydrophobic association between hydrocarbon chains. Payne *et al.*[13] in a review article on the limitations of liposomes, concluded that such carriers were chemically and physically unstable.

Chapter 2

Section 2:

Characterization Techniques

2.2.1 Introduction

The functionalized and modified magnetic particles are characterized by X-ray photoelectron spectroscopy (XPS), to obtain both a qualitative and quantitative confirmation of the presence of the monolayers, ligand, and metal. The use of diffuse reflectance Fourier transform infrared spectroscopy (DRIFTS) allows for a more detailed investigation of the different coordinations of the carboxylic acid groups and of the general molecular orientation of the monolayers on the surface of the maghemite particles. The density of surface functional groups and their reactivity with the ligand is characterized by potentiometric titration, while the loading capacity of the prepared magnetic carriers is measured by complexometric titration. Imaging of the functionalized and modified magnetic particles is performed by transmission electron spectroscopy (TEM).

2.2.2 Infrared Spectroscopy

Infrared (IR) radiation refers broadly to the part of the electromagnetic spectrum between the visible and microwave regions. Infrared radiation in the range from about 10,000-100 cm^{-1} is absorbed and converted by a molecule into energy of molecular vibration. One form of a vibration between two atoms which form a bond (say in the molecule CO) is when the bond length alternately becomes longer and shorter during the course of the vibration (i.e., a stretching vibration). In this case, the frequency (ω) of the vibration may be related to the (reduced) masses (μ) of the atoms and the strength of the bond (defined

by the force constant, k) by the following relation:

$$\omega = \frac{1}{2\pi}\sqrt{\frac{k}{\mu}} \qquad [2\text{-}2\text{-}1]$$

It is evident that as the strength of the bond increases, the frequency of the vibration increases; and, as the masses of the atoms increase the frequency will decrease. It is also clear that the frequency of the vibration is very sensitive to the molecular properties k and μ.[14,15]

Bending is another type of molecular vibration, which may consist of a change in bond angle between bonds with a common atom or a movement of a group of atoms with respect to the remainder of the molecule. For example, twisting, rocking, and torsional vibrations involve a change in bond angles (with reference to a set of coordinates arbitrarily established within the molecule). Only those vibrations that result in a rythmical change in the dipole moment of the molecule are observed in the IR. The alternating electric field, produced by the changing charge distribution accompanying a vibration, couples the molecule vibration with the oscillating electric field of the electromagnetic radiation.

Band positions in IR spectra are given as wavenumbers (ν) whose unit is the reciprocal centimeter (cm^{-1}). Band intensities can be expressed either as transmittance

(T) or absorbance (A). Transmittance is the ratio of the radiant power transmitted by a sample (I) to the radiant power incident on the sample (I_o):[16]

$$\% \text{ Transmittance} = (I / I_o) \cdot 100 \qquad [2\text{-}2\text{-}2]$$

Absorbance is the logarithm, to the base 10, of the reciprocal of the transmittance:

$$\text{Absorbance} = \text{Log}\,(1/T). \qquad [2\text{-}2\text{-}3]$$

An IR spectrum usually consists of a plot of the amount of energy absorbed by the compound under investigation against wavenumber. Usually this means that all the frequencies of the IR region are scanned individually and the amount absorbed by the sample recorded. The instrument that is used in these experiments is a FT-IR instrument, which has the advantage of being able to analyze all the frequencies in the IR region simultaneously. This means that spectra can be collected in a much shorter time.

The main component of the FT-IR is an interferometer, which consists of two mirrors, one having a fixed position and the other being free to move.[17] The two mirrors are usually at right angles to each other. At 45° to these two mirrors is a beamsplitter, which allows 50 % of the light to pass through and 50 % to be reflected. The 50 % that is reflected onto the moving mirror is also reflected back to the beamsplitter. If the distance between the moving mirror and the fixed mirror is different, the phasing of the IR radiation, once it recombines at the beamsplitter, will be different. This means that either constructive or destructive interference will occur. The output of the interferometer is a measurement of the intensity of IR radiation coming from the beamsplitter (once the two

beams have been recombined) as a function of the moving mirror distance (or retardation). The Fourier-Transform takes this data and converts it to an intensity versus frequency plot, the IR spectrum.

When scanning by this method, a background spectrum has to be obtained, for which usually a blank cell is used. The spectrum of the sample is then obtained and ratioed against the background spectrum. This means that two separate spectra have to be obtained to get one sample spectra. However, if the samples are under similar conditions, the same background can be used.

2.2.2.1 Diffuse Reflectance Infrared Fourier-Transform Spectroscopy (DRIFTS)

DRIFT spectroscopy allows for a rapid analysis of powdered samples, paper, cloth, or simply chunks of intractable materials.[18] Dilution of the sample in a non-absorbing matrix is required by this technique, to reduce spectral distortions caused by the mixing of reflectance components of the measured radiation. To overcome the low signal-to-noise ratio in highly absorbing samples, increased data collection times or the use of a sensitive detector, such as the mercury cadmium telluride (MCT), are necessary.

Three types of reflectance occur when a beam of infrared radiation is focused onto the surface of a sample consisting of discrete particles, as seen in Figure 2-2-1.[16] True specular reflectance occurs when a ray simply reflects from a crystal surface and reflects away from the particle at an angle equivalent to the incident angle. Diffuse specular reflectance is characteristic of a ray which has undergone multiple "mirror like" reflections within the sample, and which may ultimately emerge at any angle relative to the incident

radiation. Both these rays are not absorbed by the sample. The ray labeled as absorption/reflection has, as the name indicates, been reflected within the sample and has also penetrated through the particles. Only this last ray contains information about the absorptivity (α) of the sample. This absorption/reflection radiation eventually will be diffusely scattered out of the sample where it can be collected and focused onto an infrared detector. A typical optical path for a DRIFTS accessory is shown in Figure 2-2-2. Two flat mirrors are used to pass the focused beam to a spherical mirror. This mirror re-focuses the infrared radiation onto the surface of the sample, held in a cup. The sample is positioned at the focal point, using a screw adjuster. The scattered radiation is collected by a second spherical mirror and passed onto the detector optics by two other flat mirrors.

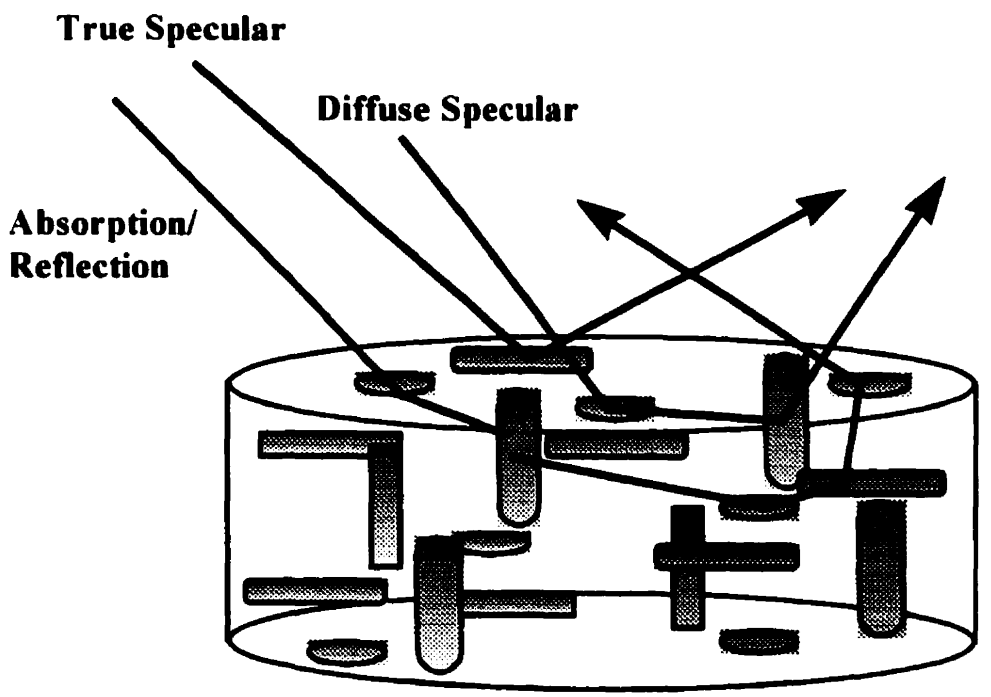

Figure 2-2-1: Three types of reflections from a powdered surface.

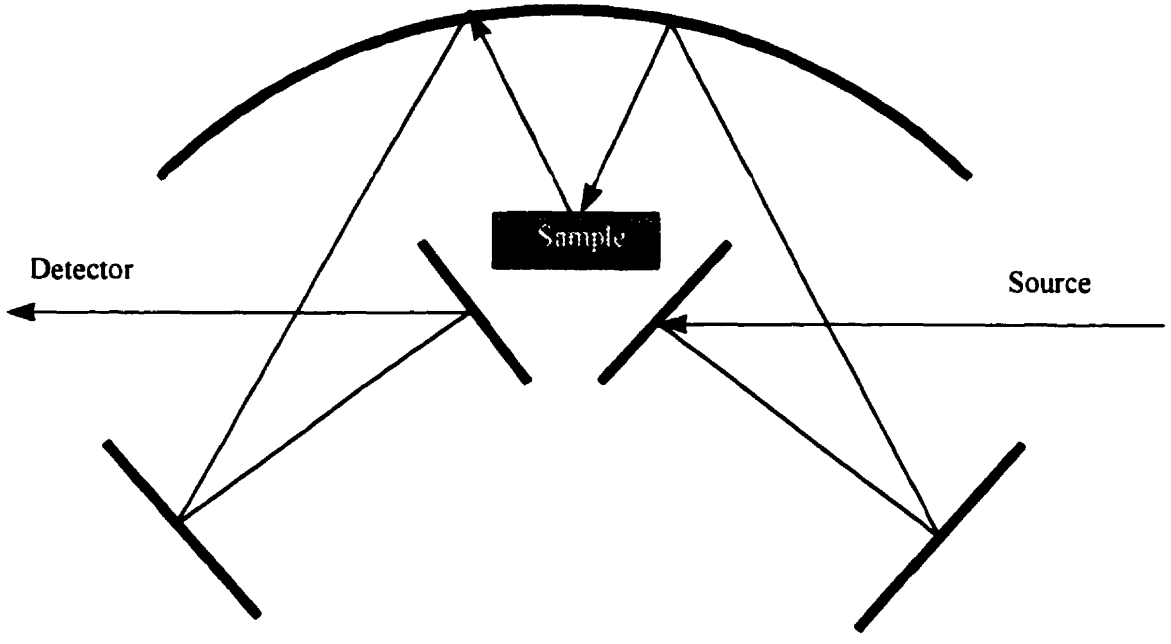

Figure 2-2-2: Optical diagram of a DRIFTS accessory.

A general theory for diffuse reflectance at scattering layers within powdered samples has been developed by Kubelka and Munk.[19] This theory relates sample concentration and scattered radiation intensity. For an infinitely thick layer, the Kubelka-Munk equation is summarized as:

$$f(R_\infty) = \frac{(1-R_\infty)^2}{2R_\infty} = \frac{k}{s} \qquad [2\text{-}2\text{-}4]$$

where R_∞ is the absolute reflectance of the layer, s is a scattering coefficient, and k is the molar absorption coefficient.

In practice, R_∞ is replaced by R_∞':

$$R_\infty' = \frac{R_\infty'(sample)}{R_\infty'(standard)} \qquad [2\text{-}2\text{-}5]$$

where R_∞' (sample) is the single beam reflectance spectrum of the sample and R_∞' (standard) is the single beam reflectance spectrum of a nonabsorbing standard. Furthermore, it has been shown[19] that for dilute samples in low absorbing matrices:

$$k = 2.303\varepsilon c \qquad [2\text{-}2\text{-}6]$$

where ε is the molar absorptivity and c is the molar concentration. Therefore:

$$f(R_\infty) = \frac{(1-R_\infty)^2}{2R_\infty} = \frac{c}{k'} \qquad [2\text{-}2\text{-}7]$$

where $k' = s/2.303\varepsilon$.

To ensure a linear response, there are two factors to be considered. First, the scattering coefficient is dependent on a number of physical variables including particle shape, size and packing density, and so care must be taken to maintain a consistent sampling protocol. Secondly, it must be remembered that the KM equation is linear only over a limited range of analyte concentrations. When c becomes large, the scattering coefficient (s) is no longer solely dependent on the non-absorbing matrix. This can result in anomalous dispersion effects. Despite its limitations, the KM model has been used for DRIFT spectra throughout this thesis.

2.2.3 X-ray Photoelectron Spectroscopy (XPS)

The XPS experiment involves the irradiation of a specimen in ultra high vacuum, usually with a non-monochromatic X-ray source (e.g., Al/Mg) of low energy. Liberated photoelectrons are detected as a function of energy by an electrostatic spherical sector analyser. The XPS spectrum, then consists of a plot of electron counts or intensity versus kinetic or binding energy. Sharp lines of intensity reflect the origin of photoelectrons in orbits around the atomic nucleus. Each element, having a finger print spectrum, can be clearly identified and its chemical state ascertained from its photoelectron binding energy.

An outline of a typical spectrometer is shown in Figure 2-2-3. The main component parts are the rotating anode X-ray source, quartz crystal monochromator, high transmission/imaging lens, hemispherical analyser and multichannel detector.[20]

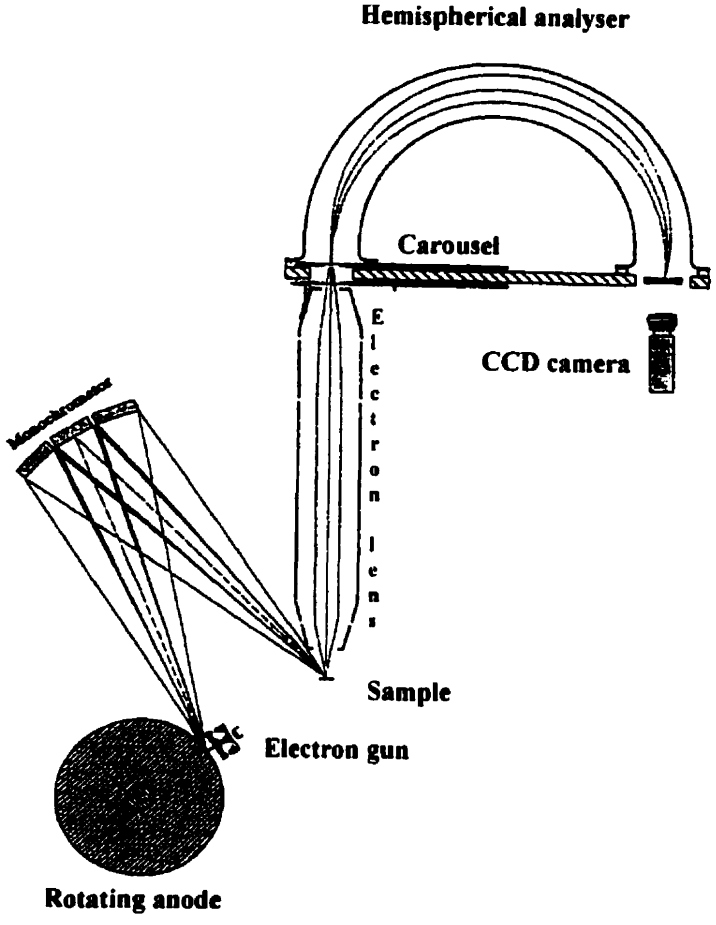

Figure 2-2-3: Schematic of a typical XPS spectrometer. (Modified from Beamson, G., Briggs, D., "High Resolution XPS of Organic Polymers", John Wiley & Sons, England (1992)).

The principles of XPS are presented in Figure 2-2-4. Soft x-rays usually derived from Al and Mg targets, due to their narrow characteristic Kα lines, excite photoelectrons from a specimen according to the photoelectron equation:[21]

$$E_K = h\nu - E_B - \Phi \qquad [2\text{-}2\text{-}8]$$

where E_K is the measured electron kinetic energy, $h\nu$ the energy of the exciting radiation, E_B the binding energy of the electron in the solid, and Φ the work function of the analyser or spectrometer.

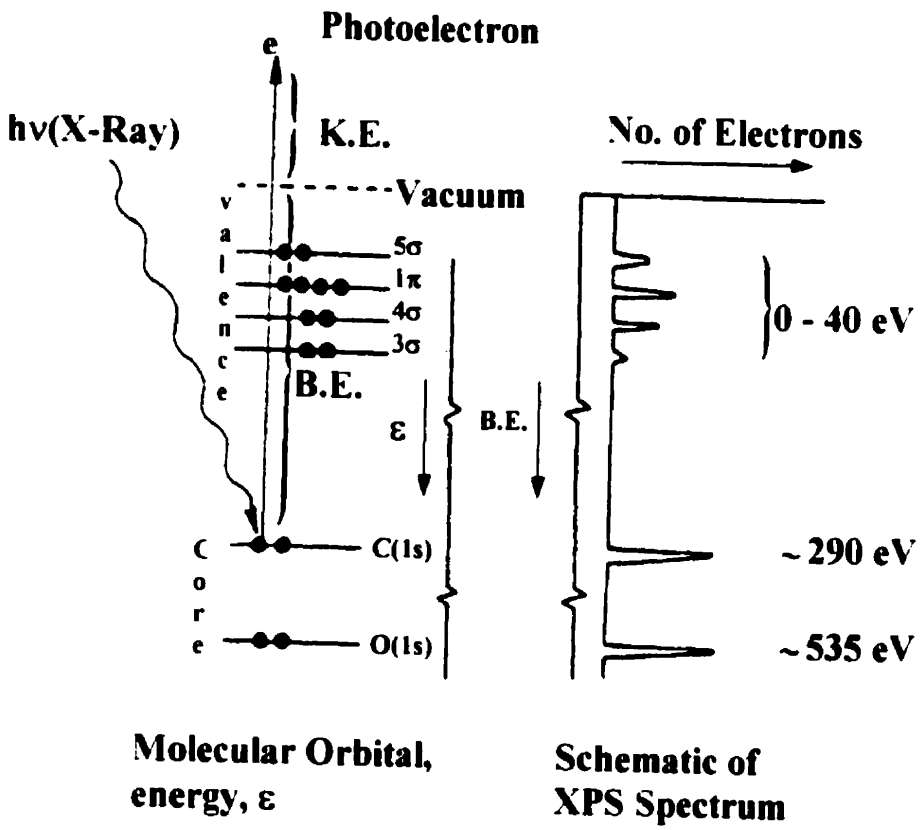

Figure 2-2-4: Principles of XPS.

Thus each characteristic X-ray will give rise to a series of photoelectron peaks reflecting the discrete binding energies of the electrons present in the solid. Unpaired valence electrons cause spin multiplet splitting due to the coupling of remaining core electrons with these unpaired valence electrons. This produces more photoemission peaks, some of which may not be resolved.

Curve fitting is performed by an XPS peak fitting software, which describes each of the components of a complex envelope as a Gaussian-Lorentzian sum function, i.e.

$$\frac{F(E)}{A} = m\exp[-4\ln(2x^2)] + \frac{(1-m)}{(1+4x^2)} \qquad [2\text{-}2\text{-}9]$$

and

$$x = \frac{(E-E_0)^2}{(FWHM)^2} \qquad [2\text{-}2\text{-}10]$$

where $F(E)$ is the intensity at energy E, A is the peak area (used as a better way of correlating the concentration ratios than peak height), E_0 is the peak center, $FWHM$ is the full width at half maximum, and m is the mixing ratio (1 = pure Gaussian, 0 = pure Lorentzian).[21] These five parameters and the parameters for the background describe each component of the envelope. These are input as initial values to the curve-fitting program. On each iteration a direction set method is used to adjust every parameter and minimize the chi-squared value. Iterations continue until chi-squared converges. It is possible to fix the value of a parameter during the curve-fitting procedure or to link parameters.

There are three methods for performing quantification in XPS, using either calibration standards, theoretical cross sections, or empirical sensitivity factors.[21,22] The

actual process of systematic measurements that constitutes the use of calibration standards can be quite tedious, however accuracies of the order of 1% can sometimes be achieved. The second method uses theoretical cross sections which describe the probability of the core level being ionized by photons. Cross sections are a function of the core level, the energy of incident photons, and of the detection angle with respect to incident photons. Theoretical cross sections can be calculated from theory (Scofield)[21,22] or measured experimentally.

The empirical sensitivity factors (SFs), mainly due to Wagner,[21,22] are more commonly used. The process of quantification involves first the identification of all elements present on the surface. Then it is necessary to measure the peak area or peak height intensity of the most intense core-level peak of each of the elements from the spectrum. Finally, each peak is divided by its empirical sensitivity factor modified by the instrument transmission function. Normalised peak area intensities (NPA, in cps) are then calculated from the raw peak intensities (RPA) by:

$$NPA = RPA / (TF \cdot SFW) \qquad [2\text{-}2\text{-}11]$$

where *TF* is the theoretical instrument transmission function based on the kinetic energy of the core-level, and *SFW* is the Wagner empirical sensitivity factor.

The concentration in atomic % is then calculated as follows:

$$C_x = \frac{NPA_x}{\left(NPA_x + NPA_y + NPA_z\right)} \cdot 100 \qquad [2\text{-}2\text{-}12]$$

where C_x is the concentration of element x in % in a matrix of elements x, y, and z. A possible source of error arising from this method involves the method of background subtraction used for calculation of peak area intensity. There is also the uncertainty in the sensitivity factor values and the instrument transmission functions. Non-homogeneous surface distribution of the particular element or elements within the analysis area may also be another factor of error.

2.2.4 Potentiometry

Potentiometric methods embrace two major types of analyses. One involves the direct measurements of an electrolyte potential from which the activity (or concentration) of an active ion may be derived. The other type involves measuring the changes in the electromotive force (emf) brought about by the addition of titrant to the sample.

In a potentiometric type of sensor, a membrane or sensing surface acts as a half-cell, generating a potential proportional to the logarithm of the analyte activity (concentration). This potential is measured relative to an inert reference electrode, also in contact with the sample. For a complete electrochemical cell, the emf is given by:[23]

$$E_{cell} = E_{ind} - E_{ref} + E_j \qquad [2\text{-}2\text{-}13]$$

where E_{ind}, E_{ref}, and E_j are the potentials of the indicator electrode, the reference electrode, and the liquid-junction potential, respectively. In a properly designed system, E_{ref} is a constant and E_j is either constant or negligible. If the indicator electrode senses the presence of the analyte in the sample solution, and the reference electrode is independent of the sample solution composition, and the liquid junction is an interface between dissimilar solutions, the indicator electrode can supply information about ion activities.

A combined glass electrode can be used as an indicating electrode. The electrochemical cell that incorporates the electrode in this work is:[11,24]

Ag/AgCl, KCl (sat) | glass membrane | unknown solution | KCl (sat), Ag/Ag/Cl

It obeys an electrode relationship of the form:

$$E_{cell} = E_{constant} + 0.0592\,pH \qquad [2\text{-}2\text{-}14]$$

or

$$pH = \frac{E_{cell} - E_{constant}}{0.0592} \qquad [2\text{-}2\text{-}15]$$

where $E_{constant}$ is the sum of all the boundary potentials in the cell plus the constant potential arising from the filling solution. The pH of a reference buffer, measured with the combined electrode and cell just described, is:

$$pH_s = \frac{E_{cell} - E_{constant}}{0.0592} \qquad [2\text{-}2\text{-}16]$$

in which pH_s is the pH and E_s is the emf of the reference buffer solution. Combining equations 2-2-15 and 2-2-16 to eliminate the undetermined $E_{constant}$ results in the expression:

$$pH = pH_s + \frac{E_{cell} - E_s}{0.0592} \qquad [2\text{-}2\text{-}17]$$

Another type of indicator electrode used in this work is the copper ion-selective electrode. The electrochemical cell formed by this electrode and a calomel reference electrode can be represented as:[11]

$Hg/Hg_2Cl_2 | Cl^-$, KCl (sat) $||$ polycrystalline sensing element $|$ external unknown solution

which obeys the relation:[25]

$$E_{cell} = E_{ref} + \frac{0.0592}{n}\log(a_{Cu^{2+}}) \qquad [2\text{-}2\text{-}18]$$

where $a_{Cu^{2+}}$ is the cupric ion activity and n is the valence which is equal to 2 in this case. The cupric ion activity is related to concentration by the following equation:

$$a_{Cu^{2+}} = f_{Cu^{2+}} \cdot c_{Cu^{2+}} \qquad [2\text{-}2\text{-}19]$$

where $f_{Cu^{2+}}$ denotes the activity coefficient. In very dilute solution the acitivity coefficient is equal to 1, so that:

$$c_{Cu^{2+}} = a_{Cu^{2+}} \qquad [2\text{-}2\text{-}20]$$

Both types of electrodes can be used with a millivoltmeter to measure cell emf for potentiometric acid-base or ionic titrations. The change in potential of the electrode is measured as a volume of titrant of a known concentration is added. The titration curves are obtained by plotting E_{cell}, usually in millivolts, against the volume of titrant added. When the slope of the emf versus the volume of titrant added is plotted, a differential curve is obtained, the maximum point of which represents the endpoint of the titration..

2.2.5 Transmission Electron Microscopy (TEM)

In a conventional transmission electron microscope (TEM), Figure 2-2-5, a thin specimen is irradiated with an electron beam of uniform current density. The acceleration voltage of routine instruments is 80-120 kV.[26] Electrons are emitted in the electron gun by thermionic, Schottky or field emission. The latter are used when high gun-brightness and coherence are needed. A two- or three-stage condenser-lens system permits variation of the illumination aperture and of the area of the specimen illuminated. The electron-intensity distribution behind the specimen is imaged with a three- or four-stage lens system onto a fluorescent screen. The image can be recorded by direct exposure of a photographic emulsion or an image plate inside the vacuum or digitally via a fluorescent screen coupled by a fibre-optic plate to a CCD camera.

Electrons interact strongly with atoms by elastic and inelastic scattering. The specimen must therefore be very thin, typically of the order of 5-100 nm for 100 keV electrons, depending on the density and elemental composition of the object and the resolution desired. Special preparation techniques are needed for this, such as

electropolishing and ion-beam etching (as used in materials science) and ultramicrotomy of stained and embedded tissues or cryo-fixation (as used in the biosciences).

TEM provides a wealth of information about the physical and chemical nature of surfaces. It has had important applications to phase studies in metallurgy and ceramics, the investigation of grain boundaries in alloys, the determination of diffusion rates of impurities in semiconductors, the analysis of occluded species in crystals, and the studies of the active sites of heterogeneous catalysts.[26] In all these applications, both qualitative and quantitative information about surfaces are obtained.

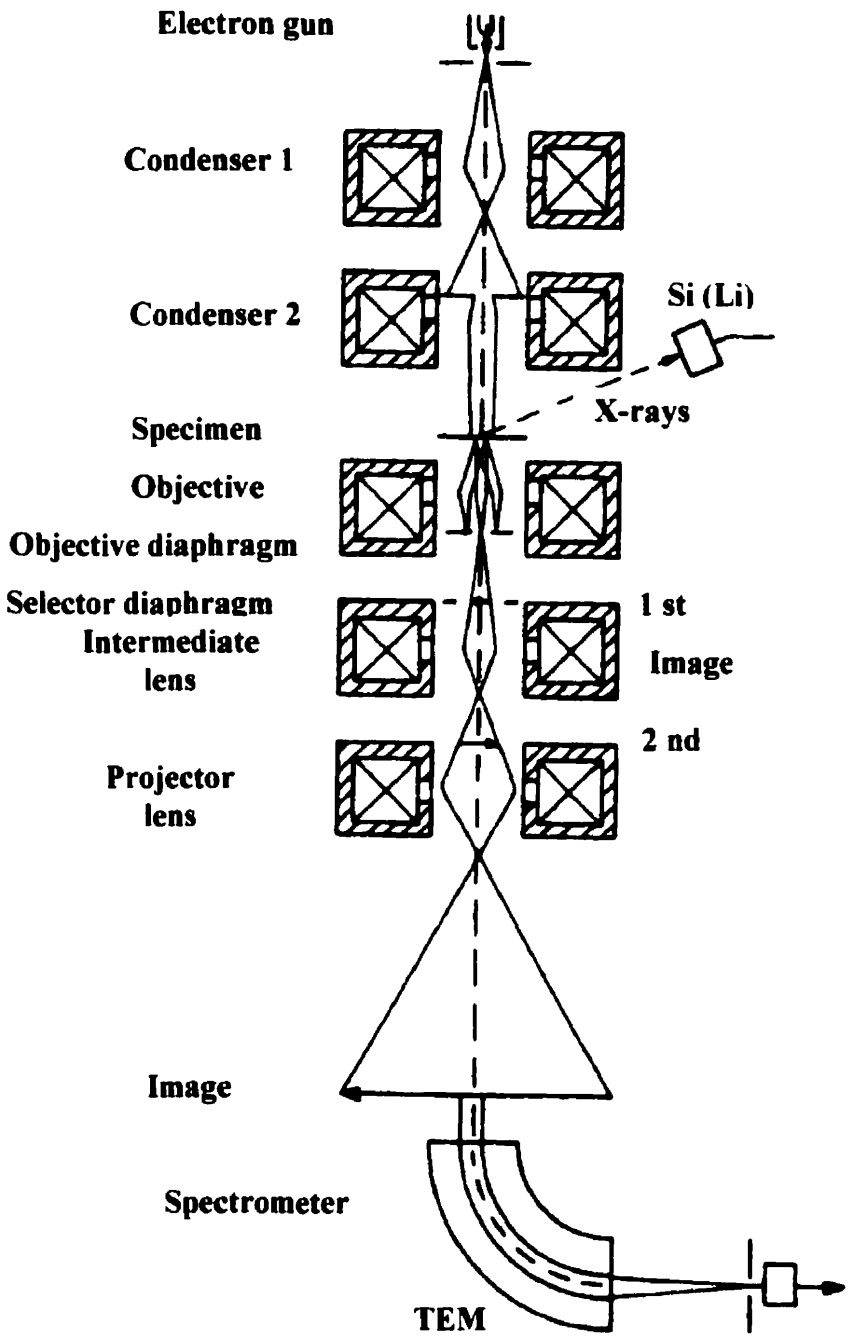

Figure 2-2-5: Schematic ray path for a TEM equipped for additional x-ray and electron energy-loss spectroscopy. (Modified from Reimer, L., "Transmission Electron Microscopy", 4th edition, Springer Series in Optical Sciences, USA (1997)).

References

[1] de Latour, C., Journal of American Water Works Association, **68**, 443-446 (1976).

[2] Terashima Y., Ozaki, H., Sekine, M., Wat. Res., 5, 537-545 (1986).

[3] Anderson, N.J., Bolto, B.A., Elderidge, R.J., Jackson, M.B., Reactive Polymers, **19**, 87-95 (1993).

[4] Bolto, B.A., J. Macromol. Sci. Chem., **A14** (1), 107-120 (1980).

[5] Ugelstad, J., Ellingsen, T., Berge, A., Helgee, B., Patent **WO 83/03920** (1993).

[6] Senna, M., Lee, J., Colloid Polym. Sci. , **273**, 76 (1975).

[7] Furusawa, K., Nagashima, K., Anzai, C., Colloid PolymSci. , **272**, 1104 (1994).

[8] Butterworth, M.D., Bell, S.A., Armes, S.P., Simpson,W., J. Colloid Interface Sci. , **183**, 91-99 (1996).

[9] Whitehead, R.A. et al. U.S. Patent 4,695,393 (1987).

[10] Liu, Q., Xu, Z., Langmuir, **11** (12), 1995.

[11] Martin, A., in "Physical Pharmacy", 4th edition, Lea & Febiger, USA (1993).

[12] Hwang, J.Y., U.S. Patent 4,906,382 (1990).

[13] Payne, N.I., Timmins, P., Ambrose, C.V., Ward, M.D., Ridgway, J. Pharm. Sci. , **75**, 325 (1986) and Payne, N.I., Browning I., Haynes, C.A., J. Pharm. Sci. , 75, 330 (1986).

[14] Skoog, D.A., West, D.M., in "Principles of Instrumental Analysis", 2nd edition, Saunders College, USA (1980).

[15] Loudon, G.M., in "Organic Chemistry", 2nd edition, Benjamin/Cummings, USA (1988).

[16] Fuller, M., Nicolet FT-IR Technical Note TN-9033.

[17] Silverstein, R.M., in "Spectrometric Identification of Organic Compounds", 5th edition, Wiley & Sons, USA (1991).

[18] Fuller, M.P., Griffiths, P.R., American Laboratory, 69-80, (October 1978).

[19] Fuller, M.P., Griffiths, P.R., Analytical Chemistry, **50** (13), 1906 (1978).

[20] Beamson, G., Briggs, D., in "High Resolution XPS of Organic Polymers", John Wiley & Sons, England (1992).

[21] Adam, E., XPS Handbook from VG Scientific ADP-OPINST17, UK (1991).

[22] Briggs, D., Seah, M.P., in "Practical Surface Analysis", 2nd edition., vol(1), John Wiley & Sons, England (1990).

[23] Willard, H.H, Merritt, L.L. Jr., Dean, J.A., Settle, F.A, Jr., in "Instrumental Methods of Analysis", 7th edition, Wadsworth, USA (1988).

[24] Chang, R., in "Physical Chemistry with Applications to Biological Systems", 2nd edition, Macmillan, USA (1991).

[25] Radiometer Copenhagen, ISE25Cu Copper Electrode Operating Instructions D31M017, France.

[26] Reimer, L., in "Transmission Electron Microscopy", 4th edition, Springer Series in Optical Sciences, USA (1997).

Chapter 3

Characterization of Rigid and Stable Monolayers of a Dibenzoic Acid Diamide Bolaamphiphile on Nanosized Maghemite Particles

Summary

The self-assembly of a dibenzoic acid diamide bolaamphiphile onto the surface of nanosized maghemite (γ-Fe_2O_3) particles is described. The nature and structure of the prepared monolayers were characterized by X-ray photoelectron spectroscopy (XPS) and diffuse reflectance infrared Fourier transform spectroscopy (DRIFTS). The results show that the bolaamphiphile anchors to the surface through chemical bonding between one of the carboxylic head groups and the iron of the maghemite, leaving a pendant carboxylic moiety reactive. The coordination at the maghemite surface is of the unidentate type, as seen by a difference in wavelength between symmetric and asymmetric carboxylate bands of 249 cm^{-1}. The amide linkages of the bolaamphiphile stitch the self-assembled molecules together by providing hydrogen bonding sites, thus forming a rigid monolayer. The structure of the bolaamphiphile is further confirmed by quantitative XPS analysis. Finally, rinsing the monolayer with HCl at pH 3 results in no significant IR spectral changes, thus confirming the stability of the monolayer in acidic conditions.

3.1 Introduction

Self-assembled monolayers (SAMs) have been intensively studied in the past few years because of their potential applications in corrosion prevention, wear protection, biosensing devices, etc.[1] Our particular interest is their potential for metal ion control in effluents from the mining and metallurgical industries.

Given the ability to readily deposit stable self-assembled monolayers on a variety of surfaces, two issues determine the utility of such assemblies for the creation of functionalized surfaces: the range of functionality that could be tolerated in the deposition process and the scope of chemical transformations that could be achieved within the monolayer environment.[2] Self-assembled monolayers of alkanethiols and alkyl disulfides on gold are extensively reviewed.[3,4] Monosilicic acid monolayers on hydroxylated surfaces such as silica and alumina are also reported.[5] More recently, self-assembled monolayers of surfactants containing a head group on each end of a hydrophobic skeleton, called bolaamphiphiles, were prepared on flat metal or metal oxide surfaces such as gold,[6] silica,[7] and aluminum oxide.[8]

One publication has so far confirmed the preparation and characterization of self-assembled coatings using a bolaamphiphile with dissimilar reactive head groups, 16-mercaptohexadecanoic acid (MHA), on the surface of nanosized maghemite particles.[9] It was found that the carboxylic head group (-COOH) of MHA anchors on the surface of magnetic particles so that the thiol (-SH) on the outer end remains available for different uses. To allow for a wider range of applications of such fabricated magnetic particles, the

addition of a second reactive carboxylic head group is sought, increasing the difficulty of the control of the reactivity of the functional groups to the substrate.

Recently, the preparation of monolayers of bolaamphiphiles with similar reactive head groups on polyacrylonitrile surfaces has been reported.[10] In that particular work, the presence of amide linkages in the formulation of the bolaamphiphile used offers the distinct feature of hydrogen bonding between the amide nitrogen of one molecule and the carbonyl on another once these molecules are self-assembled on a surface. This feature has since been used in the self-assembly of polymers by Jenekhe and Chen.[11]

In an attempt to prepare carboxy-functionalized magnetic particles, monolayers of a symmetrical dicarboxylic diamide bolaamphiphile on the surface of nanosized maghemite particles were self-assembled and characterized. The stability of these functionalized particles in acidic conditions was also assessed, to check that the monolayer is sufficiently dense to prevent access to the substrate.

3.2 Experimental

3.2.1 Materials

Nanosized maghemite particles, or γ-Fe_2O_3 (99+%) were used as received from Alfa Aesar (USA). These particles have an average diameter of 30 nm and a surface area of 50 m^2/g. The solvent N,N-dimethylformamide 99.9+% HPLC grade was used as received from Sigma-Aldrich (USA). For stability experiments, 0.1 N hydrocholoric acid in distilled water was prepared from 10 N HCl (Sigma-Aldrich, USA). Chemicals for the synthesis

were used as received from Sigma-Aldrich (USA).

3.2.2 Synthesis

N,N'-Di-*p*-benzoic Acid Decane Diacid Diamide (DBSC-10)

Dodecanedioyl dichloride (2.34 ml, 0.0094 mol) is added dropwise to a solution of 6.4 g (0.047 mol) of *p*-aminobenzoic acid and 7.3 ml (0.1 mol) of triethylamine in 100 ml of N,N-dimethylformamide. After stirring for 2 h, the solution is heated to 50°C for an additional 12 h. The residue is filtered and washed with water The remaining white solid is suspended in hydrochloric acid (0.1 M) at 60°C and stirred for 15 min. After filtration and drying the crude product (0.419 g) is obtained and used without further purification: proton-NMR, (DMSO) δ 1.3 (CH_2), 1.6 (β-CH_2), 2.3 (α-CH_2), 7.7/7.9 (aromatic ring), 10.1 (amide), 12.7 (acid); IR (diluted in KBr powder) ν(NH) = 3320 cm^{-1}, ν(C=O, amide + acid) = 1678 cm^{-1}.

3.2.3 Monolayer Preparation

Monolayers are formed on maghemite particles by molecular self-assembly. Typically, solutions of 28 mg of bolaamphiphile in 20 ml DMF (3 mmol) are prepared. Maghemite particles (50 mg) are added and the suspensions shaken overnight in a laboratory shaker at room temperature. The coated particles are collected by centrifugation, washed three times with DMF and dried in a vacuum oven at 40°C, which gives a solvent free film as proven by the absence of DMF infrared absorption bands.

3.2.4 Stability Experiment

For stability tests, the coated particles are briefly contacted with a water/HCL solution at pH 3, washed three times with DMF and dried in a vacuum oven at 40°C.

3.2.5 Infrared Measurement

The starting bolaamphiphile and the coated particles are characterized by diffuse reflectance infrared Fourier transform spectroscopy (DRIFTS) on a Bruker IFS 66 FTIR spectrometer with an on-axis ellipsoidal mirror, diffuse reflectance accessory (Spectra-Tech. Inc). The spectrometer is equipped with a liquid N_2 cooled narrow-band MCT mid-infrared (MIR) detector. A sample of KBr powder (IR grade, Aldrich) is used as the background. Samples are diluted by grinding with a mortar and pestle to approximately 20% by volume in KBr for MIR spectra. DRIFTS spectra are obtained using 100 scans at a nominal resolution of 4 cm^{-1} and are presented without base-line correction.

3.2.6 X-ray photoelectron spectroscopy (XPS)

XPS spectra are obtained on an ESCALAB 220i-XL Fisons Instruments with a Al monochromatic source at a take-off angle of 90° to the sample. The instrument is calibrated using the $Ag_{3d5/2}$ band (368.25 eV) of pure silver. The survey spectra is recorded using a constant analyzer energy (CAE) of 100 eV and the element spectra uses a CAE of 50 eV corresponding to an energy resolution of 1.2 eV. The powder sample is placed on a copper ribbon and maintained under a background pressure of $1x10^{-9}$ torr for approximately one hour in the sample chamber before spectral acquisition. The flood gun is set at 6 eV. Background charging is determined by the shift in the C_{1s} band normally at 284.8 eV at the end of a series of narrow scans for each sample. The software XPS Peak

Fitting Program for Win95 (XPSPEAK95) version 3.1 (Raymund W.M. Kwok editor) is used for deconvolution work.

3.2.7 TEM

In order to image the maghemite particles, dilute samples were prepared by dispersing particles onto carbon supported TEM grids, using deionized water. TEM investigation was performed with a JEOL 2000 FX at an accelerating voltage of 100 kV.

3.3 Results and Discussion

3.3.1 Maghemite Particles

Nanosized maghemite particles, or γ-Fe_2O_3, are classified as type A magnetic nanostructures materials.[12] These noninteracting (i.e. nonaggregating) systems derive their unique magnetic properties strictly from the reduced size of the components, with no contribution from interparticle interactions. Type-A materials include the ideal ultrafine particle system, with interparticle spacing large enough to approximate the particles as noninteracting. Magnetic particles, such as maghemite, surrounded by a surfactant preventing interactions, are a subgroup of Type-A materials.

The maghemite particles are single domain, since as the particle size decreases toward some critical particle diameter, D_c, the formation of domain walls becomes energetically unfavorable. Also, as the particle size continues to decrease below the single domain value, the spins are increasingly affected by thermal fluctuations and the system becomes superparamagnetic. The experimental criteria for supermagnetism are (1) the magnetization curve exhibits no hysteresis and (2) the magnetization (M) curves at

different temperatures must superpose in a plot of M vs H/T, where H is the magnetic field strength.

Figure 3-1 is a micrograph of a maghemite sample obtained by transmission electron microscopy (TEM). The first observation is the wide size distribution of the particles. The diameter of all particles is however well below the critical size (D_c) of 166 nm for γ-Fe_2O_3 as seen in estimates of single-domain size for spherical particles with no shape anisotropy, made by Kittel et al.[13] In fact, it can further be seen from the micrograph that the particles exhibit some shape anisotropy, which allows the particles to remain single domain to much larger dimensions than their spherical counterparts.

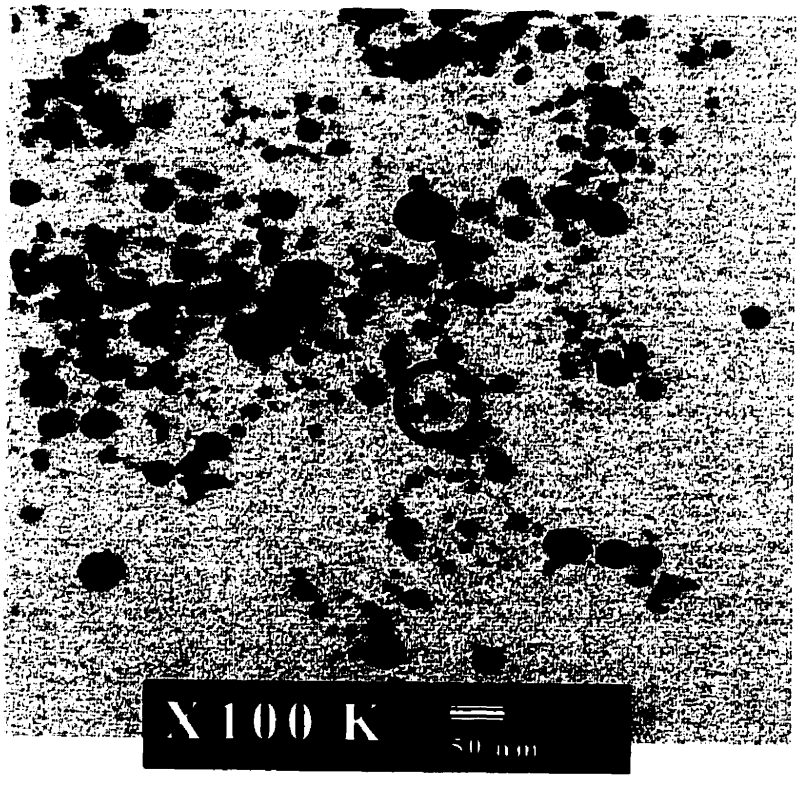

Figure 3-1: Maghemite sample by transmission electron microscopy (TEM), with nanodiffraction patterns in circled particle.

Nanodiffraction patterns can be distinguished on some of the particles indicating the presence of a crystal structure typical of maghemite and similar to that of magnetite.

Fabrication via molecular self-assembly is increasingly used to produce materials with highly uniform morphologies. The surfactant molecules help prevent unwanted particle growth and may also protect from oxidation. This technique has the advantage of keeping the particles separated during synthesis and providing passivation. Confirmation of the presence of a surfactant on the surface of untreated (not dried, not washed) maghemite is shown in Figure 3-2 for not treated, DMF washed, and dried (350°C) particles, respectively.

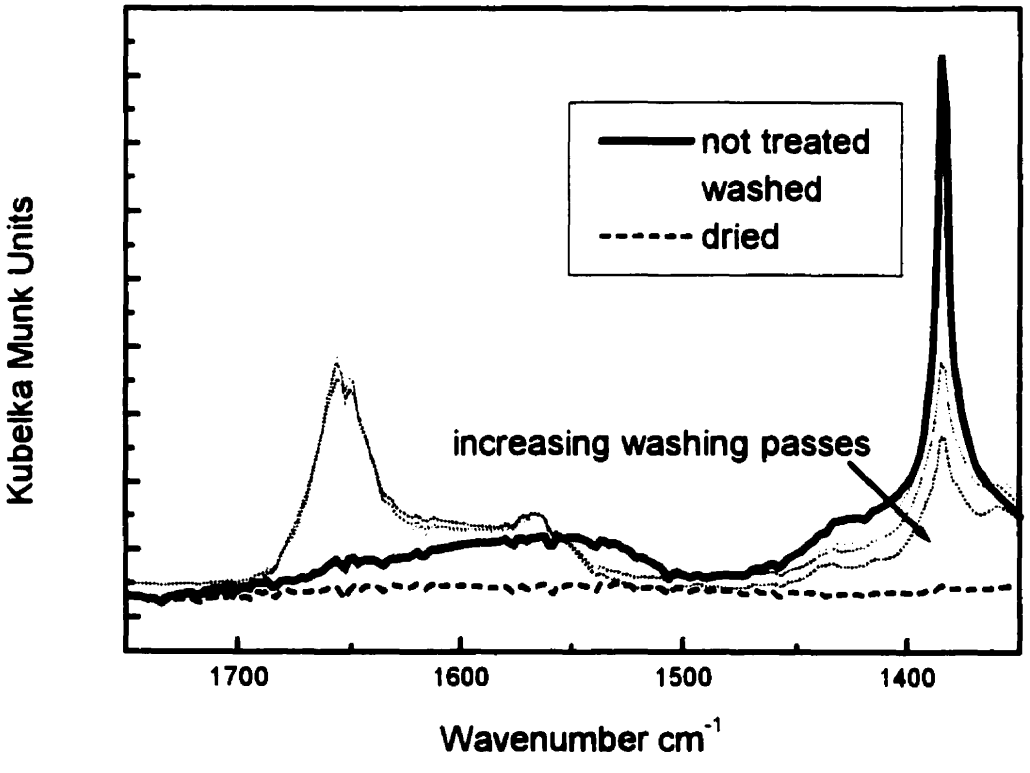

Figure 3-2: DRIFTS spectra of not treated, washed and dried maghemite particles.

The sharp peak at 1385 cm^{-1} is assigned to an ionic nitrate, sufficient to establish the presence of an anionic amine-based surfactant on the surface of untreated maghemite, from the manufacturing process of the particles.[14] The nitrate peak completely disappears from the spectrum of the dried particles, indicating complete removal of the amine-based surfactant from the maghemite surface at a temperature of 350°C. Washed spectra correspond to one, two, and three passes of DMF washed maghemite. The decrease in nitrate peak intensity with increasing washing passes indicates progressive removal of surfactant from surface, this surfactant being replaced by DMF molecules as seen from the appearance of an amide-I band at 1652 cm^{-1}. There is no significant change in the intensity of this amide band, since the drying procedure (under fumehood at room temperature) to remove DMF from the surface before IR analysis is the same for each sample.

In practice, there is no need to completely remove the surfactant from the surface of maghemite, since this only promotes aggregation of the particles in suspension, which consequently inhibits the self-assembly process. Since self-assembly takes place in DMF, with time and an excess of amide-based surfactant molecules, the original surfactant molecules will be displaced by DMF and the added surfactant molecules will be able to self-assemble on the maghemite surface. This allowed the use of maghemite particles as received for all further self-assembly work.

3.3.2 Molecular Self-Assembled Monolayers

DRIFTS spectra of the pure compound DBSC-10 (a) and its associated monolayer (b) are presented in Figure 3-3. In both spectra the peak at 3317 cm^{-1} is from the N-H stretch of the amide groups. This peak is broader in the monolayer spectrum indicating hydrogen bonding of the amides between self-assembled molecules of DBSC-10.

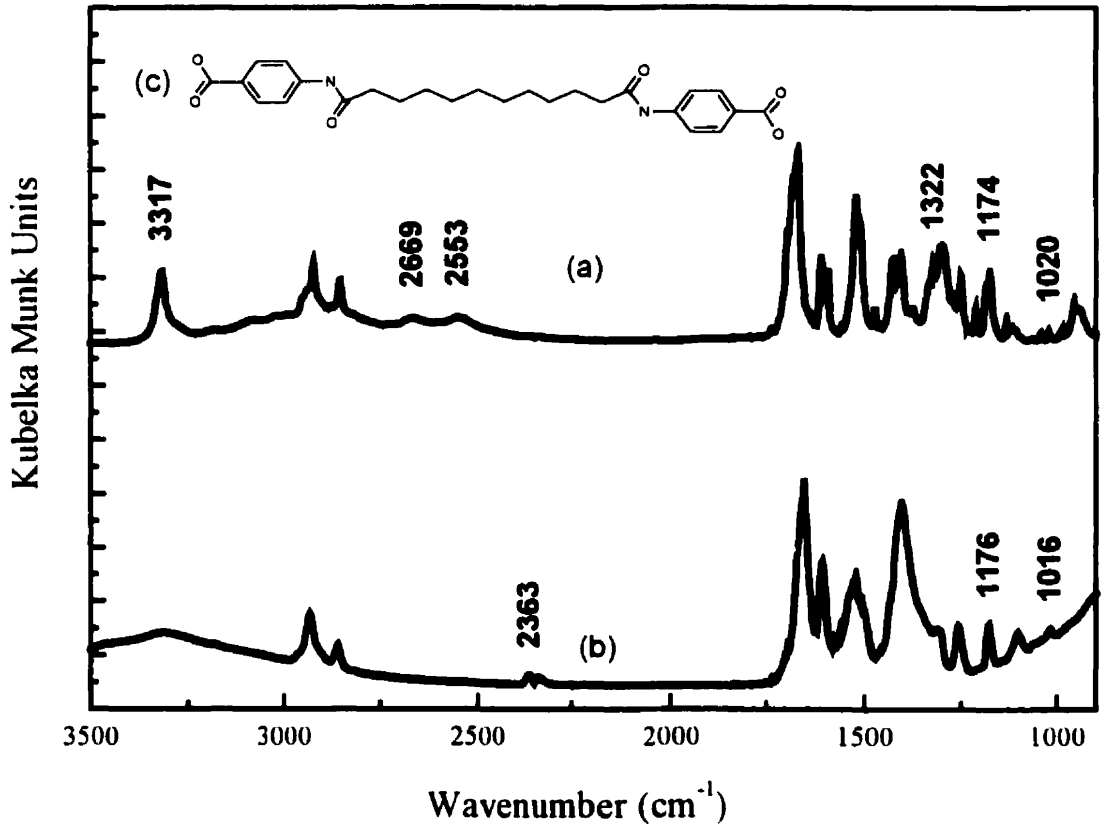

Figure 3-3: DRIFTS spectra of (a) pure DBSC-10, and (b) monolayer, with the structure of DBSC-10 in (c).

In both spectra, a broad band centered near 3000 cm^{-1} is due to OH stretching of the carboxylic group.[15,16] Two distinctive shoulders at 2669 and 2553 cm^{-1}, again due to OH stretching of the carboxylic group, are seen in the pure compound spectrum since in the solid state, carboxylic acids exist as dimers due to strong hydrogen bonding. The absence of these dimer bands in the monolayer spectrum confirms the preparation of a monolayer as opposed to multilayers of H-bonded DBSC-10 molecules. The intense band near 1322 cm^{-1} is generally referred to as the C-O stretching band.

The band 2363 cm^{-1} is due to CO_2 not completely purged from the IR chamber at the time of analysis.

An enlargement of the region 1750-1400 cm^{-1} is presented in Figure 3-4, for (a) pure DBSC-10 and (b) monolayer. A spectrum of bare maghemite (c) showing no spectral features in that particular region is also presented to confirm the presence of surfactant on the maghemite surface.

For both samples (a) and (b), a broad peak around 1670 cm^{-1} is observed, which is a superposition of three peaks: the 1695 cm^{-1} peak from the H-bonded acid dimer $\nu(COOH)_{as}$, the 1684 cm^{-1} due to the carbonyl (C=O) group vibration of the free acid, and the 1668 cm^{-1} peak, which is assigned to the carbonyl vibration of the amide group (amide I band). The presence of strong peaks at 1604 in (b), assigned as the skeletal C=C stretching vibration for the benzene ring,[17] and 1176 and 1016 cm^{-1} (see Figure 3-3), assigned as the in-plane C-H bending,[18] excludes a parallel orientation of the aromatic nucleus on the surface of maghemite. The intensified 1591 cm^{-1} band in spectrum (a)

results directly from conjugation to the ring and is due to the fact that the electron delocalisation allows a considerable dipole-moment change to occur during the vibration.[14]

It is interesting to note that the peak height ratios of the 1695, 1684 cm^{-1} peaks to that of 1604 cm^{-1} decreased to about half in the monolayer spectrum, indicating an increased involvement of the carboxylic acid groups in surface coordination.

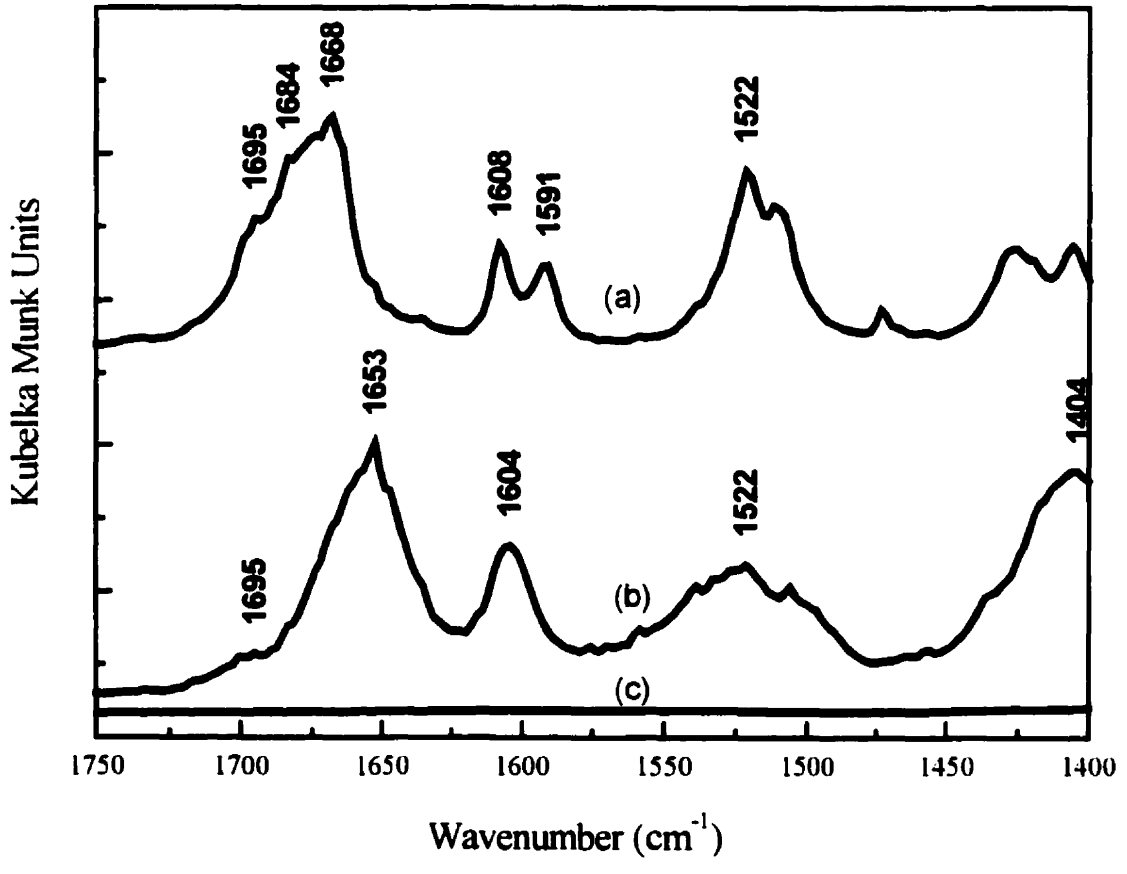

Figure 3-4: DRIFTS spectra of (a) pure DBSC-10, (b) monolayer, and (c) bare maghemite.

A ratio of two is also found between the bands at 1322 cm^{-1} and 1604 cm^{-1} (see Figure 3-3), for similar reasons.

The peak at 1522 cm^{-1} is the amide II band, made up of the N-H stretching vibration.[14] This peak is broader in the monolayer, as seen previously for the amine peak at 3317 cm^{-1}, confirming hydrogen bonding of the amide groups from the DBSC-10 molecules.

The appearance of intense new bands in spectrum (b) at 1653 cm^{-1} and 1404 cm^{-1} is due to the asymmetric and symmetric stretchings of the carboxylate moiety as a result of the coordination of carboxylic groups with the iron of maghemite particles. The difference between the asymmetrical and symmetrical peak positions indicates the type of coordination: unidentate, chelating (bidentate), bridging, or ionic, as seen in Figure 3-5.[19] The difference of 249 cm^{-1} here indicates the formation of unidentate complexes.

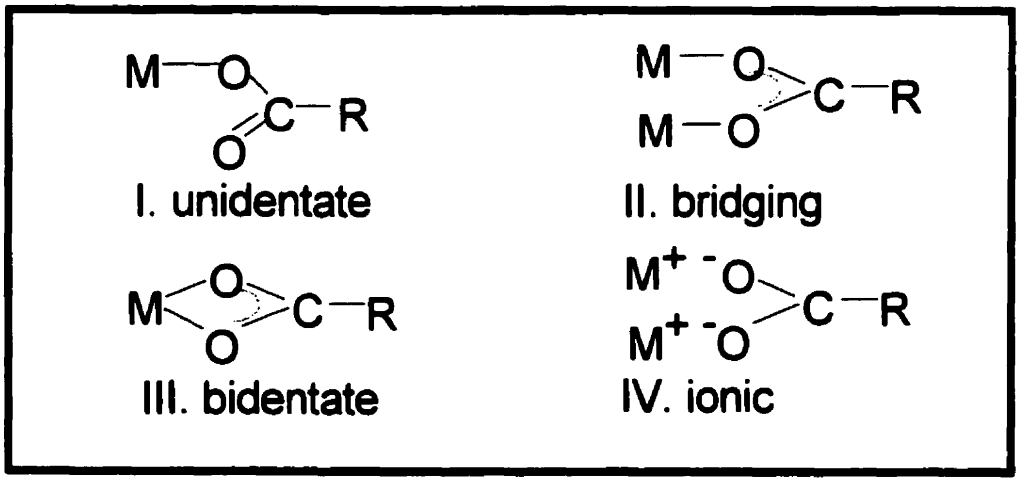

Figure 3-5: Coordination modes of the carboxylate ion.

Figure 3-6 expands the region 2950-2800 cm^{-1} of the spectra in Figure 3-3. For dehydrated monolayers of bolaamphiphiles with identical α- and ω-head groups, the distance between the monomers is fixed by the head groups, since they have a slightly larger cross-sectional area than the oligomethylene chains connecting them.[10] One therefore expects more mobility of these chains as compared to surface monolayers of single-headed amphiphiles, where area differences are adjusted by tilting.[10] Mobility of the DBSC-10 chains is seen by the shift of $\nu(CH_2)_{as}$ and $\nu(CH_2)_s$ from 2922 and 2852 cm^{-1}, respectively in the isotropic DBSC-10 spectrum, to 2931 and 2858 cm^{-1} in the monolayer spectrum.

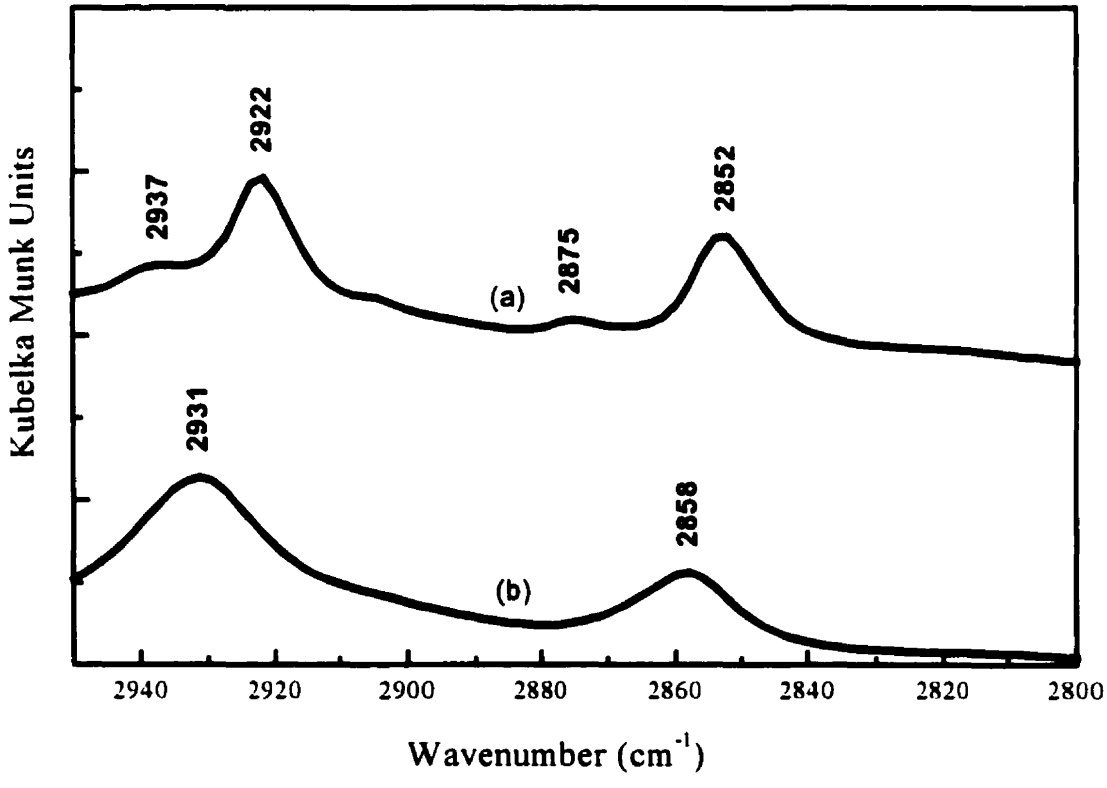

Figure 3-6: DRIFTS spectra of methylene associated peaks for (a) pure DBSC-10, and (b) monolayer.

The peaks at 2875 and 2937 cm^{-1} in (a) are associated with the symmetric mode $\nu(CH_3)_s$ (the lower energy peak for a Fermi resonance couple) and the asymmetric mode $\nu(CH_3)_{as}$, respectively. Their appearance is possibly due to triethylamine still present from the DBSC-10 preparation procedure. It should be noted that the relative geometrical orientation (i.e., tilt angle of alkyl chains) of DBSC-10 on γ-Fe_2O_3 cannot be determined directly using the DRIFTS technique, because of the random orientation of the particle surfaces with respect to the IR beam. The IR peaks of interest are summarized in Table 3-1.

Table 3-1: Assignment of IR peaks obtained from DRIFTS spectra of the surfactant pure and self-assembled.

Mode Assignment	DBSC-10 in KBr	DBSC-10 in monolayer
ν(OH stretch)	2669	nd
	2553	nd
ν(CH_2 asym stretch)	2922	2931
ν(CH_2 sym stretch)	2852	2858
ν(C=O) free acid	1684	1684
ν(COO^- asym stretch)	nd	1653
ν(COO^- sym stretch)	nd	1404
ν(C=C ring stretch)	1608	1604
	1591	
ν(amide I)	1668	1668
ν(amide II)	1522	1522
ν(NH stretch)	3317	3317

nd: not detectable.

XPS spectra of γ-Fe_2O_3, with (a) and without (b) self-assembled monolayers, are shown in Figure 3-7. The band positions in XPS spectra of untreated maghemite are given in Table 3-2. The bands at 724.5, 711.2 and 530.2 eV are attributed to iron ($Fe_{2p3/2,\ 2p1/2}$) and oxygen (O_{1s}), and are consistent with those reported previously.[20] There are no spectral changes of the $Fe_{2p3/2}$ bands in the spectrum of the monolayer coated sample. The presence of a higher energy O_{1s} shoulder for both (a) and (b) is due to the presence of DBSC-10 or surfactant from the maghemite preparation (see section 3.3.1), respectively. A band position of 533.0 eV for untreated maghemite indicates the presence of either a ketone oxygen (C-O) or an oxide oxygen (NO_2).[21]

Surfactant on the surface of untreated maghemite is also confirmed from the presence of peaks for carbon C_{1s} (b) (288.6, 286.2, 284.7 eV) and nitrogen N_{1s} (b) (407.4, 403.9, 400.3 eV), even though the intensities of these bands are significantly reduced when compared with their monolayer (a) counterparts. Three peaks are reported for each C_{1s} (b) and N_{1s} (b), indicating the presence of quite a complex molecule, which cannot be easily resolved. Nonetheless, the N_{1s} higher energy band at 407.4 eV from nitrogen oxide supports the theory established earlier from the position of the higher energy O_{1s} band, narrowing down the nature of the surfactant (from the manufacture of maghemite) to a nitrate.

The dotted lines in spectra (a) of Figure 3-7 show deconvoluted $Fe_{2p3/2}$, O_{1s}, C_{1s}, and N_{1s} peaks which are summarized in Table 3-2. The numbers associated to the O_{1s} and C_{1s} bands are referred to the ones seen in Figure 3-8 of the DBSC-10 molecular structure, and reflect the different chemical environments of these atoms. These individual

components are further characterized in the table by their full width at half maximum (FWHM). The fractional area of each component, rounded to the nearest 1 atom % is also given.

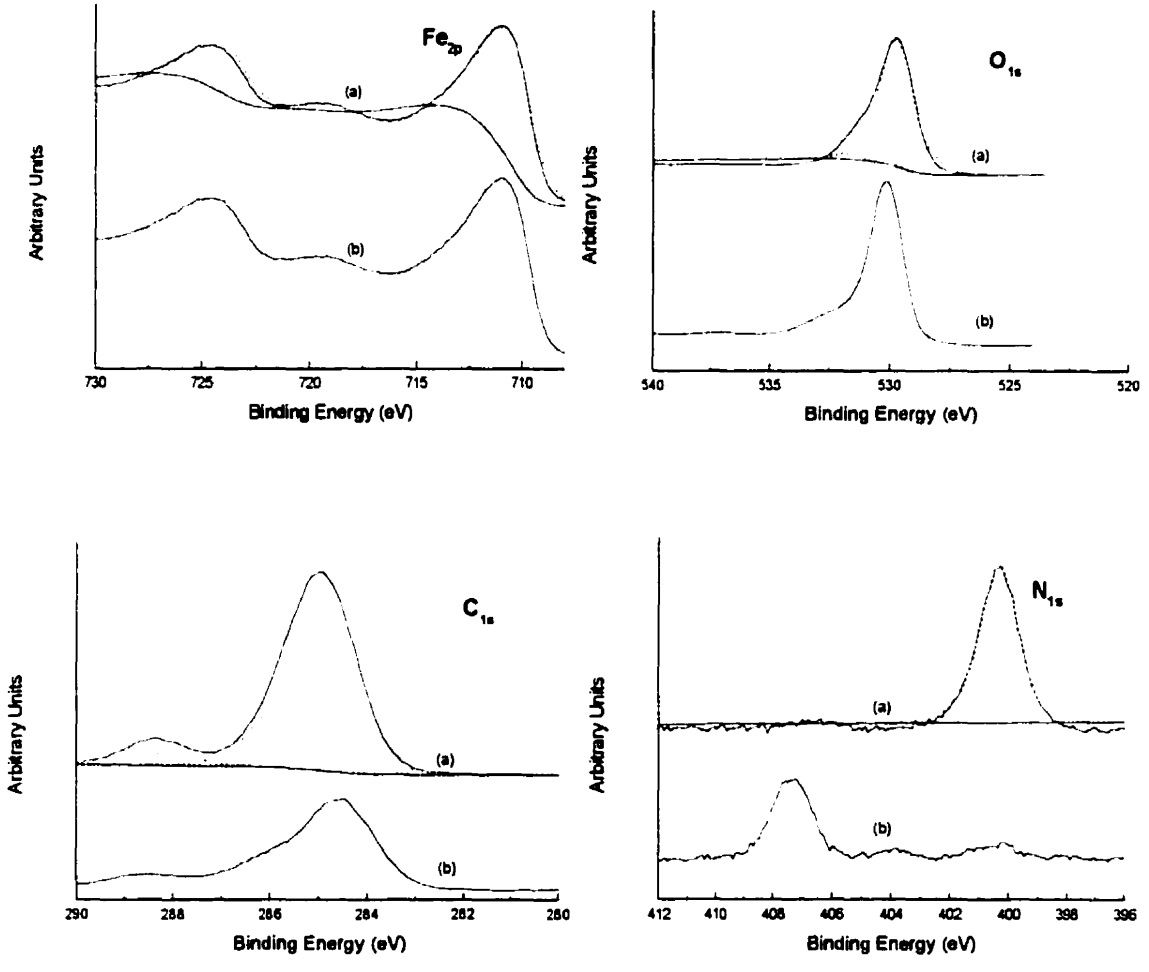

Figure 3-7: XPS spectra of narrow scans for the elements of interest on γ-Fe_2O_3 surfaces with (a) and without (b) self-assembled DBSC-10.

Table 3-2: Binding energies (eV) of X-ray photoelectrons at band maxima.[a]

System	Fe_{2p}	O_{1s}	C_{1s}	N_{1s}
γ-Fe_2O_3	724.5	533.0	288.6	407.4
	711.2	530.2	286.2	403.9
			284.7	400.3

[a]Band positions are accurate to ± 0.5 eV.

The O_{1s} band at 529.8 eV is from γ-Fe_2O_3.[22] The higher energy band at 531.0 eV corresponds to carbonyl oxygen from carboxylic and amide groups (4 C atoms), while the one at 532.0 eV indicates a single bonded oxygen from carboxylic (2 C atoms).[23] An area ratio of these two C_{1s} peaks of 1.6 (11:7) is consistent with the theoretical ratio of 2 (4:2).

There are five distinct carbon C_{1s} bands in the deconvoluted spectrum (a). The band at 284.6 eV originates from the carbon in the two aromatic rings (10 C atoms), while the 285.1 eV peak is characteristic of carbon in a hydrocarbon chain (8 C atoms).[23] Band 3 appears at 286.0 and corresponds to carbon atoms in the vicinity of a nitrogen atom (4 C atoms), i.e., the two end carbon atoms from the hydrocarbon chain, and the two aromatic carbon atoms positioned exactly next to the nitrogen atoms.[23] The higher energy bands at 288.0 and 288.7 eV, are characteristic of amide carbonyl (2 C atoms) and carboxylic carbonyl (2 C atoms), respectively.[23] An inspection of Table 3-3 shows the area % of these five bands are again in good agreement with the theoretical structure of DBSC-10.

Finally, a band position of 400.3 eV for nitrogen N_{1s} is in good agreement with the referenced values obtained for nitrogen originating from amide linkages.

Table 3-3: Binding energies (eV) of X-ray photoelectrons and related area percentages.

Peak		BE (eV)	FWHM (eV)	Area %
$Fe_{2p3/2}$		710.8	2.84	
O_{1s}	oxide	529.8	1.51	82
	1	531.0	1.30	11
	2	532.0	1.30	7
C_{1s}	1	284.6	1.02	37
	2	285.1	1.00	36
	3	286.0	1.12	17
	4	288.0	0.85	5
	5	288.7	0.98	5
N_{1s}		400.3	1.44	

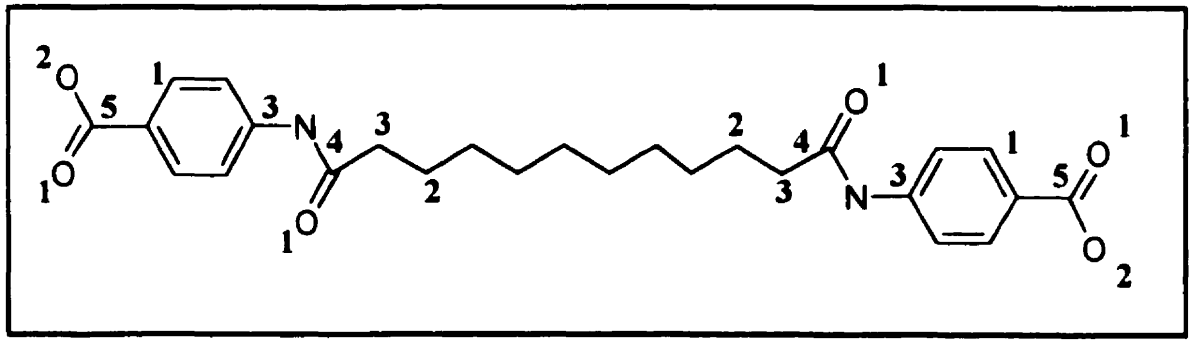

Figure 3-8: Structure of DBSC-10 with labeled atoms.

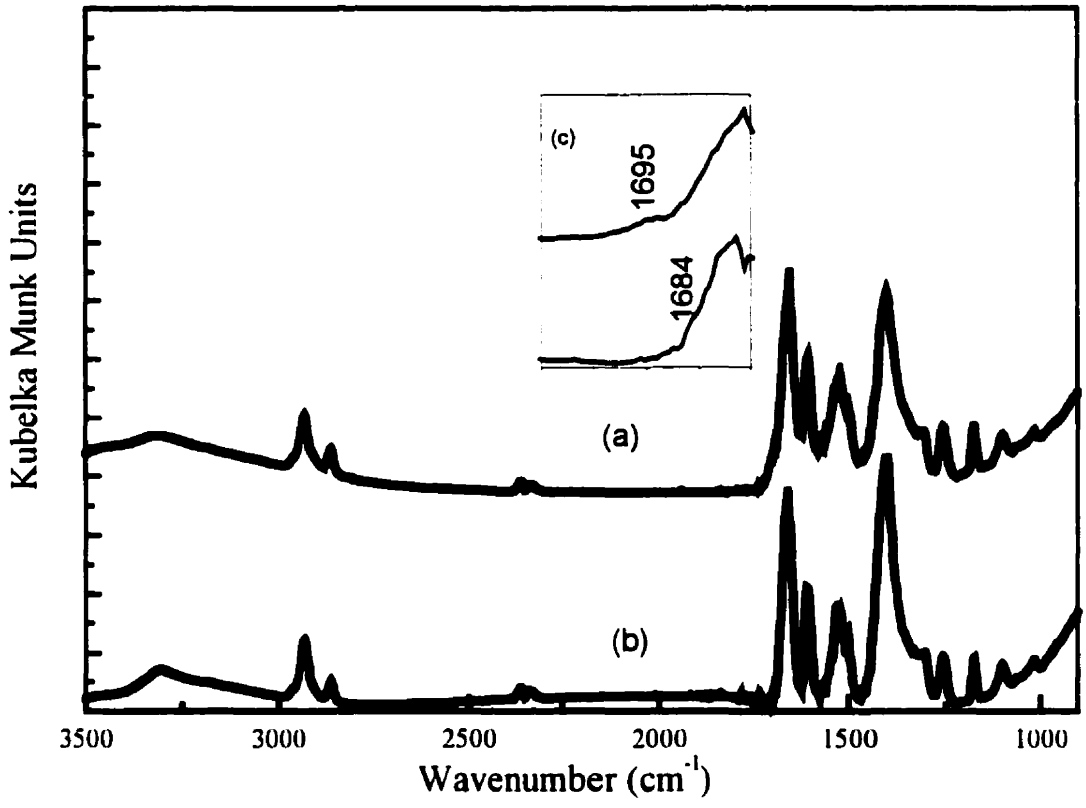

Figure 3-9: DRIFTS spectra of monolayer at (a) neutral pH and (b) pH 3, with acid related peaks presented in insert (c).

The previously shown DRIFTS and XPS results have established the self-assembly of DBSC-10 on the surface of maghemite at neutral pH. Figure 3-9, presents further DRIFTS spectra of self-assembled DBSC-10 at neutral pH (a) and washed by HCl:water at pH 3 (b). No significant spectral changes are seen in spectrum (b) when compared to spectrum (a), therefore confirming the formation of a close-packed self-assembled monolayer. An expansion of the area in (c) shows the complete disappearance of the COOH-bonded acid peak at 1695 cm^{-1}, which is converted to COOH free acid as seen with the increased intensity of the 1684 cm^{-1} peak.

3.4 Conclusions

It was shown that a monolayer of the bolaamphiphile DBSC-10 was formed at the surface of maghemite nanosized particles. Infrared measurements confirmed the unidentate coordination of one carboxylic end group of DBSC-10 with the iron of maghemite ($\nu_{as}(COO^-) - \nu_s(COO^-) = 249\ cm^{-1}$), and the presence of a free carboxylic moiety (free and H-bonded COOH). DRIFTS experiments showed broadening of amine and amide bands, indicating hydrogen bonding of the amides between self-assembled molecules, providing additional stitching of molecules and rigidity of the monolayer. This monolayer is stable in acidic conditions, as seen by the absence of infrared spectral changes when the samples are rinsed with HCl at pH 3. Quantitative XPS analysis of deconvoluted carbon and oxygen peaks confirmed the structure of DBSC-10 on the maghemite particles. XPS and DRIFTS measurements identified the presence of a surfactant on the received maghemite, originating from their preparation and designed to prevent agglomeration. Maghemite particles do not have to undergo pretreatment before self-assembly, however, since displacement of the original surfactant by DBSC-10 is performed by the solvent DMF.

References

[1] Ulman, A., in "Characterization of Organic Thin Films", Butterworth-Heineman, USA (1995).

[2] Balachander, N., Sukenik, C.N., Langmuir, **6** (11), 1621-1627 (1990).

[3] Whitesides, G.M , Bain, C.D., J. Am. Chem. Soc., **110**, 3665 (1988).

[4] Bain, C.D., Troughton, E.B., Tao Y.T., Evall,J., Whitesides, G.M , Nuzzo, R.G., J. Am. Chem. Soc., **111**, 321-335 (1989).

[5] Bergna, H.E., Lawrence, E.F., Swartzfager, D.G., in "The Colloid Chemistry of Silica", Bergna, H.E., 561-580 (1994).

[6] Allara, D.l., Hebard, A.F., Padden, F.J., Nuzzo, R.G., Falcone, D.R., J. Vac. Sci. Technology, **A1** (2), 376-382 (1983).

[7] Ihs, A., Liedberg, B.J., J. Colloid Interface Sci., **144**, 283 (1991) and Uvdal, J., Bodo, O., Liedberg, B.J., J. Colloid Interface Sci., **149**, 163 (1992).

[8] Smith, E.L., Alves, L.A., Andergg, J.W., Porter, M.D., Siperko,L.M., Langmuir, **8**, 2707 (1992).

[9] Liu, Q., Xu, Z., Langmuir, 11 (12) (1995).

[10] Böhme, P., Hicke H-G., Boettcher, C., Furhop, J-H., J. Am. Chem. Soc., **117**, 5824-5828 (1995).

[11] Jenekhe, S.A, Chen, X.L., Science, **279**, 1903-1907 (1998).

[12] Leslie-Pelecky, D.L., Rieke, R.D., Chem. Mater., **8**, 1770-1783 (1996).

[13] Kittell, C., Phys. Rev., **70**, 965 (1946).

[14] Bellamy, L.J., in "The Infrared Spectra of Complex Molecules", vol.1, 3 rd ed., Chapman and Hall, London (1975).

[15] Silverstein, R.M., in "Spectrometric Identification of Organic Compounds", 5 th ed., Wiley & Sons, USA (1991).

[16] Colthup, N.B., Daly, L.H., Wiberley, S.E., in "Introduction to Infrared and Raman Spectroscopy", 3 rd ed., Academic Press, USA (1990).

[17] Tao, Y-T., Lee, M-T., Chang, S-C., J. Am. Chem. Soc., **115**, 9547-9555 (1993).

[18] Chaffins, S.A, Gui, J.Y., Kahn, B.E., Lin, C-H., Lu, F., Salaita, G.N., Stern, D.A., Zapien, D.C., Hubbard, A.T., Langmuir, **6** (5), 957-970 (1990).

[19] Nakamoto, K., in "Infrared and Raman Spectra of Inorganic and Coordination Compounds", 4 th ed., Wiley & Sons, USA (1986).

[20] Liu, Q., Ph.D. Thesis, McGill University, Canada (1996).

[21] Clark, D.T., Thomas, H.R., Journal of Polymer Science: Polymer Chemistry Edition, **14**, 1671-1700 (1976).

[22] Briggs, D., Seah, M.P., in "Practical Surface Analysis", 2 nd ed., vol(1), John Wiley & Sons, England (1990).

[23] Beamson, G., Briggs, D., in "High Resolution XPS of Organic Polymers", John Wiley & Sons, England (1992).

Chapter 4

Determination of Monolayer Density by Potentiometric Titration

Summary

Potentiometric titration of acidic groups originating from the functionalization of nanosized maghemite particles by a diacidic bolaamphiphile (DBSC-10), is described. The titrations are achieved in the solvent dimethylformamide (DMF), using potassium hydroxide (KOH) 0.01 N in water as titrant. A reproducible packing density of 3.4 μmole of DBSC-10 per m^2 of maghemite is found, approximating the value estimated from molecular dimensions. Titration does not affect the stability of the monolayer at higher pHs, as confirmed by infrared measurements on titrated particles. New strong peaks do appear at 1603 cm^{-1} ν(COO^- asymmetrical stretch) and 1348 cm^{-1} ν(COO^- symmetrical stretch), indicating the formation of ionic complexes between the free carboxylic moieties of the monolayer and K^+ from titrant.

4.1 Introduction

There are available a wide range range of techniques to study surface phenomena. These include imaging techniques (AFM, STEM, etc.) where morphology of the surface is revealed and spectrometric techniques (MS, XPS, FT-IR and Raman, etc.) where atomic and molecular information is obtained. It is possible using these techniques to determine molecular orientation and surface coverage (inferred from a thickness determination) of self-assembled monolayers (SAMs).[1]

Recently, a series of publications has reported measurements of packing densities (moles adsorbed per unit area) of several aromatic and polyaromatic compounds adsorbed at Pt(111) electrodes, by means of Auger spectroscopy.[2,3,4,5] Characterization of adsorption on planar substrates has so far concentrated on the molecular orientation of hematite(α-Fe_2O_3)-stearate alternating Langmuir-Blodgett films, using grazing-angle infrared.[6,7]

The study of SAMs, particularly to determine a monolayer packing density, using these techniques, however, is limited when the morphology of the substrate is not a flat surface. This is the case here in the characterization of self-assembly on nanosized particles. One solution to the problem is to develop indirect analysis techniques based on a difference method, i.e., analyze for non-adsorbed species in solution and calculate by difference the amount of adsorbed species per area of particles. The results lack the rigor of direct analysis and are suspect as to the correct representation of the adsorption mechanism. In search of a direct technique, a potentiometric titration method is suggested.

Potentiometric titration of weak acids, as a direct and quantitative analysis technique, is well documented in the pharmaceutical field.[8] Carboxylic acids are compounds which are typically difficult to titrate in water, since well characterized and sharp inflexion points are seldom found in aqueous systems. Potentiometric titrations of dicarboxylic acids in alcohol (1-propanol)[9] and carboxylic acids in dimethylformamide (DMF)[10] have recently been reported. In the latter work, it was found that potassium hydroxide (KOH) could be successfully substituted for the traditionally used and fairly toxic titrant tetrabutylammonium hydroxide (TBAH), while achieving comparable inflexion point determinations. They also note hydrolysis of the DMF upon addition of titrant (i.e. water). Since hydrolysis is a slower process than the neutralization of acids in solution, fast titrant additions are necessary to insure no effect of hydrolysis on the titration curves.

In this work, potentiometric titration is based on the neutralization of surface carboxylic groups originating from the functionalization of nanosized maghemite particles (average particle size 30 nm) by a diacidic bolaamphiphile (see Figure 4-1). The titrant used is a solution of potassium hydroxide (KOH) in water and the titration medium (solvent) is dimethylformamide (DMF). Solution potential as a function of volume of titrant added to solution are obtained, from which the packing density of the bolaamphiphile per area of maghemite can be obtained.

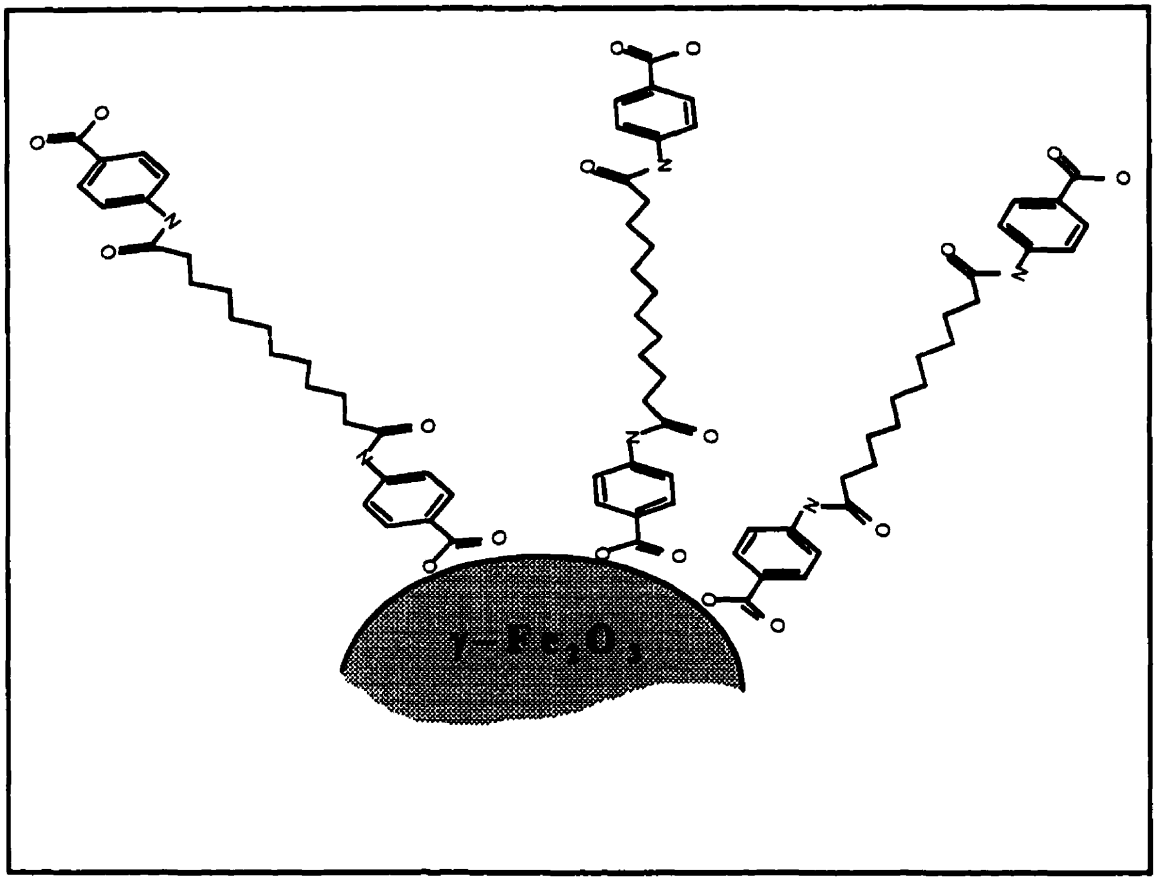

Figure 4-1: Schematic of a DBSC-10 monolayer onto a maghemite (γ-Fe_2O_3) particle.

4.2 Experimental

4.2.1 Materials

Nanosized maghemite particles, or γ-Fe_2O_3 (99+%), were used as received from Alfa Aesar (USA). These particles have an average diameter of 30 nm and a surface area of 50 m^2/g. The solvent N,N-dimethylformamide 99.9+% HPLC grade and 0.01 N-potassium hydroxide in water was prepared from a 0.1 N KOH stock solution received from Sigma-Aldrich (USA). All the chemicals used for the DBSC-10 bolaamphiphile synthesis were obtained from Sigma-Aldrich (USA).

4.2.2 Synthesis

The synthesis of *N,N'*-Di-*p*-benzoic Acid Decane Diacid Diamide (DBSC-10) of molecular weight 468.55, is described in section 3.2.2. Titrations of DBSC-10 are performed in 20 ml DMF.

4.2.3 Monolayer Preparation

Monolayers are formed on maghemite particles by molecular self-assembly. Typically, solutions of 28 mg of DBSC-10 in 20 mls of DMF (3 mmol) are prepared. Different amounts of maghemite particles (25, 50, 75 and 100 mg) are added and the suspensions shaken overnight at room temperature. The coated particles were centrifuged, washed three times with DMF, and suspended in 20 ml DMF for titration.

4.2.4 Titration Apparatus

All titration experiments are done at room temperature using a TitraLab titration laboratory (Radiometer Analytical Copenhagen, Denmark) composed of a TIM90 Titration Manager, a ABU91 Autoburette high-precision burette station, and a SAM90 Sample Station. The samples are stirred using an overhead stirrer part of the SAM90. Titrations are performed using a combined pH electrode (Radiometer pHC2401). Nitrogen is bubbled throughout the titration preventing CO_2 contamination.

4.2.5 Titration Procedure

Titrations are run in the continuous inflexion point IP mode, without predose and with a minimum/maximum speed fixed at 2%/min of a 10 ml burette. A smoothing parameter of 8 is used in the calculation of inflexion points. Note that titrations of bare iron oxide

(maghemite) surfaces are performed on oven dried (350°C) maghemite particles to model surfactant free surfaces (see section 3.3.1).

4.2.6 Infrared Measurement

The DRIFT spectrum is recorded on a Bruker IFS-66 FT spectrometer with an ellipsoidal mirror, diffuse reflectance accessory (Spectra-Tech, Inc.). The spectrometer is equipped with a liquid N_2-cooled MCT mid infrared (MIR) detector. The spectrum is measured at 4 cm^{-1} resolution and 100 scans are coadded. The MIR Kubelka-Munk spectrum is obtained by ratioing the resulting spectrum against a background of KBr (IR grade, Aldrich). The sample is diluted by grinding with a mortar and pestle to approximately 20% by volume in KBr.

4.3 Results and Discussion

4.3.1 DBSC-10 Titration

When adding KOH to a solution of DBSC-10, the following reaction takes place, based on the neutralization of a weak diacid:

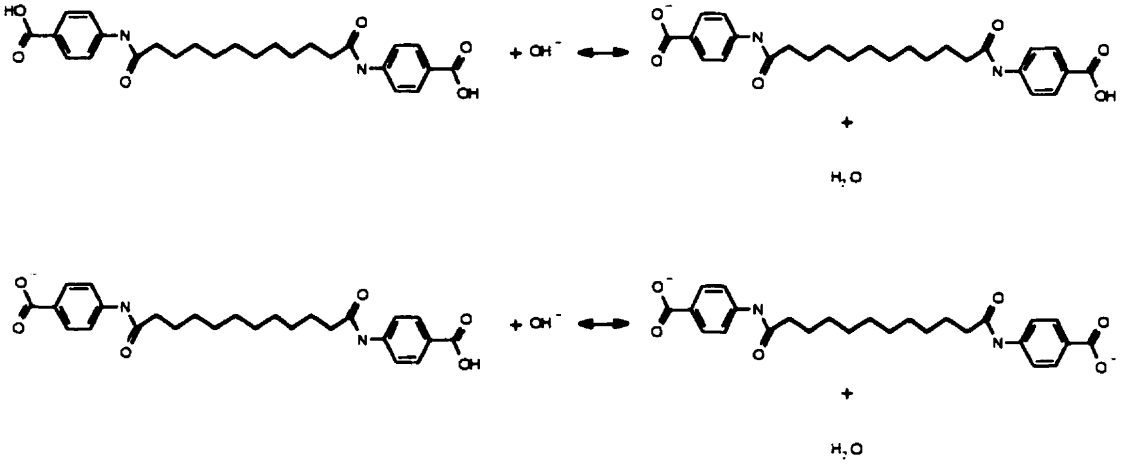

[4-1]

Assuming the reaction between DBSC-10 and OH^- is complete, the equivalence point is then characterized by:

$$2C_{DBSC\text{-}10}\, V_{Sample} = C_{Base}\, V_{Base\ total} \qquad [4\text{-}2]$$

where $C_{DBSC\text{-}10}$ and C_{Base} are the concentrations of surfactant and base, respectively, and V_{Sample} and $V_{base\ total}$ are the volumes of sample and total base added, respectively.

Figure 4-2 shows the titration curves obtained from the neutralization of (a) 4.4 mg and (b) 8 mg of DBSC-10. The shape of these curves up to the equivalence point compares with the results obtained for benzoic acid in DMF by Nickel and Weber.[10] It is characterized by the presence of two potential minima and one potential maximum, not

seen in the titration of weak acids in water systems. The presence of two inflexion points around the equivalence point is typical of the titration of a diprotic acid, i.e., successive titration of two ionizable protons. Their proximity indicates that the long hydrocarbon chain of DBSC-10 is almost sufficient to approximate the titration of two separate weak acids. Furthermore, the plateau or region of constant potential on curves (a) and (b), corresponds to the point where both the acid and the ionized species predominate, i.e., the buffer zone. The error between the experimental and theoretical (prepared) concentrations of DBSC-10 is ± 5%.

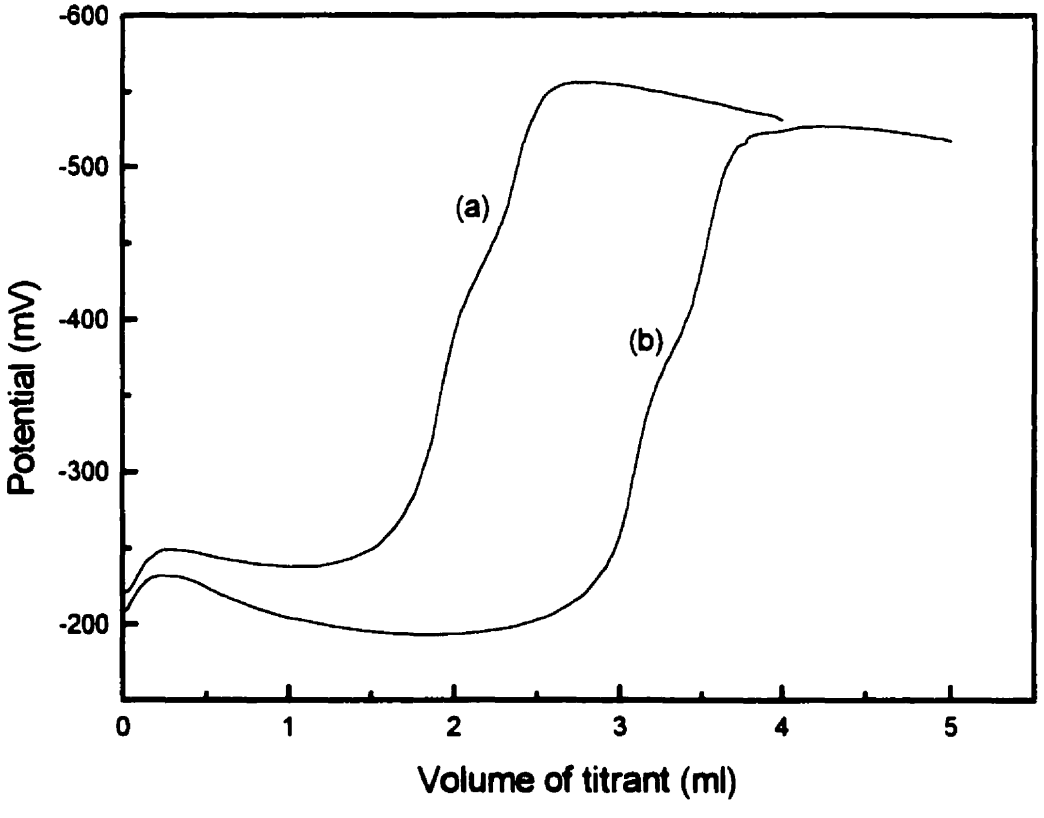

Figure 4-2: Titration curves from the neutralization of (a) 4.4 mg and (b) 8 mg of DBSC-10.

4.3.2 Titration of DBSC-10 Coated Particles

Figure 4-3 shows the titration curves of 50 mg of (a) bare maghemite and (b) DBSC-10 coated particles. The shape of curve (a) is indicative of the background response of the bare particle system. The unresolved inflexion point around a potential of -450 mV can be attributed to the titration of some hydroxy species adsorbing on the bare surface of maghemite. The shape of curve (b) does indicate the titration of a weak acid, as seen from the presence of both a potential plateau around -350 mV and a single sharp inflexion point (titration of a monoacid) at -500 mV.[11]

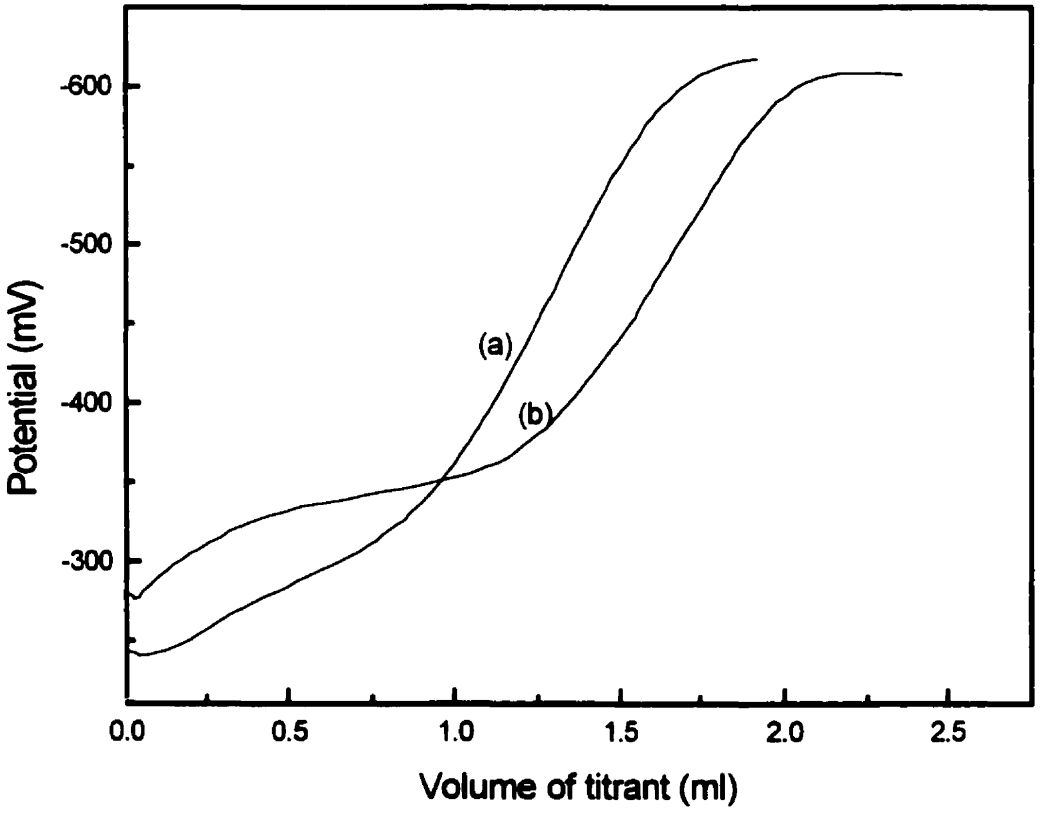

Figure 4-3: Titration curves of 50 mg of (a) bare maghemite and (b) DBSC-10 coated particles.

Curve (b) can be further divided in four different regions as seen in Figure 4-4:

- region A of the acid species, where the potential increases rapidly with the addition of base;

- region T where the titration takes place and the potential increases slowly with the addition of base;

- region E of the equivalence point where the jump in potential is observed;

- region B dominated by the ionized species and where the potential increases very slowly with increasing addition of base.

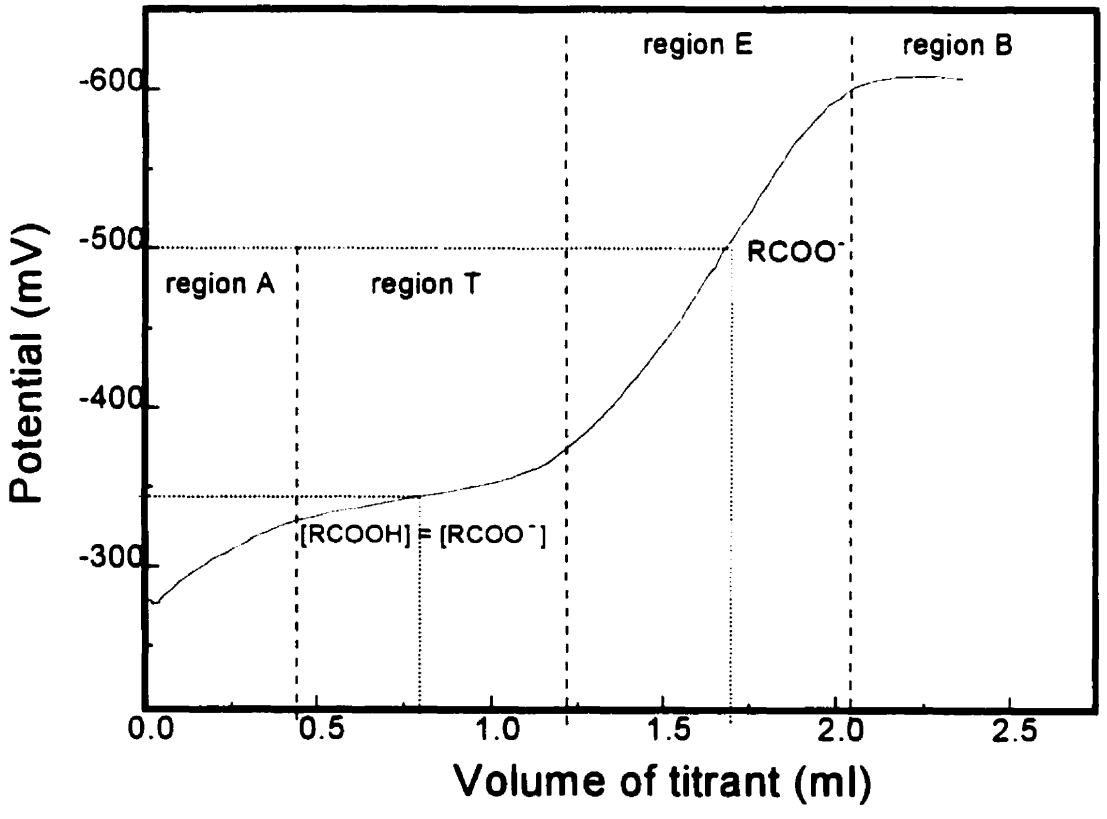

Figure 4-4: Titration of 50 mg of DBSC-10 coated particles by KOH.

Figure 4-5 presents curves corresponding to the titration of increasing amounts of DBSC-10 coated particles (a) 25 mg, (b) 50 mg, (c) 75 mg, and (d) 100 mg. The dashed line of 75 mg of bare maghemite is also presented and provides a background for comparison. Increasing the amount of titrated particles results in a right shift of the curves, as seen in (a), (b), (c) and (d). As expected from the titration of more acid, the associated T regions of each successive curves becomes longer. The slight decrease in potentials of all four B regions is due to the dilution effect of increasing the volume of titrant necessary for the titration of more acid. All three associated inflexion point (equivalence points) are observed around a potential of -500 mV.

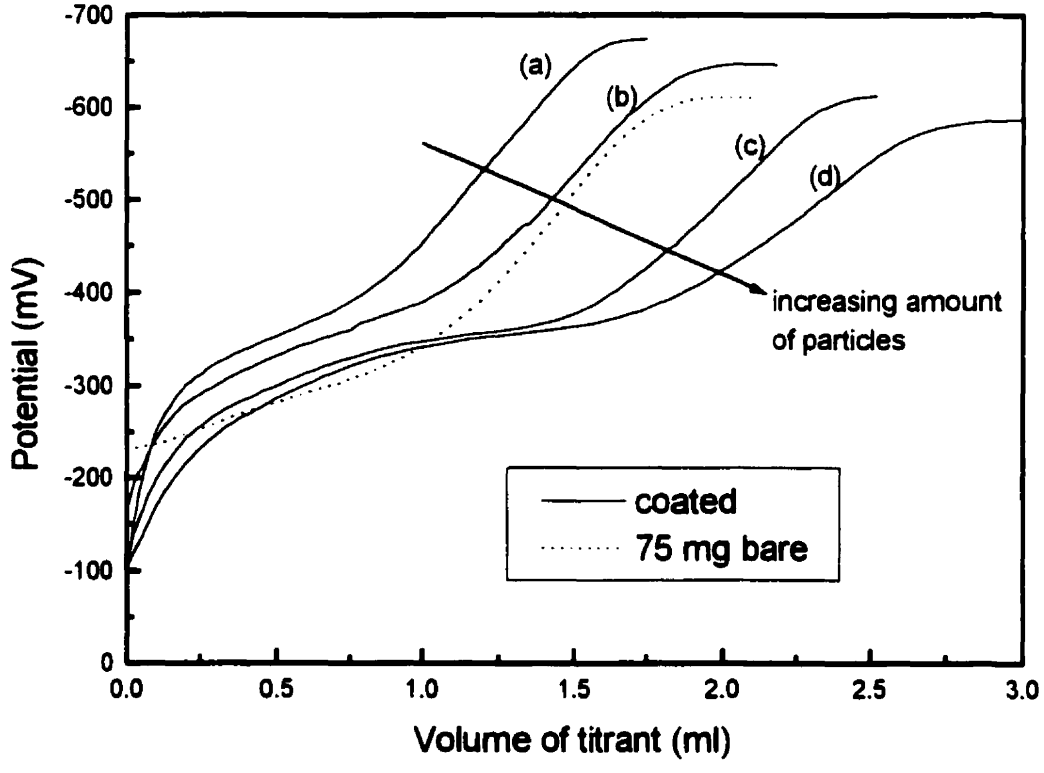

Figure 4-5: Titration of DBSC-10 coated particles (a) 25 mg, (b) 50 mg, (c) 75 mg, (d) 100 mg, and 75 mg of bare maghemite.

The volume of titrant added does not double from curve (a) to (b), indicating the presence of a systematic background effect occuring during the titration. One such effect could be the adsorption of hydroxy species onto glassware and titration components (electrode, titrant dispenser, stirrer, etc.). For this reason, only difference between the inflexion points of the curves will be considered.

The corresponding inflexion points of curves (a), (b), (c) and (d) from Figure 4-5 are shown in Figure 4-6. The difference in volume of titrant added per 25 mg increment of coated particles is seen to be approximately 0.43 ml. Table 4-1 shows this value to be reproducible within 28% of the replicate titrations mean.

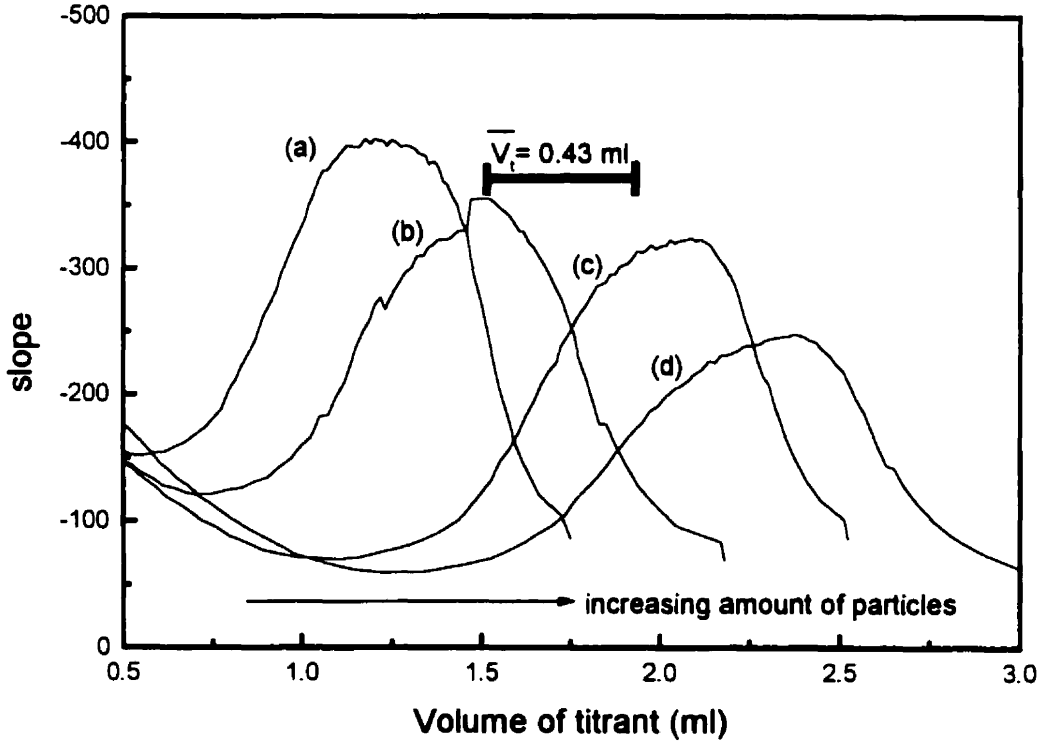

Figure 4-6: Inflexion points of DBSC-10 coated particles (a) 25 mg, (b) 50 mg, (c) 75 mg, (d) 100 mg.

Table 4-1: Reproducibility of the volume difference between 25 mg increments of coated particles.

Number of replicates	Mean difference of inflexion points	Sample standard deviation	90% confidence interval
5	0.43	0.13	0.43 ± 0.12

This average volume corresponds to 4.3 μmole of DBSC-10, and to a density of 3.4 μmole of DBSC-10 per m^2 of maghemite. This value corresponds with the calculated density, obtained using the surface area of maghemite and Avogadro's number, and assuming a cross-sectional area of a DBSC-10 molecule of 30 nm^2.[12] For 50 mg of particles , we have:

$$0.05\ g \cdot 50\ m^2/g = 2.5\ m^2 \qquad [4\text{-}3]$$

Then taking the cross sectional area of a DBSC-10 molecule as 30 nm^2,

$$2.5\ m^2 / 30\ E\text{-}20\ m^2 \text{ per molecule} = 8.33\ E18 \text{ molecules} \qquad [4\text{-}4]$$

Using Avogadro's number,

8.33 E18 molecules/ 6.02 E23 molecules per mole = 13.8 μmole of DBSC-10

or,

13.8 μmole of DBSC-10/ 2.5 m^2 = 5.5 μmole of DBSC-10/ m^2 of particle.

Note that an error on the calculated density is generated by using the average surface area of a maghemite sample in this calculation.

DRIFTS spectra of DBSC-10 coated particles after (a) and before (b) titration with KOH are shown in Figure 4-7. The presence of surfactant on (a) is confirmed. The IR region scanned reveals the asymmetrical and symmetrical carboxylate vibrational peaks. It is interesting to note the presence of new strong peaks in (a) at 1603 cm^{-1} and 1348 cm^{-1}, assigned as the $\nu(COO^-$ asym stretch) and $\nu(COO^-$ sym stretch) of the free carboxylic moieties forming complexes with the K^+ ions. A difference between the asymmetrical and symmetrical wavelengths of 255 cm^{-1}, although in the high range, is consistent with these ionic species.[13]

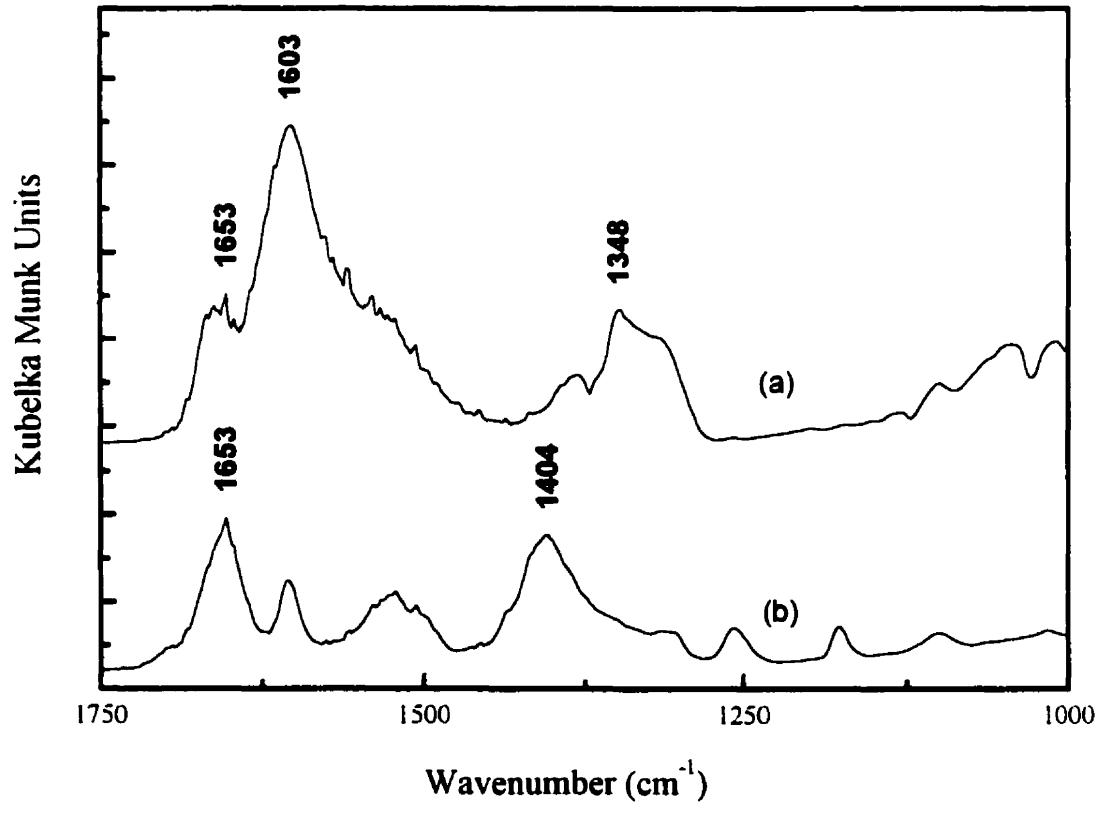

Figure 4-7: DRIFTS of DBSC-10 coated particles (a) after and (b) before titration with KOH.

4.4 Conclusions

Potentiometric titration has proven a successful and novel technique in the determination of the packing density of a self-assembled monolayer of a weak acid DBSC-10 onto maghemite particles. The system, KOH/DMF introduced by Nickel and Weber, has been proven successful in this titration. A reproducible packing density of 3.4 μmole of DBSC-10 per m^2 of maghemite was determined. This value compares with the calculated value of 5.5 μmole of DBSC-10 per m^2 of maghemite, based on the average surface area of particles. Infrared measurement confirmed the surfactant is not removed after titration. New strong peaks at 1603 cm^{-1} and 1348 cm^{-1}, associated with the asymmetrical and symmetrical vibrations of a carboylate group, confirm the formation of ionic complexes between the free carboylic moieties of the coated maghemite and K^+ ions from the titrant.

References

[1] Ulman, A., in "Characterization of Organic Thin Films", Butterworth-Heineman, USA (1995).

[2] Stern, D., Laguren-Davidson, L., Frank, D.G., Gui, J.Y., Lin, C-H., Lu, F., Salaita, G.N., Walton, N., Zapien, D.C., Hubbard, A.T., J. Am. Chem. Soc., **111**, 877-891 (1989).

[3] Chaffins, S.A., Gui, J.Y., Kahn, B.E., Lin, C-H., Lu, F., Salaita, G.N., Stern, D.A., Zapien, D.C., Hubbard, A.T., Langmuir, **6**, 957-970 (1990).

[4] Chaffins, S.A., Gui, J.Y., Lin, C-H, Lu, F., Salaita, G.N., Stern, D.A., Hubbard, A.T., Langmuir, **6**, 1273-1281 (1990).

[5] Gao, P., Lin, C-H., Shannon, C., Salaita, G.N., White, J.H., Chaffins, S.A., Hubbard, A.T., Langmuir, **7**, 1515-1524 (1991).

[6] Peng, X., Zhang, Y., Yang, J., Zou, B., Xiao, L., Li, T., J. Phys. Chem., 96, 3412-3415 (1992).

[7] Yang, J., Peng, X-G., Zhang, Y., Wang, H., Li, T-J., J. Phys. Chem., **97**, 4484-4487 (1993).

[8] Martin, A, in "Physical Pharmacy", 4 th ed., Lea & Febiger, USA (1993).

[9] Bozdogan, A., Ozeroglu, C., Kunt, G., Sarac, S., Revue Roumaine de Chimie, **38** (12), 1415-1419 (1993).

[10] Nickel,P., Weber, W., Pharm.Ztg., Wiss., **2·2** (134), 13-17 (1989).

[11] Chang, R., in "Physical Chemistry with Applications to Biological Systems", 2 nd ed., Macmillan, USA (1981).

[12] Böhme, P., Hicke H-G., Boettcher, C., Furhop, J-H., J. Am. Chem. Soc., **117**, 5824-5828 (1995).

[13] Nakamoto, K, in "Inrared and Raman Spectra of Inorganic and Coordination Compounds", 5 th ed., John Wiley & Sons, USA (1997).

Chapter 5

Section 1:

Coupling of Diethylenetriamine to Carboxyl-Terminated Magnetic Particles

Summary

The ligand diethylenetriamine (DETA) has been successfully coupled to carboxy-terminated magnetic particles, using the carbodiimide EDCI. Amine related peaks from DETA are seen in infrared measurements. The reaction with DETA involves a rearrangement of the self-assembled DBSC-10 molecules on the maghemite, as seen from a shift of methylene peaks, indicating less mobile hydrocarbon chains. XPS measurements and a deconvolution of peaks indicate that one out of two molecules of DBSC-10 is reacting with DETA to form new amide linkages. This would give an amount of DETA-reacted DBSC-10 molecules on the surface of 84 μmole per g of carboxy-terminated particles. Titration of the DETA-reacted particles show the titration of two different types of protons, amine and carboxylic, and the ratio of 1:1. Finally, the amount of base required for the complete titration of DETA-reacted particles (0.5 ml per 25 mg of titrated particles) excludes the possible cross-linking reaction of DETA with free carboxylic groups from DBSC-10.

5.1.1 Introduction

Complexing agents have been used extensively in the metals extraction industry. They have been employed for leaching, solvent extraction, design of coordinating resins, and flotation.[1] When ligands are attached to solid supports such as magnetic particles, metals can be selectively absorbed and removed from dilute streams.[2]

Complexes of macrocyclic ligands, with low pH of complexation, are known to display particular extra thermodynamic stability and selectivity.[3,4,5] While the sulfur-donor macrocycles are weakly complexing with all metal ions, the nitrogen donor macrocycles complex well with transition metal ions, as well as the post-transition metal ions. As a simple model nitrogen donor macrocycle, the ligand diethylenetriamine (DETA) was chosen for attachement to a carboxyl-terminated magnetic carrier, prepared by the functionalization of nanosized maghemite particles by a diacid bolaamphiphile (see Chapter 3).

Carbodiimides are the most common reagent in peptide synthesis and in other amide bond-forming reactions of primary and secondary amines with carboxylic acids (reaction 5-1-1).[6] Dimethylaminopropyl ethylcarbodiimide hydrochloride (EDCI) promotes amide formation by reacting with the carboxyl group of an acid and by activating it towards nucleophilic substitution.[7]

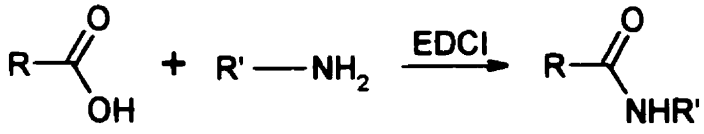

[5-1-1]

Since DETA has two primary amines, cross-linking to carboxyl-terminated magnetic particles is also possible. Further characterization of the DETA-activated carboxyl-surface by spectroscopy techniques such as infrared and X-ray photoelectron, as well as by potentiometric titration will give an assessment of the extent of DETA reaction.

5.1.2 Experimental

5.1.2.1 Materials

The preparation procedure of the carboxyl-terminated magnetic particles is described in section 3.2.3. The prepared particles are not dried, but rather sequentially washed with distilled water (three times) to remove traces of dimethylformamide (DMF), and prepare them for DETA-reaction. All chemicals used in the preparation of the coupling buffer, the coupling agent 1-ethyl-3-(3-dimethylaminopropyl)carbodiimide (EDCI) and DETA were obtained from Sigma-Aldrich (USA). The titrant (0.01 N-potassium hydroxide in water) was prepared from a 0.1 N KOH stock solution received from Sigma-Aldrich (USA).

5.1.2.2 Preparation of Stock Solutions

Coupling Buffer 0.01 M potassium phosphate containing 0.15 M sodium chloride; pH is adjusted to 5.5 with 6 N HCl.

Coupling Agent Solution Prepared immediately before use, by adding 28.6 mg of EDCI to 50 ml of distilled water.

5.1.2.3 Coupling of DETA Procedure

This procedure was supplied by Sigma-Aldrich (USA), and is adapted for 50 mg of starting carboxyl-terminated magnetic particles.

Activation Particles are suspended by shaking vigorously in 10 ml of coupling buffer. After centrifugation, the supernatant is decantated. This activation is repeated three times. Finally, the particles are resuspended in 10 ml of coupling buffer.

Coupling of DETA First, 5 µl of DETA is dissolved in 50 ml of distilled water. Then, 4 ml of coupling agent solution is added to washed and resuspended particles. The particles are resuspended by shaking vigorously, and 10 ml of DETA solution are added. The solution is shaken gently at room temperature for 16-24 hours, while maintaining the pH between 4.5 and 6.0 with 0.1 M HCl. After the reaction has taken place, the solution is centrifuged, and the supernatant decanted off. The particles are further washed three times with distilled water, and either dried at 40°C in a vacuum oven prior to spectroscopic characterization, or washed (twice), reacidified in water at pH 3, and finaliy resuspended in 20 ml of DMF for titration.

5.1.2.4 Titration Apparatus

The titration experiments are done at room temperature using a TitraLab titration laboratory (Radiometer Analytical Copenhagen, Denmark) composed of a TIM90 Titration Manager, a ABU91 Autoburette high-precision burette station, and a SAM90 Sample Station. The samples are stirred using an overhead stirrer part of the SAM90. Titrations are performed using a combined pH electrode (Radiometer pHC2401). Nitrogen is bubbled throughout the titration, preventing CO_2 contamination.

5.1.2.5 Titration Procedure

Titrations are run in the continuous inflexion point IP mode, without predose and with a minimum/maximum speed fixed at 1%/min of a 10 ml burette. A smoothing parameter of 8 is used in the calculation of inflexion points.

5.1.2.6 Infrared Measurement

The DRIFT spectra of the DBSC-10 monolayer and DETA-reacted particles were obtained on a Bruker IFS-66 FT spectrometer, with an ellipsoidal mirror and a diffuse reflectance accessory (Spectra-Tech, Inc.). The spectrometer is equipped with a liquid N_2-cooled MCT mid infrared (MIR) detector. The spectra were obtained using 100 scans at a nominal resolution of 4 cm^{-1} and are presented without base-line correction. A sample of KBr powder (IR, grade, Aldrich) is used as the background. The sample is diluted by grinding with a mortar and pestle to approximately 20% by volume in KBr.

5.1.2.7 X-ray photoelectron spectroscopy (XPS)

XPS spectra are obtained on an ESCALAB 220i-XL Fisons Instruments with a Al monochromatic source at a take-off angle of 90° to the sample. The instrument is calibrated using the pure $Ag_{3d5/2}$ band (368.25 eV). The survey spectrum is recorded using a constant analyzer energy (CAE) of 100 eV and the element spectra uses a CAE of 50 eV corresponding to an energy resolution of 1.2 eV. The powder sample is placed on a copper ribbon and maintained under a background pressure of $1x10^{-9}$ torr for approximately one hour in the sample chamber before spectral acquisition. The flood gun is set at 6 eV. Background charging is determined by the shift in the C_{1s} band normally at 284.8 eV at the end of a series of narrow scans for each sample. The software XPS Peak

Fitting Program for Win95 (XPSPEAK95) version 3.1 (Raymund W.M. Kwok editor) is used for deconvolution work.

5.1.3 Results and Discussion

5.1.3.1 DRIFTS

DRIFTS spectra of the DBSC-10 monolayer before (a) and after (b) DETA reaction are presented in Figure 5-1-1. In both spectra a strong N-H stretch band is seen at 3319 cm^{-1} in (a) and 3315 cm^{-1} in (b).[9,10] The sharper peak in (b) indicates the presence of weaker hydrogen bonded amide groups. A rearrangement of the DBSC-10 molecules on the surface of the maghemite from DETA-reaction accounts for less hydrogen-bonding of the amide groups of DBSC-10. At the same time, the new amide linkage of DBSC-10 and DETA can be involved (H-bonded) or not with other amide or carboxylic head groups. A confirmation of the presence of DETA in (b) is seen with the appearance of a strong peak at 1018 cm^{-1}, associated with the C-N stretch of alkyl amines.[11]

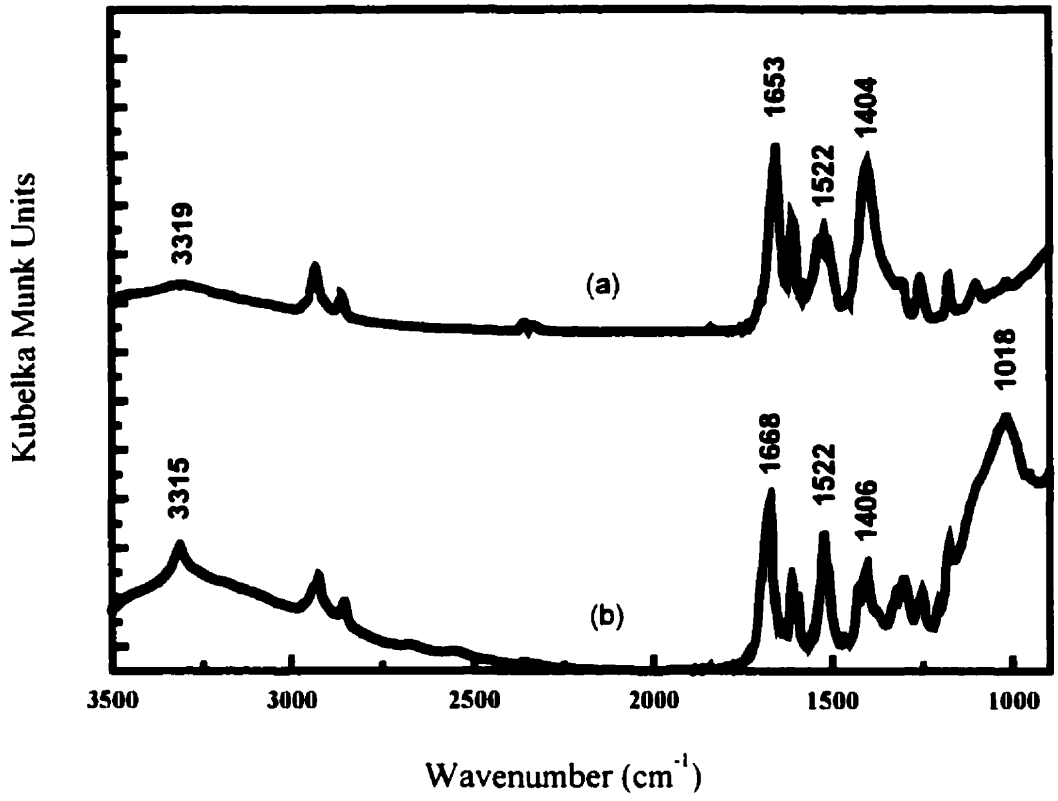

Figure 5-1-1: DRIFTS spectra of the DBSC-10 monolayer before (a) and after (b) reaction with DETA.

Figure 5-1-2 expands the methylene region 3000-2800 cm^{-1} of the spectra in Figure 5-1-1. Here again can be seen an effect of the rearrangement of the DBSC-10 molecules onto maghemite upon DETA reaction, with shifts of both asymmetrical and symmetrical CH_2 bands to lower wavenumbers; from 2931 to 2858 cm^{-1}, respectively in (a), to 2924 and 2852 cm^{-1} in (b). More information about the tilt angle of alkyl chains cannot be determined directly by DRIFTS, since the maghemite surface is not a flat substrate which can be analyzed by grazing angle methods.

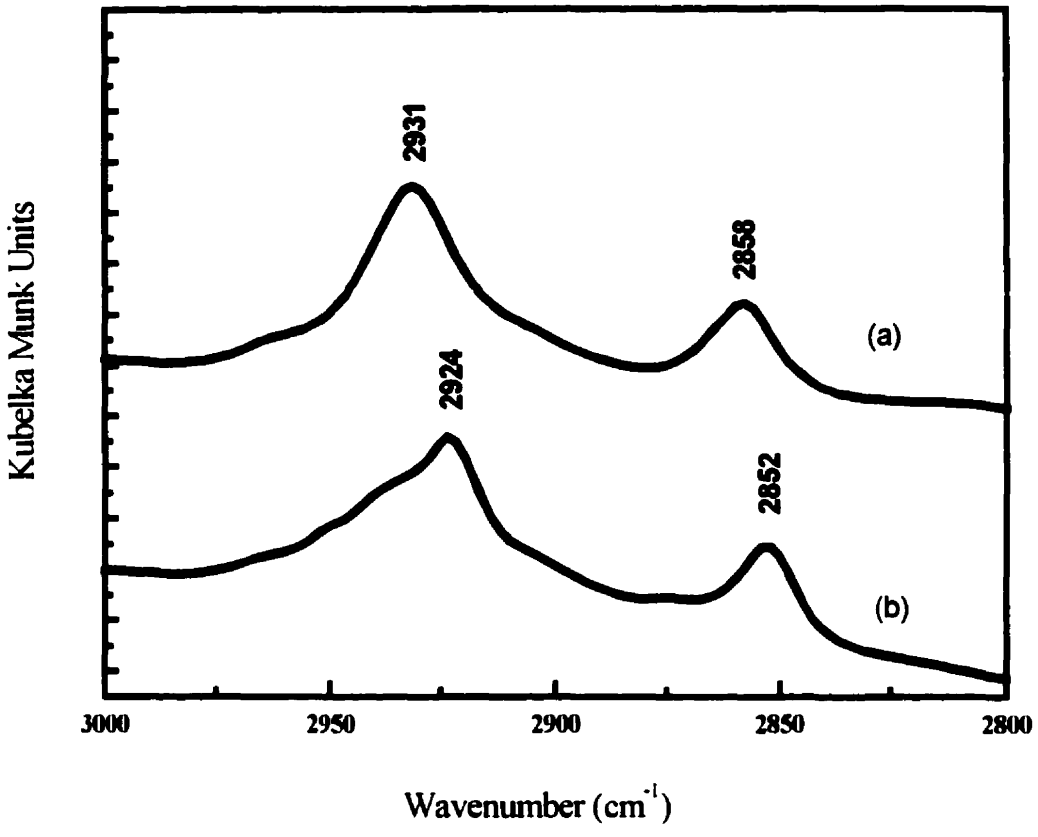

Figure 5-1-2: DRIFTS spectra of methylene associated peaks for the DBSC-10 monolayer before (a) and after (b) reaction with DETA.

An enlargement of the region 1750-1400 cm^{-1} is presented in Figure 5-1-3, for the monolayer before (a) and after (b) DETA reaction. Evidence of rearrangement of the DBSC-10 molecules in (b) is seen in the shift of the 1653 cm^{-1} band, corresponding to the asymmetrical stretch of the carboxylate group, to 1672 cm^{-1}. Less mobility of the oligomethylene chains, as seen in Figure 5-1-2 seems to therefore be adjusted by tilting of the headgroups. The position of the symmetrical band of the carboylate group remains practically unchanged, varying only from 1404 cm^{-1} to 1406 cm^{-1}. The difference between the asymmetrical and symmetrical peak positions in (b), $\Delta\nu = 266$ cm^{-1}, is still high enough

to indicate the presence of unidentate complexes (see Section 3.3.2 and Figure 3-5), while tending towards the values associated with asymmetrical bidentates.[12]

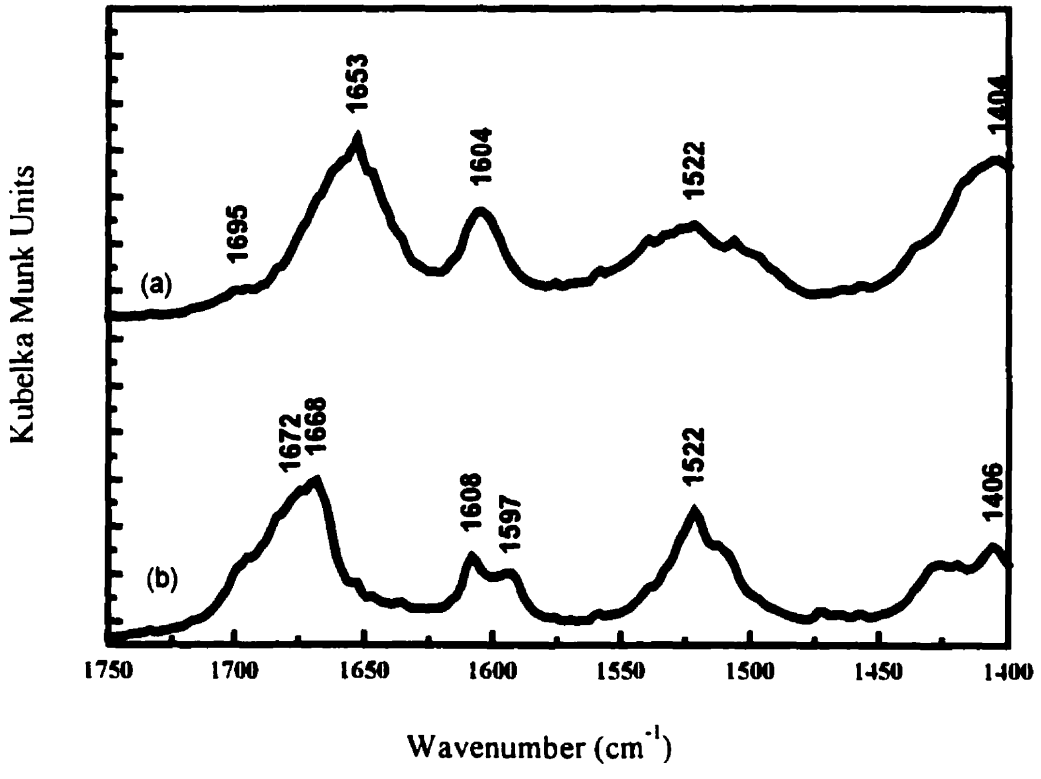

Figure 5-1-3: DRIFTS spectra of the DBSC-10 monolayer before (a) and after (b) reaction with DETA.

In both spectra (a) and (b) bands associated with amide I and amide II vibrations are seen around 1668 and 1522 cm^{-1}, respectively. Furthermore, a new amine band appears at 1597 cm^{-1} in (b), which is associated with the deformation vibration of the primary amine of DETA. The IR peaks of interest are summarized in Table 5-1-1.

Table 5-1-1: Assignment of IR peaks obtained from DRIFTS spectra of the DBSC-10 monolayer before and after reaction with DETA.

Mode Assignment	Before DETA	After DETA
ν(CH_2 asym stretch)	2931	2924
ν(CH_2 sym stretch)	2858	2852
ν(C=O) H-bonded acid	1695	1695
ν(COO^- asym stretch)	1653	1672 (shoulder)
ν(COO^- sym stretch)	1404	1406
ν(C=C ring stretch)	1604	1608
ν(amide I)	1668	1666
ν(amide II)	1522	1522
ν(NH stretch)	3319	3315
ν(NH_2 deform)	nd	1597
ν(C-N stretch) alkyl amines	nd	1018

nd: not detectable.

5.1.3.2 XPS

XPS spectra of the DBSC-10 monolayer before (a) and after (b) DETA reaction, are shown in Figure 5-1-4. The dotted lines in both spectra show deconvoluted $Fe_{2p3/2}$, O_{1s}, C_{1s}, and N_{1s} peaks which are summarized in Table 5-1-2. The numbered O_{1s}, C_{1s}, and N_{1s} bands are referred to the ones seen in Figure 5-1-5 of the DBSC-10 and DBSC-10-DETA-reacted molecular structures, and reflect the different chemical environments of these atoms. The fractional area of each component rounded to the nearest 1% is also given.

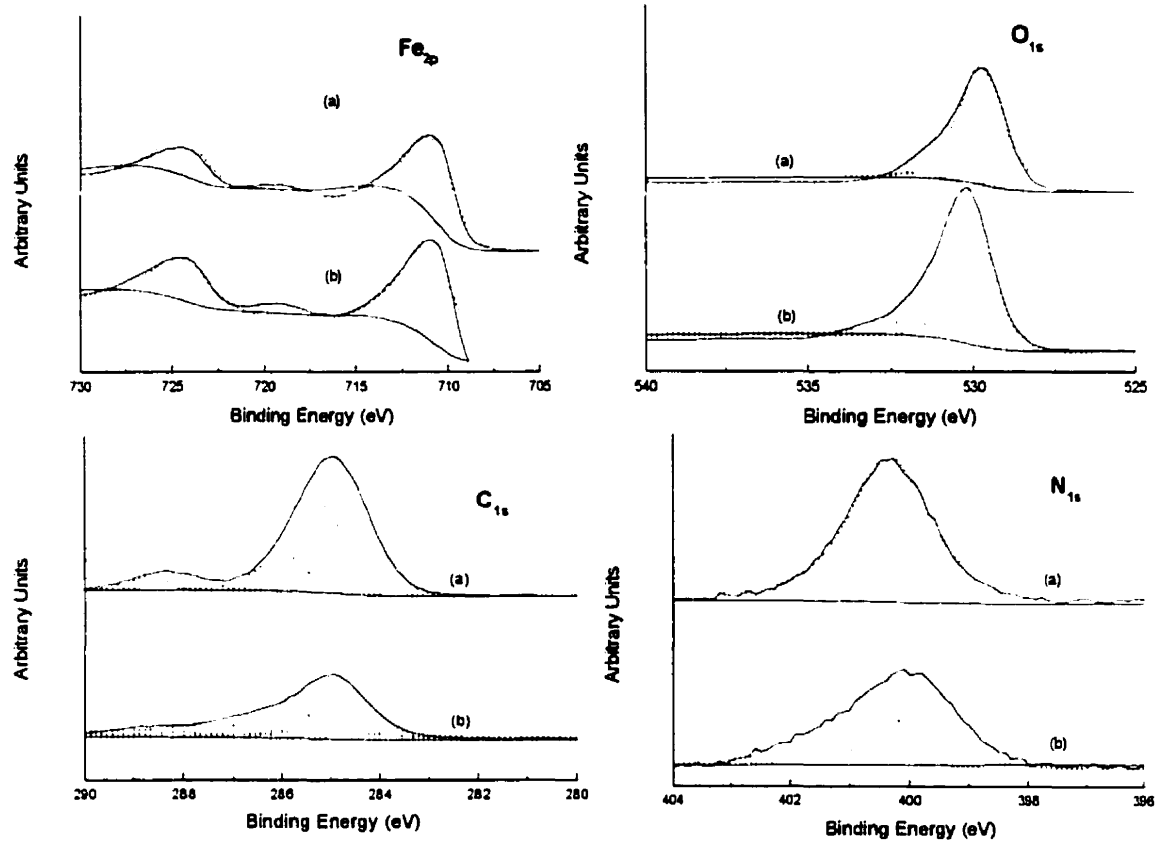

Figure 5-1-4: XPS spectrum of narrow scans for the elements of interest on carboxy-terminated maghemite surfaces before (a) and after (b) reaction with DETA.

Table 5-1-2: Binding energies (eV) of X-ray photoelectrons and related area percentages.

Peak		BE (eV)	Area % Before DETA	Area % After DETA
$Fe_{2p3/2}$		710.8		
O_{1s}	oxide	529.8	82	60
	1	530.8	11	30
	2	532.0	7.0	11
C_{1s}	1	284.6	37	26
	2	285.1	36	26
	3	286.0	17	32
	4	287.6	5.0	11
	5	289.0	5.0	6.2
N_{1s}	1	399.8		33
	2	400.3	100	51
	3	401.5		15

Band positions are accurate to ± 0.5 eV.

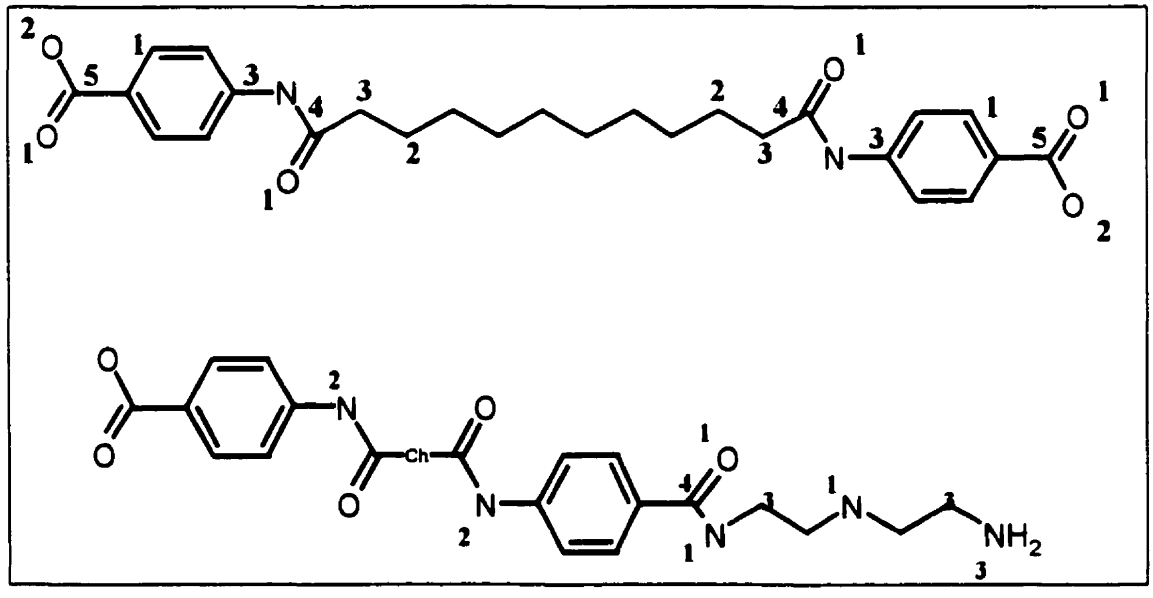

Figure 5-1-5: Structures of DBSC-10 and DETA-reacted DBSC-10 with labeled atoms.

As expected, there are no spectral changes in the bands at 724.3 and 710.8 eV of iron ($Fe_{2p3/2,\ 2p1/2}$) before and after the DETA-reaction.[13] The band in the oxygen (O_{1s}) spectrum (b) is more symmetrical than the band in (a), due to oxygen species present at higher binding energies. Deconvolution of spectrum (b) still indicates the presence of oxides at 529.8 eV. There is an increase in both the higher energy bands at 530.8 eV, corresponding to carbonyl oxygen from carboxylic and amide groups, and 532.0 eV, corresponding to single bonded oxygen from carboxylic.[14] An area % ratio of these last two oxygen peaks of 3 (30:11), suggests that not all DBSC-10 molecules have reacted with DETA.

The XPS spectrum of carbon C_{1s} after the DETA reaction does not reveal the valley between higher and lower binding energies seen in spectrum (a). There are still five distinct carbon bands in the deconvoluted spectrum (b). The band at 284.6 eV originates from the carbon in the two aromatic rings, while the position 285.1 eV is characteristic of carbon in a hydrocarbon chain. Band 3 is seen at 286.0 and corresponds to carbon atoms in the vicinity of a nitrogen atom, i.e. the two end carbon atoms from the hydrocarbon chain, the two aromatic carbon atoms positioned exactly next to the nitrogen atoms, and the DETA carbon atoms. The higher energy bands 287.6 and 289.0, are characteristic of amide carbonyl (from DBSC-10, not reacted and DETA-reacted) and carboxylic carbonyl, respectively. Inspection of Table 5-1-2 shows that the area % of bands 1 and 2 have decreased with respect to the higher energy ones after DETA reaction. A net increase in both bands 3 and 4 is associated with the presence of reacted DETA molecules. The ratio of bands 4 to 5 which used to be 1 (5:5) before DETA, is now at 1.8 (11:6.2), which

seems to indicate that one out of two DBSC-10 molecules, which gives a ratio of 1.7 (5:3), has reacted with DETA to form new amide linkages.

A close examination of the nitrogen spectrum (b) shows that the nitrogen band is broader and more asymmetric than the same band in (a). Deconvolution of the nitrogen band in (b) results in three distinct bands centered at 399.8, 400.3, and 401.5 eV, which correspond to non-hydrogen-bonded N-H from amide, secondary amine from DETA; H-bonded N-H from amide, and protonated primary amine from DETA, respectively. The free acidic head groups of DBSC-10 molecules on maghemite are responsible for the protonation of the primary amine groups of DETA molecules. The area % associated with these three nitrogen bands, 33, 50 and 15% respectively, support the hypothesis that one out of two DBSC-10 molecules has reacted with DETA, which is respectable fraction taking account the steric hindrance of these molecules assembled onto the maghemite surface. This value would correspond to an amount of DETA on the surface of about 2.1 μmole per 25 mg of particles assuming a DBSC-10 packing density as calculated in Chapter 4.

5.1.3.3 Titration

Figure 5-1-6 presents the titration curves of 25, 50 and 75 mg of DETA-reacted particles. The general shape of the curves differs from the one obtained in the titration of DBSC-10 coated particles (see Chapter 4), in that it does not solely indicate the titration of a weak acid anymore, i.e. presence of a plateau and one single sharp inflexion point (see

section 4.3.1). In fact, there are two inflexion points in the titration curves of Figure 5-1-6 and no discernable plateau.

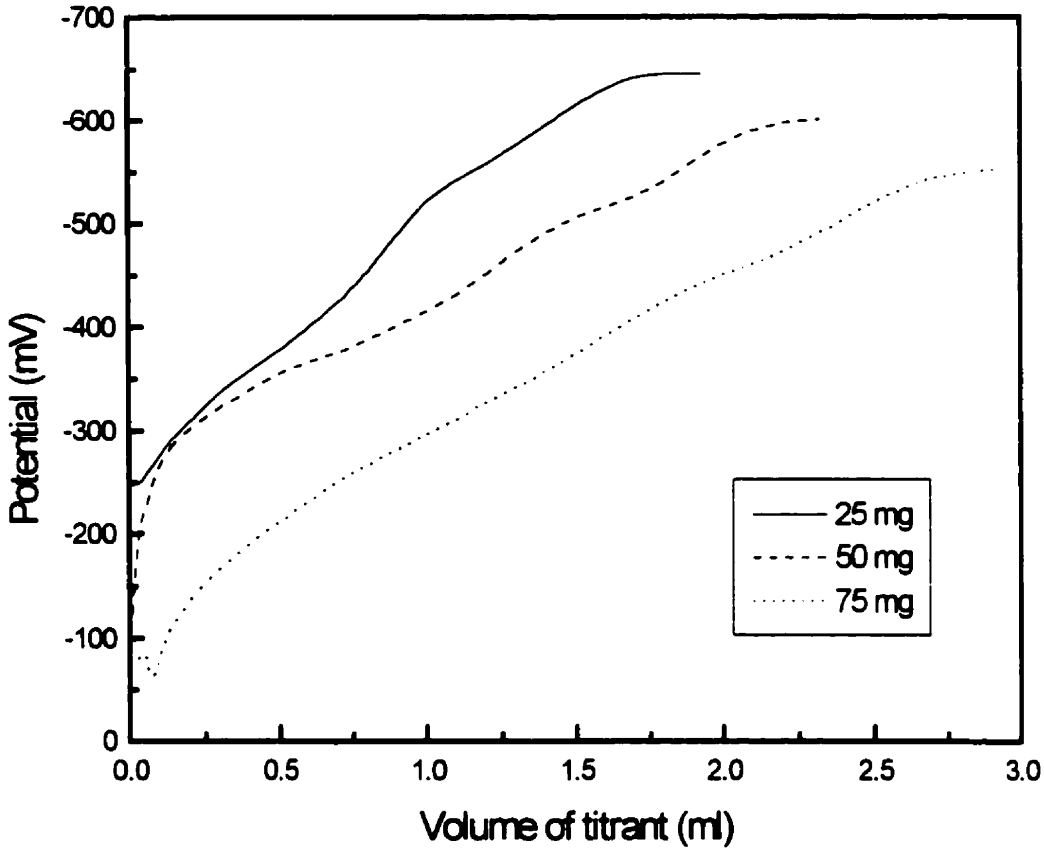

Figure 5-1-6: Titration of DETA reacted particles (—) 25 mg, (—) 50 mg, and (···) 75 mg.

The corresponding inflexion points, calculated by the first derivative of the curves in Figure 5-1-6, are seen in Figure 5-1-7. The height of the inflexion points decreases from 25 to 75 mg, due to dilution effects, but the difference between the titrations endpoints, corresponding to the volume of titrant added at the second inflexion point, is constant at 0.5 ml.

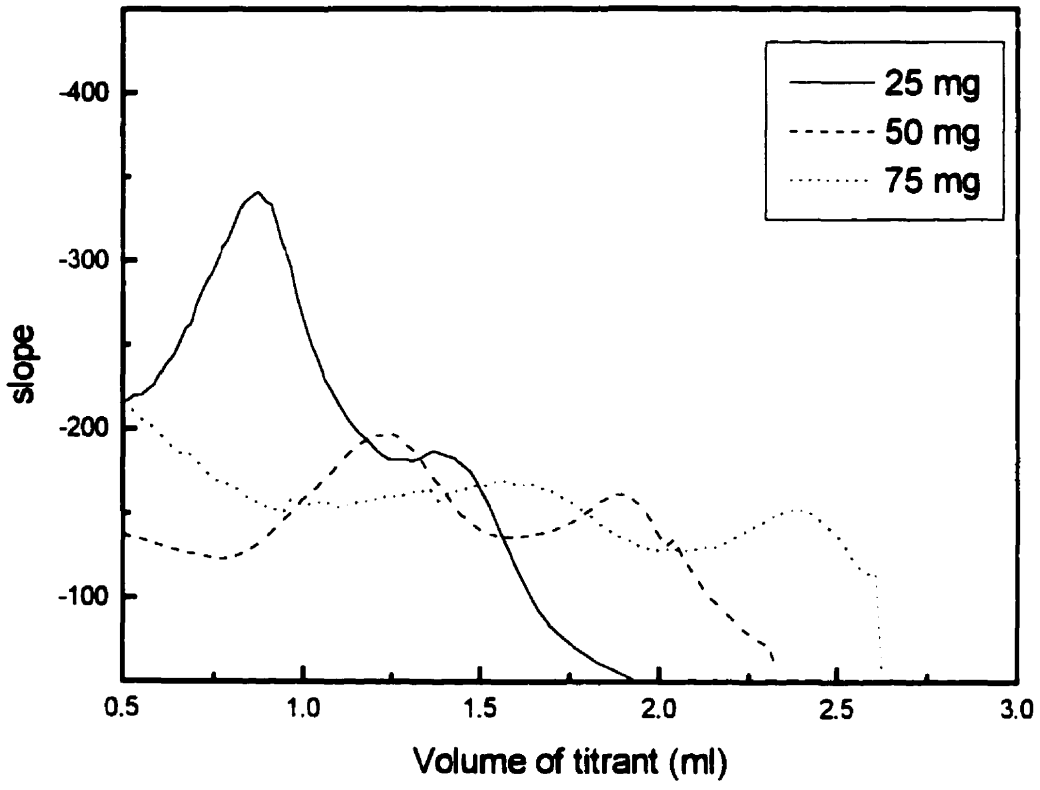

Figure 5-1-7: Inflexion points of DETA reacted particles (—) 25 mg, (—) 50 mg, and (···) 75 mg.

The two inflexion points are due to the titration of both the protonated amine and protonated carboxylic groups present after reacidification. As seen in Figure 5-1-8, the titration to basic form can take two different paths, similar to the titration of amino acids, i.e., either the protonated amine or the protonated carboxylic group can titrate first. The major neutral form of any α-amino acid is however, the zwitterion (minor form 1 part out of 10^5).[15] An application of this general rule could be that titration is, in this case, indicative of the ratio of DETA to DBSC-10 present on the DETA-reacted particles. The first inflexion point is associated with the titration of the carboxylic group.[16] The basic

form is attained at the second inflexion point, i.e., both the amine group and the carboxylic group are titrated. The constant volume of base added of 0.5 ml per 25 mg of DETA-reacted particles, corresponds to the average volume obtained in the titration of DBSC-10 coated particles (see section 4.3.2), and excludes the possibility of cross-linking of DETA molecules to carboxyl-terminated maghemite surface, which would decrease the amount of base required for titration.

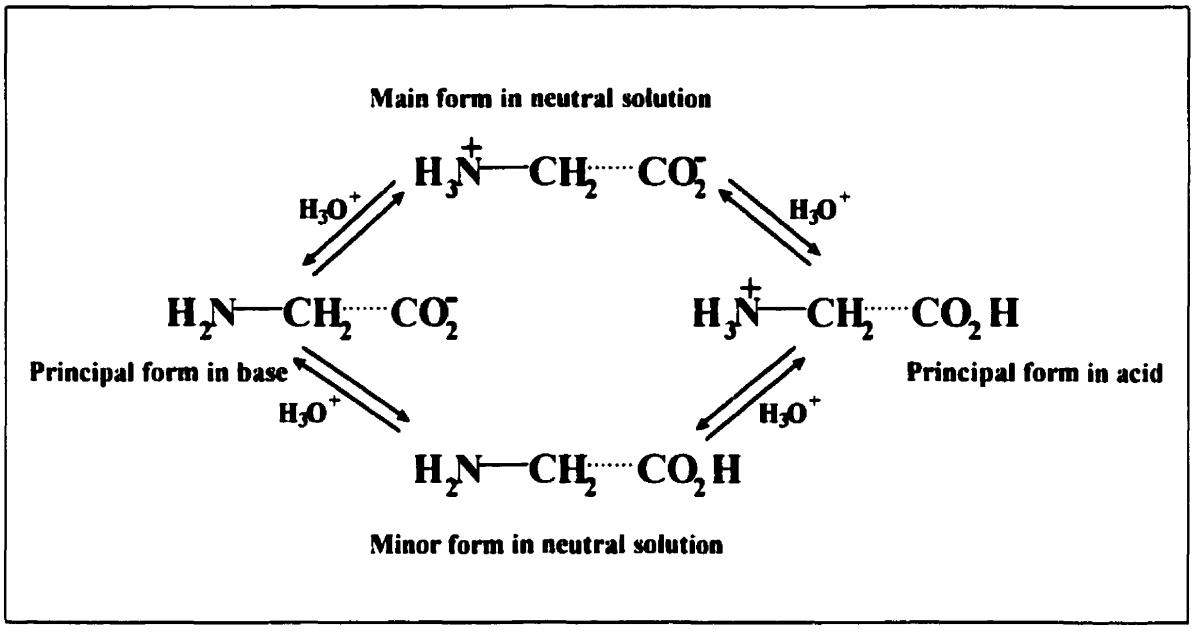

Figure 5-1-8: Acid-base properties of amino acids.

Tables 5-1-3 and 5-1-4 summarize the data used in the calculation of the amounts of carboxylic and amine groups, obtained from the inflexion points presented in Figure 5-1-7. The mean results obtained are 3.4 μmole and 1.4 μmole, for the carboxylic groups and the amine groups, respectively. Table 5-1-5 shows these values to be reproducible within about 30% of the replicate titration means.

The higher end of the reproducibility limit for amine groups, corresponding to the amount of DETA-reacted particles, i.e., 2.0 μmole, approximates the value of 2.1 μmole per 25 mg of carboxy-terminated particles, obtained from XPS results. This would again tend towards a ratio of DBSC-10 to DETA reacted molecules of 1:1.

Table 5-1-3: Inflexion points results of DETA-reacted particles.

Amount of Particles (mg)	Inflexion Point No 1 (ml)	Inflexion Point No 2 (ml)
25	0.873	1.41
50	1.24	1.90
75	1.56	2.38

Table 5-1-4: Titration results of replicates.

Replicate #	Result No 1 (μmole)	Result No 2 (μmole)
1	3.7	1.2
2	3.2	1.6

Replicates are based on 25 mg differences of magnetic carriers.

Table 5-1-5: Reproducibility of the titration results between 25 mg increments of DETA-reacted particles.

Results	Number of replicates	Mean	Sample standard deviation	80% confidence interval
No 1	2	3.4	0.35	3.4 ± 0.76
No 2	2	1.4	0.28	1.4 ± 0.61

5.1.4 Conclusions

The ligand DETA has been successfully coupled to carboxy-terminated maghemite particles using a typical carbodiimide EDCI. The reaction is through the formation of amide linkages between the free carboxylic group of self-assembled DBSC-10 molecules and a primary amine of DETA. Infrared measurements confirm the presence of DETA on the maghemite particles from the appearance of strong C-N stretch and NH_2 deformation, peaks. Even though molecules of DBSC-10 still show significant hydrogen bonding of amide linkages, reorganization of these molecules on the maghemite surface occurs from the reaction with DETA, as seen from the shift of both the asymmetrical and symmetrical CH_2 stretch peaks to lower wavenumbers. The unidentate complex carboxylate-iron from maghemite could be tending towards an asymmetrical bidentate conformation.

The various area percentages obtained from the deconvolution of XPS peaks of the atoms of interest tend to show that one molecule of DBSC-10 out of two has reacted with DETA molecules, forming new amide linkages. The ratio of C_{1s} from amide (band 4) to carboxyl (band 5) went from 1 (5:5) before DETA to 1.8 (11:6.2) after DETA.

Titration of DETA-reacted particles confirmed the presence of protons originating from different chemical environments, namely from protonated amine and protonated carboxylic groups. A 1:1 ratio of DETA-reacted DBSC-10 to DBSC-10 molecules is approximated from these results, which supports the XPS results. The amount of base required for the complete titration of both the amine and carboxylic groups is constant (0.5 ml per 25 mg of DETA-reacted particles) and agrees with the amount of base

required for the titration of self-assembled DBSC-10 molecules on maghemite, excluding the possible cross-linking reaction of DETA to free carboxylic groups.

References

[1] Kauffman, G.B. (ed.), "Coordination Chemistry. A Century of Progress", ACS Symposium Series, No. 565, American Chemical Society, Washington (1994).

[2] Liu, Q., Ph.D. Thesis, McGill University, Canada (1996).

[3] Hubbard, K.L., Darling, G.D., Finch, J.A., Minerals Engineering, **10** (1), 41-54 (1997).

[4] Martell, A.E., Hancock, R.D., in "Metal Complexes in Aqueous Solutions", Modern Inorganic Chemistry, series ed. John P. Fackcler, Jr., Plenum Press, USA (1996).

[5] Constable, E.C., in "Metals Ligand Reactivity", Series in Inorganic Chemistry, series ed. J. Burgess, Ellis Horwood, England (1990).

[6] Paquette, L.A., in "Encyclopedia of Reagents for Organic Synthesis", Wiley & Sons, USA (1995).

[7] Solomons, G.T.W., in "Organic Chemistry", 2 nd ed., Wiley & Sons, USA (1980).

[8] Procedure for Product No. I 7518 from Sigma (1994).

[9] Bellamy, L.J., in "The Infrared Spectra of Complex Molecules", vol.1, 3 rd ed., Chapman and Hall, London (1975).

[10] Silverstein, R.M., in "Spectrometric Identification of Organic Compounds", 5 th ed., Wiley & Sons, USA (1991).

[11] Colthup, N.B., Daly, L.H., Wiberley, S.E., in "Introduction to Infrared and Raman Spectroscopy", 3 rd ed., Academic Press, USA (1990).

[12] Nakamoto, K., in "Infrared and Raman Spectra of Iorganic and Coordination Compounds", 5 th ed., Wiley & Sons, USA (1997).

[13] Briggs, D., Seah, M.P., in "Practical Surface Analysis", 2 nd ed., vol(1), John Wiley & Sons, England (1990).

[14] Beamson, G., Briggs, D., in "High Resolution XPS of Organic Polymers", John Wiley & Sons, England (1992).

[15] Loudon, G.M., in "Organic Chemistry", 2 nd ed., Benjamin /Cummings, USA (1988).

[16] Anderson, N.J., Bolto, B.A., Eldridge, R.J., Jackson, M.B., Reactive Polymers, **19**, 87-95 (1993).

Chapter 5

Section 2:

TEM Imaging of DETA-Terminated Magnetic Carriers

Summary

The surface morphology of prepared maghemite based magnetic carriers has been imaged at the nanometre scale by transmission electron microscopy (TEM) using an advanced Pt/C replica technique. TEM images confirm the presence of a modified maghemite surface by the absence of dodecahedron-like structures evident in a sample of bare untreated maghemite. Surface defects are also visible from the TEM image of the carriers, probably originating from the reaction of half of the carboxylic groups of the carboxy-terminated maghemite with DETA molecules. Finally, a well-ordered monolayer is inferred by the halo seen around some of the carriers particles.

5.2.1 Introduction

The surface morphology of magnetic carriers is commonly investigated by scanning electron microscopy (SEM),[1] while molecular self-assembled films are typically analyzed by atomic force microscopy (AFM).[2] In this study, the resolution limit of SEM (0.1-1 μm) is not sufficient to determine the morphology for this sample of maghemite particles, which have an average particle size of 23 nm. Furthermore, even though AFM can study morphological features at a fine scale, it is usually applied to *in situ* investigations of smooth surfaces, and is therefore not a suitable technique in the study of monolayers at the surface of particles having rough and irregular topography. An alternative technique is imaging replicas using transmission electron microscopy (TEM). Replicas are prepared by condensation of heavy metals (e.g., Au, Ag, and Pt) on the magnetic carrier surface. This "decoration and shadowing" technique offers a unique opportunity to investigate the detailed characteristics of surface morphologies with resolution near 1 nm. Recently this technique has been applied to the study of the surface morphology of ZrO_2-Al_2O_3 fibers, where very fine grain morphologies (<50 nm) were observed.[3] In the present work, the monolayer thickness, dictated at the base by the length of the surfactant (DBSC-10) monomers, is approximately 2 nm, and consequently this replicas technique can be used to image the monolayer on the maghemite particles.

5.2.2 Experimental

5.2.2.1 Materials

A sample of bare maghemite was used without pre-treatment, i.e., no heating. The preparation procedure of the carboxyl-terminated magnetic particles is described in section 3.2.3. The preparation procedure of the DETA-magnetic carriers (DETA-reacted carboxyl-terminated magnetic particles) is described in section 5.1.2.3. A sample of each was prepared and dried at 40°C in a vacuum oven prior to spectroscopy characterization.

5.2.2.2 TEM

The surface microtopography of individual particles was examined on high-resolution replicas by TEM. The replicas consist of a thin platinum/carbon (Pt/C) film (95Pt/5C wt % and 1-2 nm thick) and a supporting carbon film (15-29 nm thick). Particles were dispersed on a freshly cleaved mica surface. The shadowing and replication procedure was performed in a freeze-etch unit (Balzer 400) under high vacuum (1.333×10^{-4} Pa) and at room temperature. An extremely fine granular Pt/C film was condensed on the crystal surface by an electron beam evaporation gun as a point source at an angle of 30° and a distance of 15 cm. Instrumental conditions (i.e., acceleration potential and emission current) allowed a Pt/C deposition rate of 0.25 nm s^{-1}. The thickness of the metal film was determined by measuring the frequency shift of a quartz crystal thin film oscillator that was mounted as close as possible to the object. The centering rod of the evaporation gun was pointed halfway between the quartz and specimen holder. In cases where the orientation of the quartz crystal and the object were the same (with respect to the angle of the incident beam), the actual thickness of the metal film was compared directly with that measured by

the quartz monitor. However, a more acurate thickness of the metal film was assessed by positioning the quartz crystal perpendicular to the direction of incident flux of Pt/C atoms. By knowing the oblique angle of the gun with respect to the specimen stage, the actual deposition rate and thickness of the metal film on the sample surface were calculated.

A supporting carbon film was immediately condensed on the Pt/C coating by a vertical electron beam gun at 90° and 12 cm away from the surface of the specimen for 6 seconds. Under the optimal operational conditions and a deposition rate of 2.5 nm s^{-1}, a total thickness of approximately 15 nm carbon film was produced. The replica was cleaned by dissolving the particles adhering to the replica with a 6% HF solution, rinsed with deionized water and transferred onto 300 mesh TEM grids. TEM imaging was performed with a JEOL 2000 FX at an accelerating voltage of 100 kV.

5.2.3 Results and Discussion

Figure 5-2-1 represents the surface microstructure of the bare maghemite sample. A TEM magnification of ×25K was used. The picture taken from the TEM image, which is the one presented here, has been magnified ×3.

This sample shows a good dispersion of the particles, which is expected from the presence of the surfactant introduced in the manufacture of maghemite to prevent aggregation. Fines are present in this sample, as seen by the presence of some particles with diameters below 10 nm.

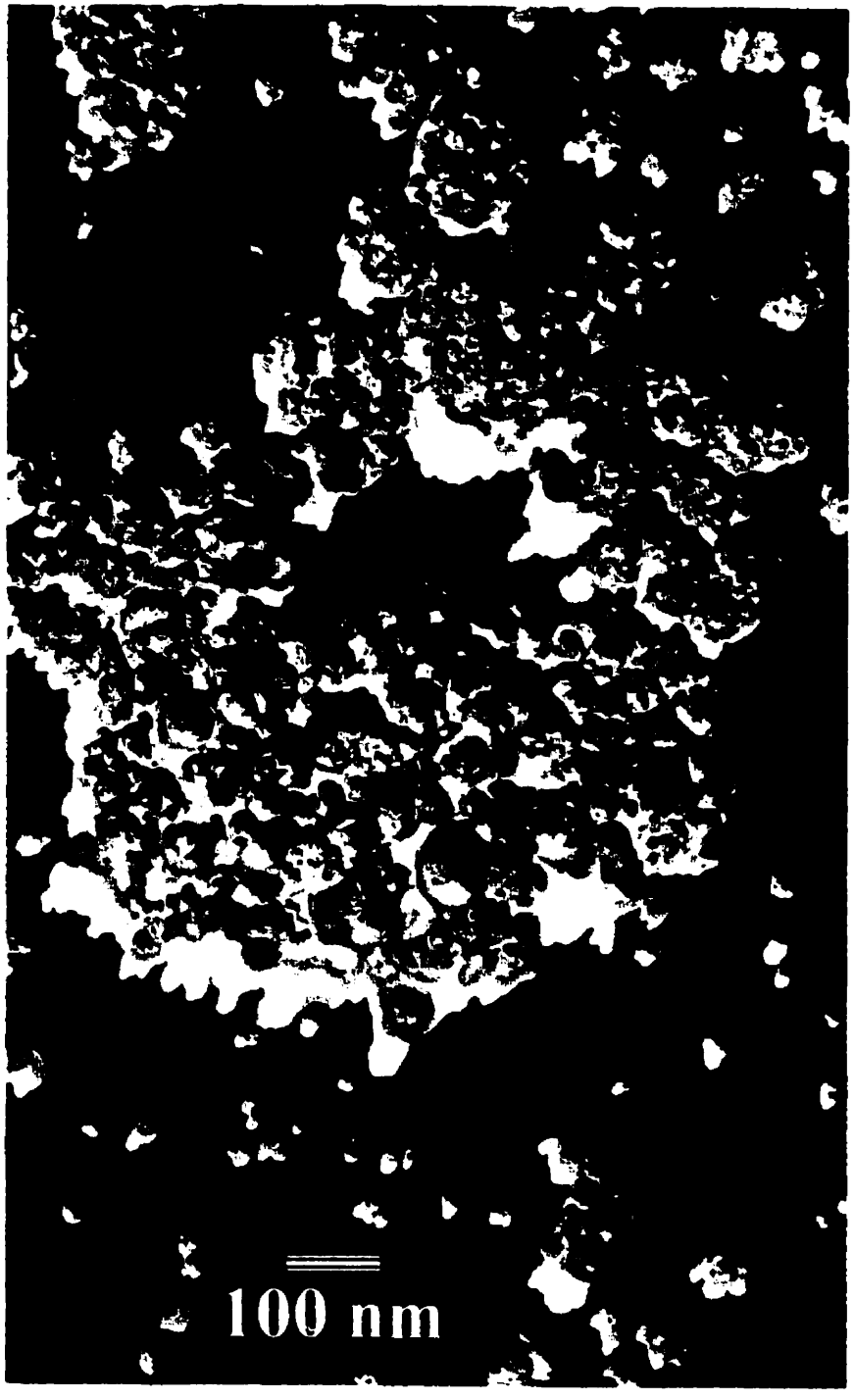

Figure 5-2-1: TEM image of a bare maghemite sample.

The TEM image at a much higher magnification, Figure 5-2-4(a) reveals the presence of faces on some of the particles, (see particle labelled 'D'), approximating the morphology of dodecahedrons (12 faces). When faces of particles are not clearly distinguishable, the perimeter can be seen to display hexagonal shapes, as seen from Figure 5-2-4(a) on the particle labelled 'E'. This seems to indicate that this "stabilization surfactant" is composed of short-chained molecules that do not self-assemble, since the original shape of maghemite particles is still distinguishable.

The surface microstructure of the maghemite carboxy-functionalized by DBSC-10, is presented in Figure 5-2-2, (at similar magnifications as in Figure 5-2-1). Less dispersion is exhibited by this sample than in the sample of bare maghemite. This is probably due to the fact that the particles were dried in a vacuum oven prior to TEM characterization, making their redispersion in water onto mica surfaces more difficult.

As seen from both Figure 5-2-2 and Figure 5-2-4 (b), the same picture at a much higher magnification, the dodecahedron shape of the individual particles in this sample, cannot be distinguished. This indicates the presence of a layer on the surface of the particle. The presence of an ordered pattern, revealed on some particles, can be extended to confirm the presence of a well-ordered layer, or self-assembled monolayer, of a longer chain-type surfactant.

The last sample analyzed by TEM, the DETA-terminated magnetic carriers, is seen in Figure 5-2-3. Here again, a TEM magnification of ×25K was used, while the picture taken from the TEM image, presented here, has been magnified ×3. The TEM image reveals the presence of a much more evenly size distributed sample (less fines below 10

nm) than seen in the previous two samples of bare and carboxy-functionalized maghemite. The particles are again here not well dispersed, as for the carboxy-functionalized sample, due to the intermediate drying step of particles prior to TEM characterization.

From the magnification of this last sample, Figure 5-2-4(c), a certain surface roughness of the particles can be detected, (similar to the "fuzz" on old tennis balls). This surface effect could be due to alternating thickness effects from a monolayer where one molecule of surfactant out of two has reacted with DETA molecules. A halo, labelled 'F' on Figure 5-2-4(c), is clearly distinguishable around some of the particles of this sample. This shadowing effect is one of the best images of the well-ordered surfactant molecules, self-assembled onto the maghemite particles.

Figure 5-2-2: TEM image of a carboxy-functionalized maghemite sample.

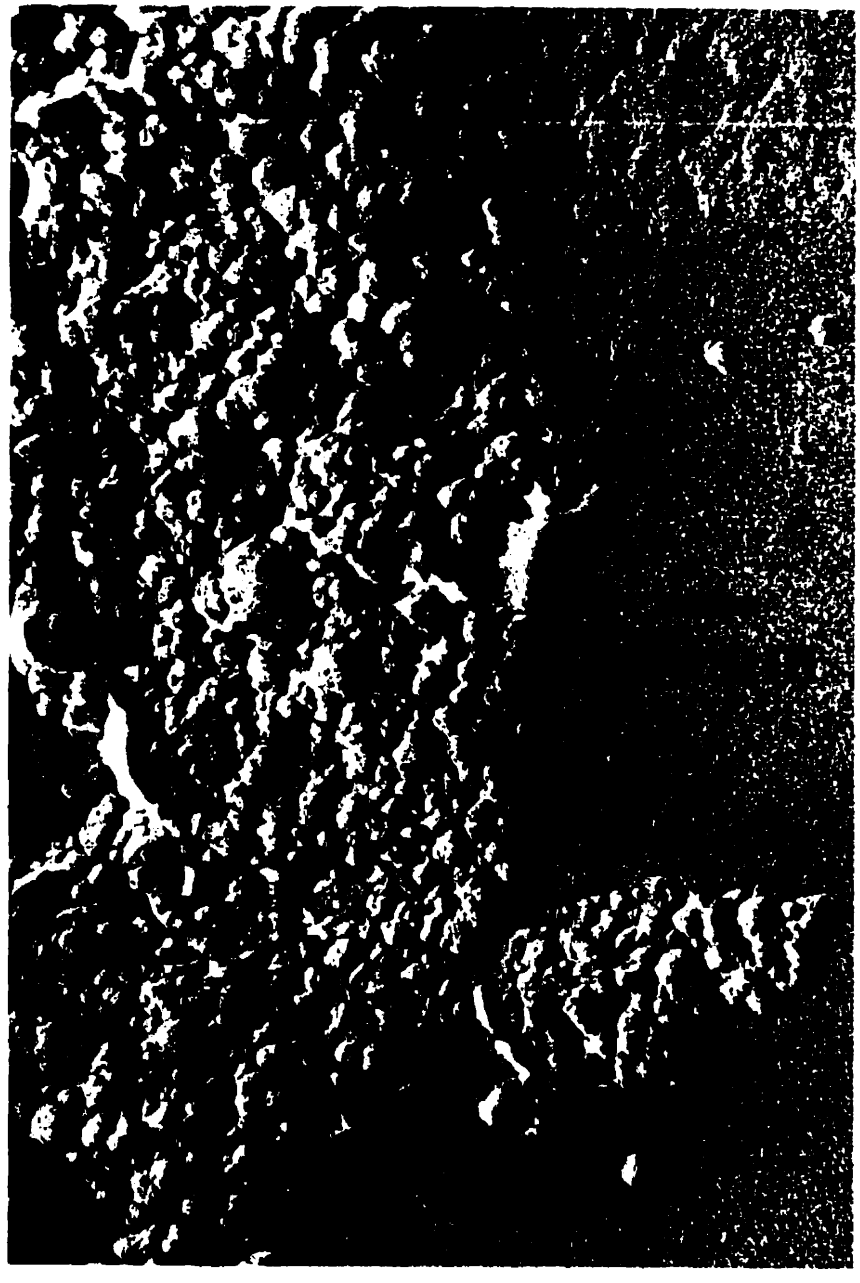

Figure 5-2-3: TEM image of DETA-modified maghemite, i.e. magnetic carriers.

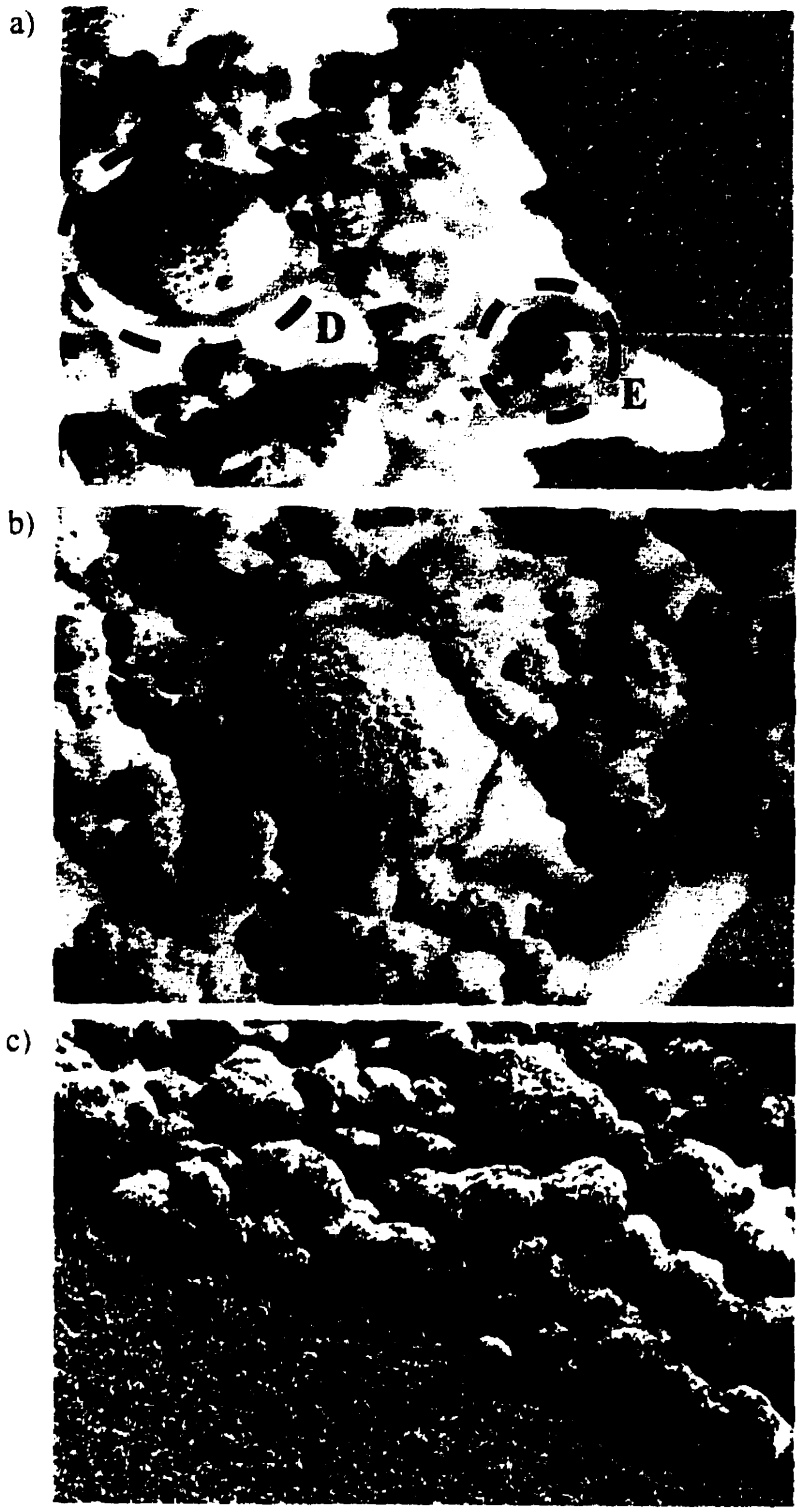

Figure 5-2-4: TEM images, at higher magnifications, of samples (a) bare, (b) carboxy-functionalized, and (c) DETA-modified maghemite, with special features (D) dodecahedron shape, (E) hexagonal perimeter, and (F) halo.

5.2.4 Conclusions

The surface morphology of bare and functionalized maghemite particles have been imaged at the nanometre scale by transmission electron spectroscopy using an advanced Pt/C replica technique. The dodecahedron shape of maghemite particles is distinguishable in a sample of untreated maghemite. The TEM images confirm the presence of a modified maghemite surface on samples of carboxy- and DETA-functionalized maghemite particles, as revealed by the absence of dodecahedron structures. Aligned patterns, already distinguished in the sample of the carboxy-terminated particles, are intensified by thickness effects in the image of the DETA-modified maghemite sample. This could be due to the reaction of half the carboxy-groups with DETA molecules. Finally, a visible halo around some of the particles in the last sample of the DETA-modified maghemite, clearly images the monolayer, formed of well-ordered surfactant molecules on the surface of particles.

References

[1] Ølsvik, O., Popovic, T., Skjerve, E., Cudjoe, K.S., Hornes, E., Ugelstad, J., Uhlen, M., Clinical Microbiology Reviews, 7 (1), 43-54 (1994).

[2] Ulman, A., in "Characterization of Organic Thin Films", Butterworth-Heineman, USA (1995).

[3] Vali, H., Allahverdi, M., Drew, R.A.L., Journal of Materials Science, **31**, 6177-6184 (1996).

Chapter 6

Complexation of Copper Ions by DETA-Terminated Magnetic Carriers

Summary

It has been shown that the prepared, DETA-functionalized, magnetic carriers are able to complex copper ions from dilute streams. Complexometric titration using a copper selective electrode indicates the complexation of 0.52 μmole of Cu^{2+} per 50 mg of magnetic carriers. This loading capacity, for example, is equivalent to the removal of 100 ppm of copper ions from a one liter solution by 3 g of magnetic carriers. XPS results confirm the presence of Cu_{2p} bands, indicating the loading of copper ions. A shift of the nitrogen N_{1s} bands to higher binding energies confirms the involvement of secondary amine and amide nitrogen atoms from DETA-functionalized carriers in copper complexation.

6.1 Introduction

Magnetic carriers offer a new perspective in wastewater treatment in two major ways. First, they offer the selectivity for targeted metal ions, which is of great importance in the separation of the metals from complex solutions.[1] Secondly, magnetic carriers can cope with effluents containing high levels of turbidity, and can easily be separated from slurries and even sludges.[2]

The ligand diethylenetriamine (DETA) is known to show excellent selectivity for the base metals Zn(II), Cu(II), and Ni(II), against Fe(III), Ca(II), Mg(II), and Al(III), present in mining effluents.[3] It is expected that the free ligand's behaviour should be similar to its behaviour once attached to the magnetic carrier, since the mode of attachment of DETA to the carboxy-terminated carrier (amide linkage) does not change the functionality of the ligand.[4]

The removal of copper ions from dilute aqueous solutions by complexation with DETA-terminated magnetic carriers, forming chelates, is studied. The ligand molecules of the magnetic carrier have four possible points of attachment to the metal ion (N and O from amide linkage, and N from NH and NH_2 groups), and are accordingly quadridentates. Note that DETA is a tridentate ligand. However, in the complexation of copper, it is possible that not all of the four groups may be involved in coordination. Water molecules can also serve has coordinating groups, since they can also donate a pair of electrons in forming a complex with a metal ion.[5,6]

Characterization of the chelates by complexometric titration using a copper selective electrode, will assess the copper loading capacity of the magnetic carriers.

Further characterization by XPS spectroscopy will give insight into the possible coordination geometry adopted by the chelates.

6.2 Experimental

6.2.1 Materials

The preparation of DETA-terminated magnetic carriers is described in section 5.1.2. The prepared particles are sequentially washed with distilled water (three times) and either dried at 40°C in a vacuum oven, prior to XPS measurements, or resuspended in 20 ml water for titration experiments. The titrant, 0.01 M cupric nitrate in water, was prepared from $Cu(NO_3)_2 \cdot 2^{1/2}H_2O$ received from Fisher Scientific (USA). The preparation of carboxy-terminated particles are described in section 4.2.3. The particles are washed three times in DMF, then sequentially washed in water (3 times), and resuspended in 10 ml water for titration.

6.2.2 Titration Apparatus

All titration experiments are done at room temperature using a TitraLab titration laboratory (Radiometer Analytical Copenhagen, Denmark) composed of a TIM90 Titration Manager, a ABU91 Autoburette high-precision burette station, and a SAM90 Sample Station. The samples are stirred using an overhead stirrer part of the SAM90. Titrations are performed using a copper selective electrode (Radiometer ISE25Cu) along with a calomel reference electrode (Radiometer REF401).

6.2.3 Titration Procedure

Titrations are run in the continuous inflexion point IP mode, without predose and with a minimum/maximum speed fixed at 2%/min of a 10 ml burette. A smoothing parameter of 8 is used in the calculation of inflexion points. Note that titrations of bare iron oxide (maghemite) surfaces are performed on oven dried (350°C) maghemite particles to model surfactant free surfaces (see section 3.3.1).

6.2.4 Copper Calibration Curve

The standard stock solutions of $Cu(NO_3)_2$ in water, corresponding to 10^{-3}, 10^{-4}, 10^{-5}, and 10^{-6} mol/L of Cu^{2+} ions are prepared. The calibration curve (Figure 6-1) is linear in the range 10^{-3} to 10^{-5} mol/L and is represented by the following equation:

$$potential(mV) = 27.75[Cu^{2+}] + 289.07 \qquad [6\text{-}1]$$

Direct measurements can be made from this titration curve as long as they are performed inside the pH 3 to 7 range. There is little need for recalibration, since the electrode sensitivity (slope) remains unchanged with time.

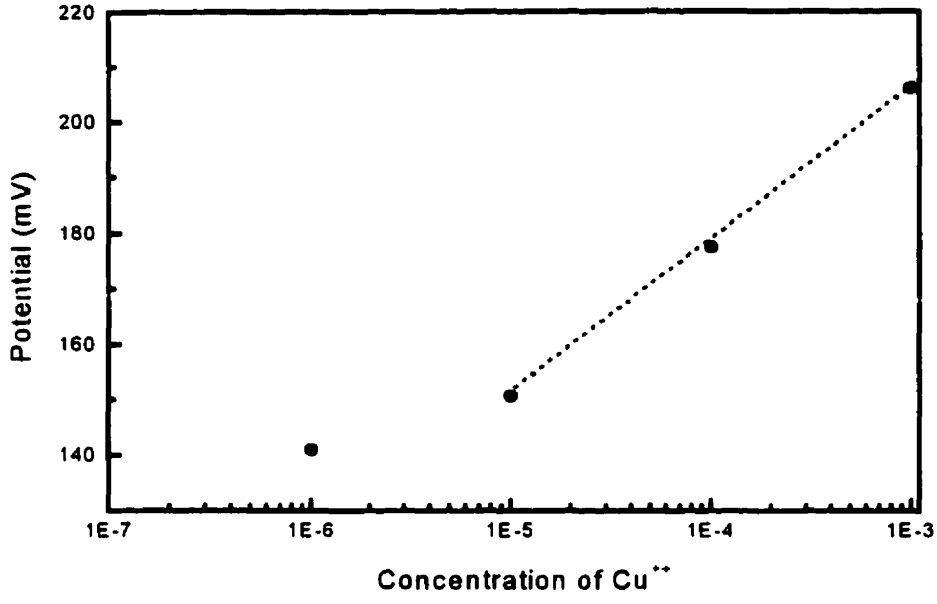

Figure 6-1: Calibration curve of the copper selective electrode.

6.2.5 X-ray Photoelectron Spectroscopy (XPS)

XPS spectra are obtained on an ESCALAB 220i-XL Fisons Instruments with a Al monochromatic source at a take-off angle of 90° to the sample. The instrument is calibrated against the pure $Ag_{3d5/2}$ band (368.25 eV). The survey spectra is recorded using a constant analyzer energy (CAE) of 100 eV and the element spectra uses a CAE of 50 eV corresponding to an energy resolution of 1.2 eV. The powder samples are placed on a copper ribbon and maintained under a background pressure of $1x10^{-9}$ torr for approximately one hour in the sample chamber before spectral acquisition. The flood gun is set at 6 eV. Background charging is determined by the shift in the C_{1s} band normally at 284.8 eV at the end of a series of narrow scans for each sample. The software XPS Peak

Fitting Program for Win95 (XPSPEAK95) version 3.1 (Raymund W.M. Kwok editor) is used for deconvolution work.

6.3 Results and Discussion

6.3.1 Complexometric Titration

Figure 6-2 shows the titration curves obtained for increasing amounts of magnetic carriers from 50 mg to 200 mg, by 50 mg increments. The complexometric titration curve of 200 mg of bare maghemite particles (dashed line) is also presented to demonstrate that the titration is not just due to the presence of particles in solution. In the case of the magnetic carriers, copper added to solution is complexed by DETA until it is detected by the selective electrode. If the first point of the linear calibration point is chosen, i.e., the lower detection limit, this corresponds to a potential of 150 mV. Note that the initial pH in solution before the first copper addition is around 6 and drops at the end of the titration, which is within the range permitted for direct measurements using the copper selective electrode. The formation of copper monohydroxy species ($CuOH^+$), between pH 5 and 6 at low concentration of copper in solution, is responsible for the decrease in pH.[7]

From Figure 6-2, the mean volume difference between 50 mg increments of magnetic carrier at 150 mV, is 0.052 ml. Table 6-1 shows this value to be reproducible within 6% of the replicate titrations mean.

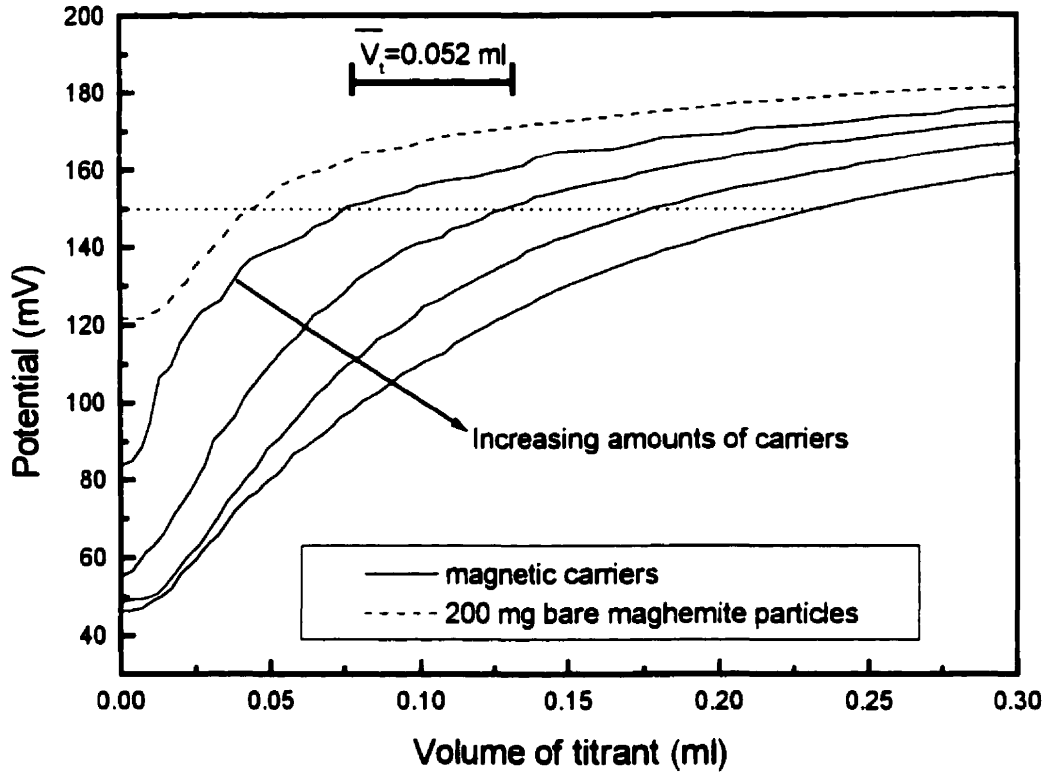

Figure 6-2: Titration of magnetic carriers and 200 mg of bare maghemite particles.

Table 6-1: Reproducibility of the volume differences.

Number of replicates	Mean difference* of titrant added	Sample standard deviation	90% confidence interval
4	0.052	0.0025	0.052 ± 0.0029

*Differences are for 50 mg increments of magnetic carriers.

This average volume corresponds to 0.52 μmole of Cu^{++} per 50 mg of magnetic carriers. The sampling volume of water being 20 ml, this also corresponds to the removal of 26 μM or 1.65 ppm of Cu^{++} from solution. With this carrying capacity value, it is estimated that 3 g of magnetic carriers is needed to remove 100 ppm of Cu^{++} from a one liter solution. This capacity value is about three times of that expected for amine-type magnetic carriers having only one primary amine functional group, i.e., where 10 g magnetic particles would remove the 100 ppm Cu^{++}.[8]

The curves obtained from the copper titration of increasing amounts of carboxyl-terminated (i.e., unmodified) magnetic carriers, from 50 mg to 100 mg, by 25 mg increments, is presented in Figure 6-3. The curve of 100 mg bare maghemite particles (dashed line) is also shown. It is seen that all the curves practically fall on the one of the bare particles, and hence it is concluded that the carboxyl-terminated carriers, as well as the bare particles, are not able to complex the Cu^{++} present in solution.

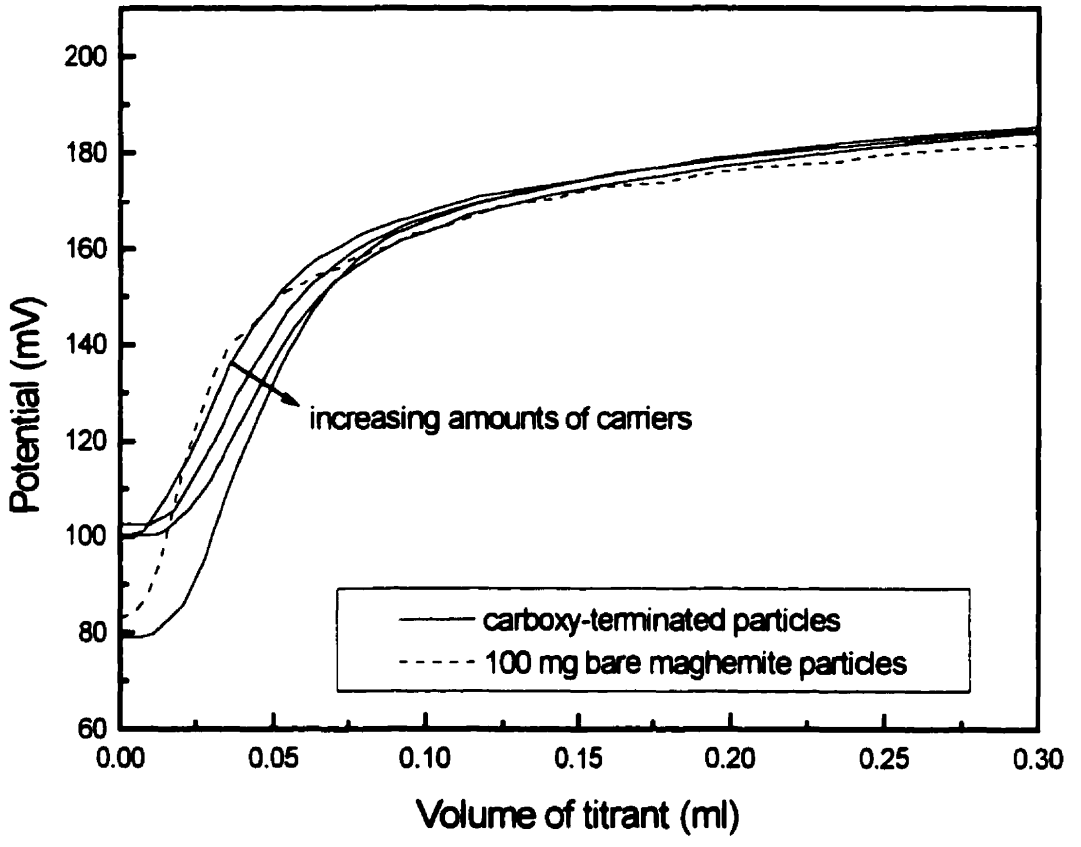

Figure 6-3: Titration of carboxy-terminated particles and 100 mg bare maghemite.

6.3.2 XPS

XPS spectra of the magnetic carriers with (a) and without (b) copper, are shown in Figure 6-4, for the regions $Fe_{2p3/2, 2p1/2}$, O_{1s}, and C_{1s}. The dotted lines in the spectra show the deconvoluted peaks of interest of each of these atoms. Few spectral changes are seen between curves (a) and (b), on the iron and oxygen spectra. The carbon spectra of (a) presents more of a deep valley between higher and lower energy peaks than (b), possibly indicating a shift of lower energy amide carbon to higher binding energies upon coordination with copper.

The interesting XPS results are seen in Figure 6-5, which presents the spectra of Cu_{2p} and N_{1s}, with (a) and without copper (b). The broad band at 938 eV in the spectrum of Cu_{2p} is associated with an Auger band of iron, not copper. The new bands centered at 933.5 and 954 eV in spectrum (a) are characteristic of copper ions, indicating their uptake by the magnetic carriers. Furthermore, the presence of a satellite band at 941 eV suggests that the majority of copper ions are in cupric form (Cu^{2+}).[9]

Inspection of the N_{1s} spectra reveals that the envelope band in (b) is shifted to a higher binding energy in (a). This indicates that both the secondary and amide nitrogen atoms originating from the DETA ligand, which used to show at 399.8 eV (see Table 6-2), are now detected at the higher binding energy of 401.3 eV after copper complexation.[10] It cannot, however, be concluded from these XPS results which nitrogen atoms are involved and to what extent, with the complexation of copper ions.

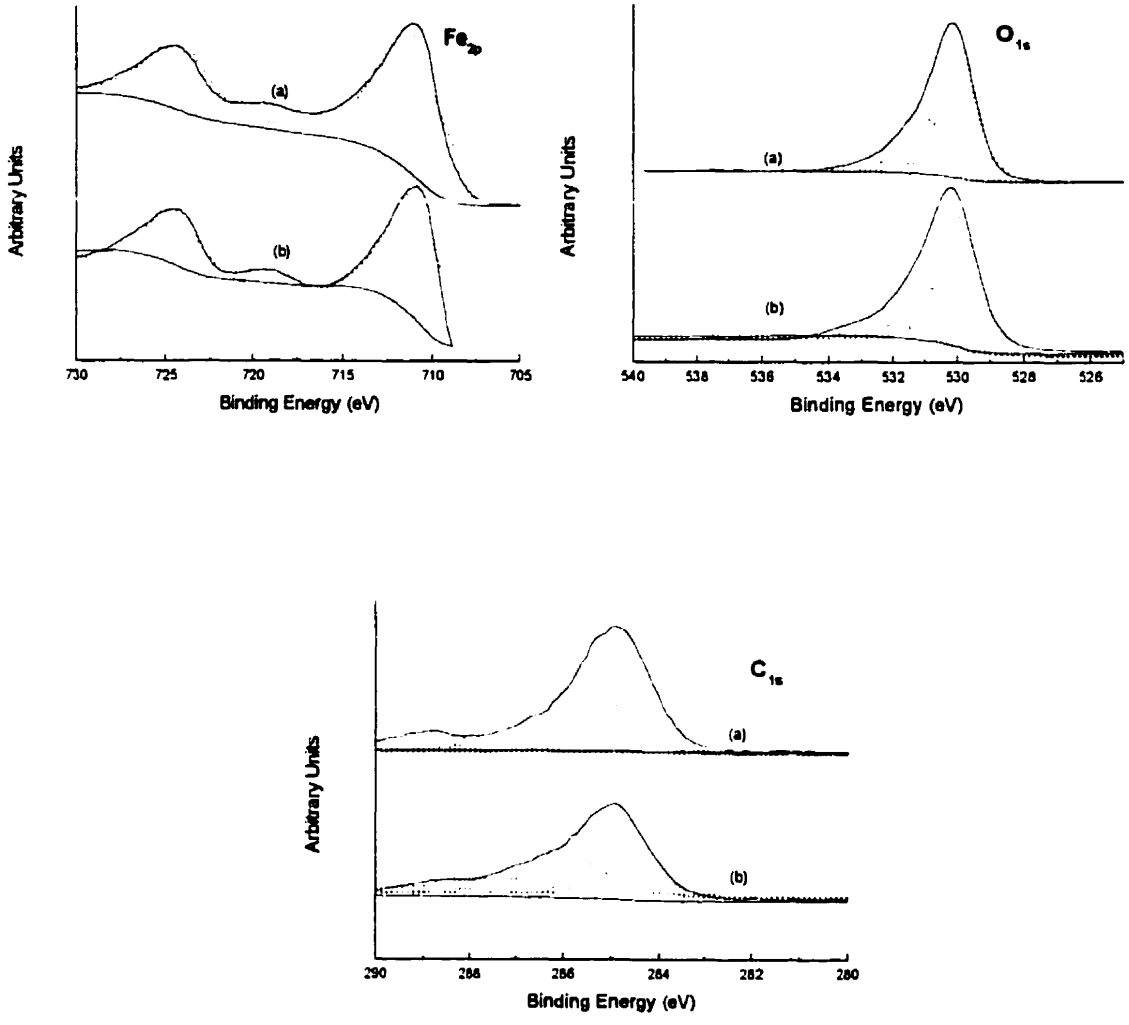

Figure 6-4: XPS spectra of narrow scans for the elements of interest on magnetic carriers after (a) and before (b) copper loading.

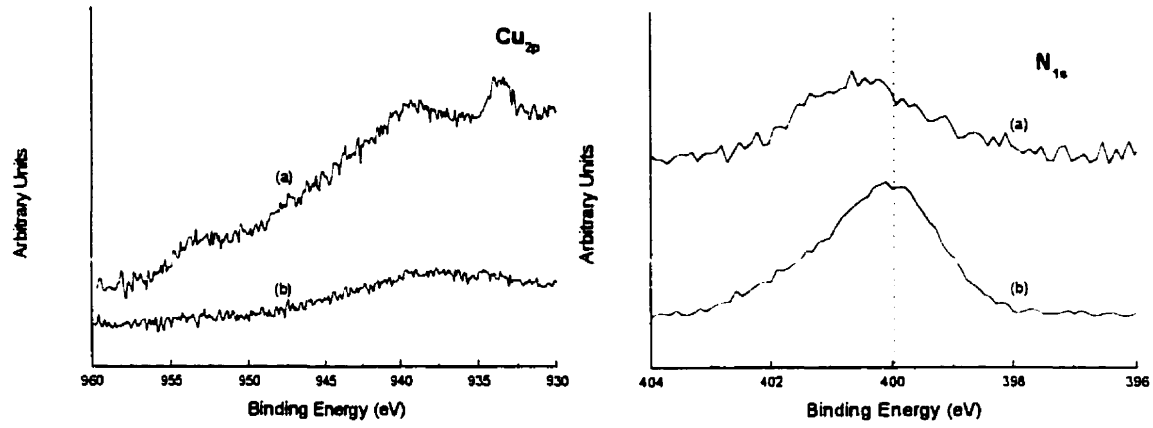

Figure 6-5: XPS spectrum of narrow scans for copper and nitrogen on magnetic carriers after (a) and before (b) copper loading.

Table 6-2: Binding energies (eV) of photoelectrons.

Peak	Magnetic Carriers BE (eV)	Copper Loaded BE (eV)
$Cu_{2p3/2}$	nd	933.5
		954.0
N_{1s}	399.8	nd
	400.3	400.3
	401.5	401.3

Band positions are accurate to ± 0.5 eV.

nd: not detectable.

6.4 Conclusions

This work confirms the complexation of copper ions by the DETA-functionalized magnetic (maghemite) carriers prepared. Complexometric titration using a copper selective electrode indicates the complexation of copper ions by magnetic carriers, a feature absent on non modified carboxy-terminated carriers and bare particles. The prepared magnetic carriers, with four possible points of attachment to metal ions, load a reproducible amount of copper of 0.52 μmole of Cu^{2+} per 50 mg of carriers. This corresponds to the removal of 1.65 ppm Cu^{2+} per 50 mg of carriers from a one liter stream. This loading capacity is three times the capacity exhibited by reported primary-amine functionalized magnetic carriers.[7] XPS results show the presence of $Cu_{2p3/2,\ 2p1/2}$ bands at 933.5 and 954.0 eV, confirming the loading of copper ions by magnetic carriers. A shift of the nitrogen envelop band to a higher energy, indicates involvement of the secondary amine and amide nitrogens in the copper complexation.

References

[1] Beauvais, R.A., Alexandratos, S.D., Reactive & Functional Polymers, **36**, 113-123 (1998).

[2] Bolto, B.A., Waste Management, **10**, 11-21 (1990).

[3] Rao, S.R., Xu, Z., Finch, J.A., in "Waste Processing and Recycling in Mineral and Metallurgical Industries II", Rao, S.R., Amaratunga L.M., Richards,G.G., Kondos,P.D. eds, Proceedings of the International Symposium, 69-77, Canada (1995).

[4] Hubbard, K.L., Darling, G.D., Finch, J.A., Minerals Engineering, **10** (1), 41-54 (1997).

[5] Martin, A, in "Physical Pharmacy", 4 th ed., Lea & Febiger, USA (1993).

[6] Constable, E.C., in "Metals Ligand Reactivity", Series in Inorganic Chemistry, series ed. J. Burgess, Ellis Horwood, England (1990).

[7] A.M. Gaudin Memorial Volume 1, "Flotation", M.C. Fuerstenau ed., USA (1976).

[8] Liu, Q., Ph.D. Thesis, McGill University, Canada (1996).

[9] Briggs, D., Seah, M.P., in "Practical Surface Analysis", 2 nd ed., vol(1), John Wiley & Sons, England (1990).

[10] Beamson, G., Briggs, D., in "High Resolution XPS of Organic Polymers", John Wiley & Sons, England (1992).

Chapter 7

Summary

7.1 Conclusions

The research presented in this thesis describes the preparation and characterization of a type of magnetic carriers, based on the functionalization of nanosized maghemite particles. The work demonstrates that a rigid and stable monolayer of a dibenzoic acid diamide bolaamphiphile self-assembles on maghemite surfaces and the exposed carboxylic groups of the functionalized surface can further react with an amine based ligand, such as DETA, allowing for the preparation of highly selective magnetic carriers.

Chapter 3 presents the characterization by spectroscopy techniques, of a self-assembled monolayer of a dibenzoic acid diamide bolaamphiphile on nanosized maghemite particles. DRIFTS results indicate the unidentate coordination of one carboxylic end group of DBSC-10 with the iron of maghemite, from a difference between the two stretching vibrations of the carboxylate, $\nu_{as}(COO^-)$ and $\nu_s(COO^-)$, of 249 cm^{-1}. The presence of H-bonded amide and free carboxylic moieties, also confirmed by DRIFTS, indicate a rigid monolayer. Structural evidence of the presence of DBSC-10 molecules on maghemite is further provided by XPS. No pre-treatment of the received maghemite is necessary prior the self-assembly of DBSC-10, which translates into a simple one-step preparation procedure of the functionalized surfaces. The stability of the monolayer in an acidic environment, at pH 3, is confirmed by DRIFTS.

A determination of the DBSC-10 monolayer density, is described in Chapter 4. This study was conducted using potentiometric titration to indicate the neutralization of surface carboxylic groups. These data are associated with the amount of DBSC-10 present on a given surface area of maghemite. Potentiometric titration gave a packing density of

3.4 μmole of DBSC-10 per m^2 of maghemite. This value was found to be in good agreement with the calculated value of 5.5 μmole of DBSC-10 per m^2 of maghemite. DRIFTS results indicate the retention of K^+ ions by the monolayer after titration.

Section one of Chapter 5 describes the coupling of the DETA ligand to carboxyl-terminated magnetic particles, using a typical carbodiimide to form peptide linkages. Characterization of the reacted monolayer by DRIFTS confirms the presence of DETA through the appearance of related peaks, namely the C-N stretch and the primary amine deformation bands. Deconvolution of XPS peaks associated with the atoms of interest, and potentiometric titration, both show that 50% of the carboxyl-terminated surface reacted with DETA. This result indicates that steric requirements, from self-assembly, may affect the accessibility of the different reactants involved, therefore decreasing the yield of reaction.

The second section of Chapter 5 presents the surface morphology of bare and functionalized maghemite particles, as imaged by TEM spectroscopy. An advanced Pt/C replica technique allows for the detection of dodecahedron-shaped bare maghemite particles. This specific shape is not distinguished in the samples of both types of functionalized particles, indicating the presence of coatings. This shadowing technique enables the visualization of a well-ordered coating.

Chapter 6 describes application of the prepared magnetic carriers in the removal of Cu^{2+} ions from dilute aqueous solution. Confirmation of the presence of copper and chelated nitrogen groups on the magnetic carriers was obtained by XPS spectroscopy. A complexometric titration technique was used to indicate the extent of complexation. A

loading of 0.52 μmole of Cu^{2+} per 50 mg of magnetic carriers was found by a difference method. With this carrying capacity value, it is estimated that 3 g of magnetic particles is needed to remove 100 ppm of copper ions from a one liter solution, indicating an improvement in metal loading capacity from single chelation site-type carriers. This adds justification to the use of ligands for the preparation of magnetic carriers for selective metal uptake and indicates potential benefit of ligands containing even more donor groups than DETA.

7.2 Contributions to Original Knowledge

1. Magnetic carriers with reactive carboxylic groups were prepared, for the first time, using a dicarboxylic bolaamphiphile, DBSC-10, through molecular self-assembly. The monolayer thus formed, was characterized by DRIFTS and XPS spectroscopy techniques, and was found to be both rigid and stable.

2. A novel potentiometric titration technique has been developed and used in the assessment of the DBSC-10 monolayer density. This technique is based on the neutralization of surface carboxylic groups of functionalized maghemite particles by the titrant KOH in water using DMF as the solvent.

3. Magnetic carriers with available reactive DETA ligand terminations, have been synthesized. The reaction is via one of the secondary amines of DETA and a carboxylic group from the DBSC-10 functionalized maghemite, using a typical carbodiimide (EDCI) to form amide linkages. The reacted monolayer was characterized by DRIFTS, XPS, and potentiometric titration, which indicated a 50% reaction yield.

4. An advanced TEM Pt/C replica technique, has been applied to the imaging of the prepared magnetic carriers. Visualization of the monolayers is either through the shadow halos around some carrier particles, or from loss of the dodecahedron shape of bare maghemite.

5. Application of the prepared magnetic carriers to metal recovery was demonstrated. The removal of Cu^{2+} ions from dilute streams, using a DETA-terminated type of carrier, was shown. A technique, complexometric titration, was adapted to this work to assess the extent, i.e., the efficiency, of copper ion removal.